

Biophysical characterization of aggregation and gelation in concentrated solutions of eye lens crystallin proteins

Dissertation

zur Erlangung des Doktorgrades der Naturwissenschaften
(Dr. rer. nat)

der

Naturwissenschaftlichen Fakultät II
Chemie, Physik und Mathematik

der Martin-Luther-Universität
Halle-Wittenberg

vorgelegt von

Frau Maria Camilles

Gutachter:

1. Prof. Dr. Kay Saalwächter (Martin Luther Universität, Halle-Wittenberg)
2. Prof. Dr. Jochen Balbach (Martin Luther Universität, Halle-Wittenberg)
3. Prof. Dr. Simon Ebbinghaus (Ruhr Universität Bochum)

Tag der öffentlichen Verteidigung: 14.10.2024

Contents

Abbreviations	4
Overview of the thesis.....	5
1 Introduction	6
1.1 Lens structure and components.....	6
1.2 Crystallin proteins.....	8
1.2.1 Alpha crystallin protein.....	8
1.2.2 Beta and gamma crystallins	9
1.3 Lens crystallin interactions.....	10
1.4 Macromolecular crowding in biological systems.....	12
1.5 Temperature dependent stability of crystallin protein (γ B and α -crystallin).....	13
1.6 Aggregation and gelation of globular protein	15
1.6.1 What drives the aggregation of globular proteins?	16
1.6.2 Gelation studies of common globular proteins	17
1.6.3 Solid state NMR and protein structure determination.	18
2 Scope of the thesis	21
3 Basics of characterization techniques.....	23
3.1 Nuclear magnetic resonance spectroscopy (NMR).....	23
3.1.1 Internal interactions	25
3.1.2 Relaxation	27
3.1.3 NMR relaxation studies for protein solutions.....	29
3.1.4 Measuring transverse relaxation	30
3.1.5 Magic-Angle Spinning solid state NMR.....	31
3.1.6 Cross polarization	31
3.1.7 Insensitive nuclei enhanced by polarization transfer (INEPT).....	32
3.1.8 Measuring relaxation in rotating frame.....	33
3.2 Small-angle X-ray scattering (SAXS).....	33
3.3 Dynamic light scattering (DLS).....	34
3.4 Attenuated total reflectance FTIR (ATR-FTIR)	35
3.5 Electron Microscopy	35
4 Material and Methods.....	36
4.1 Lens material and recombinantly synthesized protein	36

4.1.1	Culture media.....	36
4.2	Molecular biology - cell transformation.....	37
4.3	Protein expression and purification.....	37
4.3.1	H α B-crystallin	37
4.3.2	Bovine γ B crystallin.....	39
4.4	α -crystallin from bovine lens.....	39
4.5	Sample preparation.....	40
4.5.1	Solution state NMR.....	40
5	Characterization techniques.....	42
5.1	NMR relaxation.....	42
5.2	Easy NMR relaxation method.....	43
5.3	Heteronuclear Single Quantum Coherence (HSQC).....	43
5.4	Solid-state NMR.....	43
5.4.1	TUM parameters (Structural determination)	43
5.4.2	MLU parameters	44
5.5	Absorption spectroscopy for concentration determination	44
5.6	Small Angle X-ray scattering (SAXS).....	45
5.6.1	Basic analysis.....	45
5.7	ATR FTIR spectroscopy	51
5.8	Electron microscopy.....	52
5.9	Dynamic Light scattering.....	52
5.10	Transmission Experiments	53
6	Results and Discussion	54
6.1	A quantitative study of heat-induced aggregation of eye-lens crystallin proteins under crowding conditions using low-resolution NMR.....	54
6.1.1	Transverse relaxation at high protein concentration.....	56
6.1.2	Data analysis approach	57
6.1.3	Average T_2 values and aggregation kinetics	58
6.1.4	Aggregation kinetics vs concentration	60
6.1.5	Quantitative estimation of aggregated protein (γ B-crystallin).....	61
6.1.6	Transverse relaxation of the solvent	62
6.1.7	Conclusion	63

6.2	Investigation and characterization of gelation of α -crystallin eye-lens protein.....	64
6.2.1	Aggregation and gelation in globular proteins.....	64
6.2.2	Gelation in eye lens α -crystallin protein.....	65
6.2.3	Conclusion	86
6.3	Effect of Magic Angle Spinning (MAS) on solid-state NMR resolution of α B-crystallin protein probed using $T1\rho$ relaxation.....	88
6.3.1	Solution state NMR experiment with α B crystallin (HSQC).....	88
6.3.2	Solid-state MAS NMR of α B crystallin (TUM Data)	90
6.3.3	Solid-state MAS NMR of α B crystallin (MLU Data)	92
6.3.4	Correlating $T1\rho$ relaxation to MAS dependent spectral resolution.....	93
6.3.5	Conclusion	100
7	Summary.....	101
8	Table of figures.....	104
9	References	108
10	Acknowledgement	126
11	List of Publications	128
12	Curriculum Vitae	129
13	Erklärung.....	130

Abbreviations

ACD	Alpha Crystallin Domain
ATR	Attenuated Total Reflectance
CD	Circular Dichroism
CP	Cross Polarization
CTR	C – Terminal Region
DLS	Dynamic Light Scattering
FTIR	Fourier Transform Infrared Spectroscopy
GdHCl	Guanidinium hydrochloride
GELFI	Gel Filtration
H α B	Human Alpha B
HMW	High Molecular weight
HSQC	Heteronuclear Single Quantum Coherence
MAS	Magic Angle Spinning
MLU	Martin Luther Universität
NMR	Nuclear Magnetic Resonance
NTR	N – Terminal Region
RF	Radio Frequency
SAXS	Small-Angle X-ray Scattering
sHSP	Small Heat Shock Protein
TEM	Transmission Electron Microscopy
ThT	Thioflavin T
TUM	Technical University of Munich
UV	Ultraviolet

Overview of the thesis

Over the years several sources of cataract formation has been speculated, namely protein aggregation, amyloid formation, protein crystallization and liquid-liquid phase separation (Graw 2009; Benedek 1997). The exact cause of such an aggregation is although still unknown. This work is an attempt to understand the aggregation tendency of the crystallin proteins specifically under heat stress condition. The thesis is divided into several sections. In the introduction, the eye lens structure, the organization within the lens and its different components have been described in detail. Furthermore, a closer look at the individual crystallin proteins that constitute the major part of the lens, the unique characteristics of these proteins and the inherent role it plays in maintaining the transparency of the lens. An insight into the macromolecular crowding in biological systems explains the proteins' ability to exist in such a crowded environment. This is followed by a literature review of the current known temperature effects on the crystallin proteins and the aggregation and gelation tendency of the globular protein. The second section describes in details the outlook of the thesis. The basics of the characterization techniques used have been elaborated in the next section, wherein a short introduction of each of the techniques have been included. In section four, the materials and method used have been described. Here, information regarding the recombinant protein expression and purification has been detailed and in addition parameters used for the different techniques are listed. The last section is the results and discussion chapter which is split into three subsections. The first part deals with using low resolution NMR to study the heat-induced aggregation of two crystallin proteins, bovine γ B and bovine α -crystallin under crowding conditions. Both the crystallins showed varying aggregation tendency with bovine γ B crystallin forming solid aggregates and bovine α -crystallin aggregated to form a gel. In the second subsection, the gels formed by bovine α -crystallin is further explored and compared to the aggregation of human α B-crystallin. Several different characterization techniques were used to get a better understanding of the gel formation in α -crystallin. This allowed a closer look at the changes occurring during the gelation starting from a protein globular level down to molecular level. The last section was initially an attempt to see the structural changes upon gelation in α -crystallin proteins using solid state NMR. This study was then modified to correlating the resolution of solid-state NMR spectra of human α B crystallin with increasing MAS spinning frequency, by accessing the slower motions using $T_{1\rho}$ relaxation measurement.

1 Introduction

Cataract is one of the leading causes of blindness that has affected more than 51% of the total world population, which estimate to around 20 million people (Pascolini and Mariotti 2012). It is a protein condensation disease, wherein under certain detrimental circumstances eye lens proteins lose their native structure and aggregate to form a cloudy lens that hinders one's vision. Cataract can be classified into two types congenital and age - related cataract. Congenital or childhood-onset cataract results from certain point mutations in the lenticular protein that could prevent proper folding of the protein, destabilize the Greek key domain or result into disulfide bond formation. For certain aggregation prone variants of structural crystallins, such point mutations do not lead to overall structural changes. In age-related cataract the damages caused to the lens proteins due to post translational modifications accumulates over time, which is brought about primarily by UV exposure (Martin 2007). This eventually leads to formation of larger structures leading to light scattering and eventually opacification of the eye lens preventing light from falling on to the retina resulting into visual impairment (Figure 1).

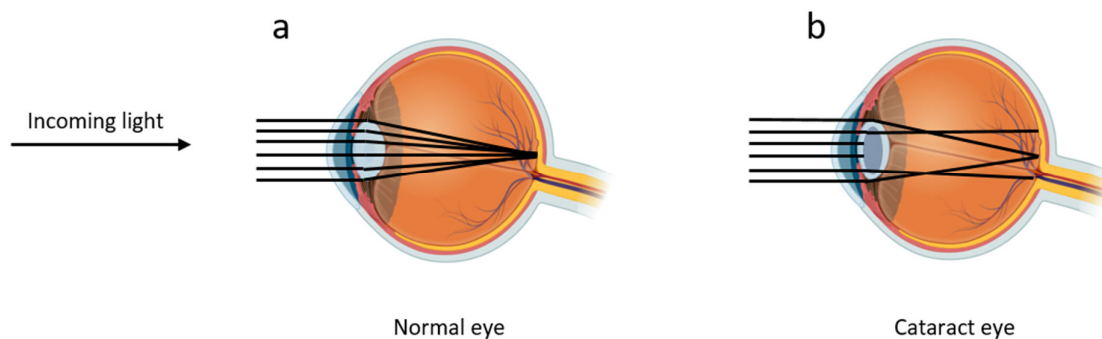


Figure 1: a. Clear eye lens permits the light to focus sharply on the retina, b. Clouded lens scatters or blocks the light from falling on to the retina. (Pictures made using Biorender)

1.1 Lens structure and components

The lens proteome is one of the major components in the eye that focuses light and directs it on to the retina. A mature lens is made up of long ribbon-like fiber cells with a hexagonal packing and arranged in the form of concentric circles such that the older cells are accumulated at the center and younger cells are on the outside, forming an extensive cytoskeleton network (Bloemendal et al. 2004; Martin 2007). The fiber cells eventually differentiate expressing fiber cell specific proteins known as crystallin in high concentrations and in the due course of embryonic development these fiber cells eliminate nuclei and other cellular organelles. This is crucial for a transparent lens. Therefore, the crystallins that were synthesized during the initial maturation stage remain in the core, while the crystallin expressed later remains in the cortex. Due to the loss of cellular organelles, the terminally differentiated fiber cells can no longer express proteins and therefore the proteins already present during the lens maturation cannot be replaced and has to remain stable throughout a lifetime (Robinson 2010).

A mature eye lens is predominantly made up of abundant water-soluble crystallin protein which amount to 90 % of the dry weight of a lens, (Horwitz et al. 1999) in contrast to ordinary tissues where the water content is about 95 % and protein is about 5 % (Riedl et al. 2020). In a human eye lens these proteins are present at an extremely high concentration ranging from 200 mg/mL at the periphery to 400 mg/mL at the center (Fagerholm et al. 1981). For aquatic organisms it goes upto 700 mg/mL due to absence of air-water interface and therefore requires higher refocusing power (Martin 2007). It was initially ascertained that such high protein concentration ensured the lens transparency as well as high refractive index gradient necessary for proper functioning of the lens. Benedek (1971) and Delaye and Tardieu (1983) in separate studies using light scattering and X-rays studies respectively, showed that the crystallins at such high concentrations are closely packed with a short-range ordered arrangement. This resembles a dense liquid or glass which facilitates the lens transparency that do not transition into a paracrystalline phase as was speculated by Trokel (1962). It is striking characteristic of these proteins to exist in such crowded conditions and be able to hold on to its hydration shells and thus avoid aggregation.

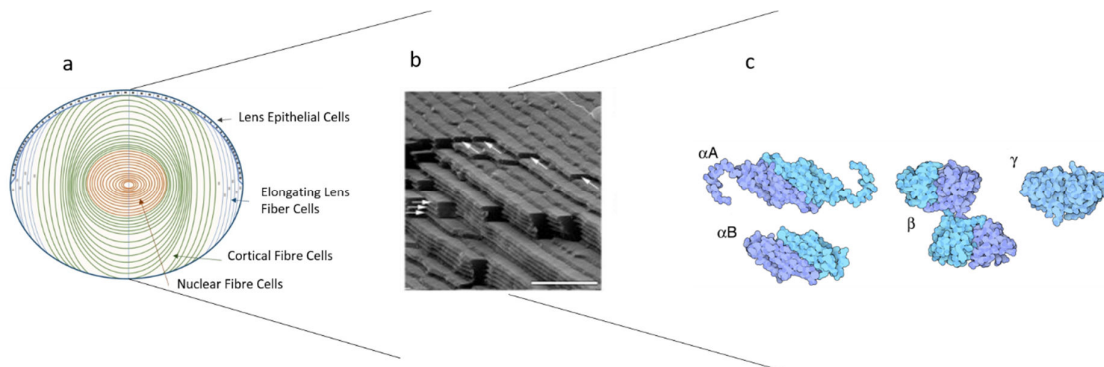


Figure 2: Organization within the eye lens a. cross-section of lens depicting the cell distribution of epithelium (Kalligeraki et al. 2020) reused with permission according to CC BY 4.0 DEED license (<http://creativecommons.org/licenses/by/4.0/>), b. Short ranged ordered packing of lens fiber cells (Song et al. 2009) reused with permission according to Copright Clearance Center, Inc, License ID – 1449356 - 1, c. Three major crystallin proteins (Goodsell 2010) reused with permission according to CC BY 4.0 license.

The lenticular proteins are collectively known as ‘Crystallin proteins’, and α -, β -, and γ -crystallins are three major classes of crystallin protein. These proteins are present as a polydisperse colloidal solution within the eye lens. The protein - protein interactions play a major role in maintaining the lens transparency brought in by the repulsive interactions of β -crystallins that results into even distributions of oligomeric components and the attractive interactions between the γ -crystallins ensure close short - range packing contributing to the high refractive index. This balance of forces between the crystallins in the lens when is impeded, can lead to lens clouding (Tardieu et al. 1992)

1.2 Crystallin proteins

1.2.1 Alpha crystallin protein

α -crystallins is one of the major lens structural proteins that constitute to around 40 % of the total lenticular protein mass in the eye. This protein comprises of two subunits α A- and α B- having 60 % sequence homology with 173 and 175 amino acid residues respectively. They exist in the eye lens in a ratio of 3:1. The monomeric weight of these proteins are \sim 20 kDa, but in the lens they are present as a heterogeneous high molecular weight aggregates with molecular weight ranging from 300 - 1200 kDa, with an average of around 800 kDa. The number of subunits range from 24 – 33 units. In the eye lens they exists as an hetero - oligomer with 12 - 14 nm diameter in size (Burgio et al. 2001; Boyle and Takemoto 1994). α -crystallins are composed of an immunoglobulin-like α -crystallin domain of \sim 90 residues flanked on both sides by an unstructured hydrophobic N-terminal, and a polar dynamic, highly flexible C - terminal extension with a conserved IXI motif (Carver et al. 2017). Figure 3 is a schematic representation of the oligomerization of α -crystallin protein through the interaction of the various domain regions. The monomeric sHSP initially assemble into a dimer through the ACD - ACD (alpha crystallin domain) interactions. Further on higher order assemblies such as hexamers are formed by the interaction of ACD - CTR (C - terminal region) interactions and the weak NTR (N - terminal region) interactions then lead the assembly of final oligomer (Delbecq et al. 2015). One major difference between both the subunits is the presence of cysteines in α A. This helps in transferring the disulfide bonds to an aggregating client. On the other hand client proteins can bind via the exposed hydrophobic surfaces with specific regions on the chaperone for both α A and α B (Roskamp et al. 2020). While α A crystallin is found primarily in the eye lens, α B crystallin have been expressed in eye lens, heart, brain and skeletal muscle. Several studies using circular dichorism and infrared measurements have indicated that the secondary structure of α -crystallin constitute around 60-70 % of β -sheet structure and very little α -helix (Augusteyn and Stevens 1998).

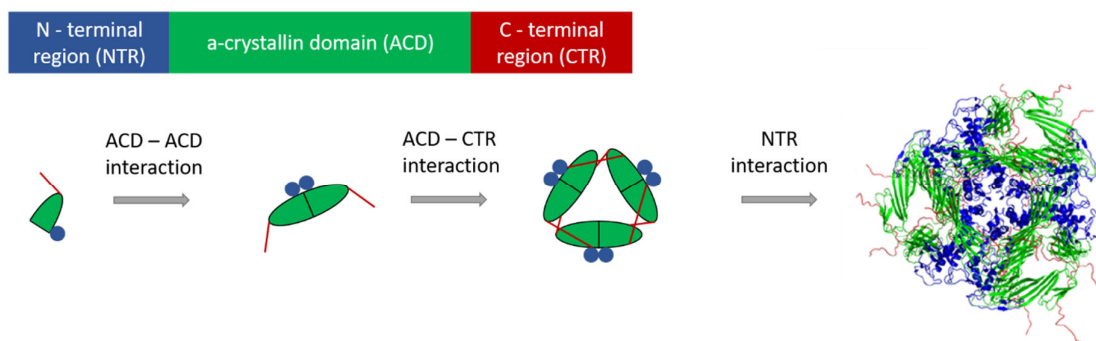


Figure 3: Oligomerization of α -crystallin via different interactions (Delbecq et al. 2015) adapted and reused according to ACS usage agreement.

1.2.1.1 Chaperoning functions

α -crystallins belong to a family of proteins known as small heat shock proteins and they act as molecular chaperones by maintaining protein homeostasis and protect cells from stress. In cells under conditions of stress such as heat, pH change, ultraviolet radiation, oxidative stress proteins in the lens tend to unfold and aggregate and in response to such stressors these sHsp's act within first line of defence as they prevent these proteins from aggregating. They bind to the unfolding protein and solubilizes them by an ATP-independent process and hence they lack the ability to refold them back to its native state. In one of the pioneering works by Horwitz, the chaperoning of crystallins were studied, which showed that only α -crystallins could suppress the aggregation of various enzymes including alcohol dehydrogenase, as well as β - and γ -crystallins. A mixture of bovine eye lens crystallins devoid of α -crystallins aggregates at 60 °C indicating its importance in the eye lens. Furthermore, α -crystallin could renature ~ 95% of γ -crystallin, that was denatured using GdHCl, which was confirmed by circular dichroism (Horwitz 1992).

This chaperoning of α -crystallin has been linked to the hydrophobicity of these proteins. It has been speculated that the interaction between hydrophobic site on the α -crystallin and the exposed hydrophobic region during denaturation of the substrate protein is responsible for its chaperone function, where the exposed site on the denatured protein would self-aggregate (Reddy et al. 2006). Subunit exchange could also play a major role in chaperoning since it helps in rearranging and accommodating the aggregating substrate (Putilina et al. 2003). It has been shown that cleaving the C-terminal end from α A results into decreased chaperoning activity towards alcohol dehydrogenase. This C-terminal plays a major role in preventing heat induced denaturation and aggregation (Takemoto et al. 1993). Mainz et al., on contrary showed that α B crystallin at 37°C exhibits different chaperoning ability towards different types of aggregates. The amyloid fibrils bind to the hydrophobic central ACD domain, while amorphous aggregates of lysozyme are taken up by the N-terminal domain (Mainz et al. 2015).

1.2.2 Beta and gamma crystallins

Beta and gamma crystallins are structural protein present in the eye lens belonging to the same crystallin superfamily (Augusteyn and Stevens 1998). They constitute the remaining 60 % of the total lens proteins, with 35 % β -crystallin and 25 % γ -crystallin (Vendra et al. 2013). They share a similar secondary structure with two domains that consists of four β -sheets arranged as two Greek Key motifs per domain (Figure 4). The major difference between these proteins is that β -crystallins have N-terminal extensions and basic β -crystallins have a C-terminal extension. β -crystallins family consists of basic (β B1, β B2, β B3) and acidic (β A1, β A2, β A3 and β A4) polypeptides forming higher order oligomers and/or also exist as homo or hetero dimers. γ -crystallins are a group of monomeric protein of molecular weight of about 20 kDa consisting of 6 homologous proteins γ A to γ E that are closely related gene products, and γ S that has characteristics intermediate between β - and γ -crystallin (Carver 1999).

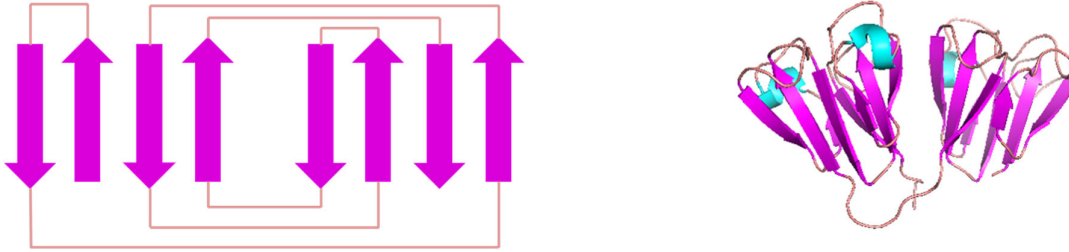


Figure 4: Basic secondary structure construct of $b\gamma$ -Crystallin, a. Two Greek key motif per domain formed from antiparallel β sheets, b. Structure of Bovine γB crystallin: pdb code: 1GCS (Najmudin et al. 1994), processed using pyMol

1.2.2.1 Bovine γB crystallin

In the bovine lens γB and γD are the most predominant γ -crystallins. The very first X-ray crystal structure determination of a lens protein was reported on bovine γB (Blundell et al. 1981). The study revealed that these proteins have a high degree of internal symmetry consisting mostly of β pleated sheet. They are folded into two domains such that each domain comprises of the N - terminal half and the C - terminal, with each of these domains being compact and stabilized by surface ion pairing. These domains possess a hydrophobic core and are tightly packed by these hydrophobic interactions, with negligible exposure of the connecting peptide. γ -crystallin are characterized by high free cysteine content, which under certain oxidative stress conditions would readily form disulfides, eventually leading to aggregation and insolubilization of these proteins. (Mandal et al. 1987; McDermott et al. 1988)

1.3 Lens crystallin interactions

The protein - protein interactions between the lens crystallins play a major role in maintaining the lens transparency, especially with the protein being in such an extremely concentrated environment. If these interactions are perturbed either due to post translational modifications during ageing or due to certain mutations, this could lead to the formation of high molecular weight aggregates which could eventually scatter light and hamper vision. Delaye and Tardieu were the first to use SAXS to confirm the short range ordered arrangement of crystallin proteins within the lens. They observed that with increasing concentration of these proteins a relatively closer packing of the lens protein makes the lens transparent, without transitioning to a crystalline order. The refractive index fluctuations decreases owing to this close packing of crystalline proteins thereby reducing the scattered light intensity (Delaye and Tardieu 1983). Tardieu further reported that the protein - protein interactions between α -crystallins were a good fit with the model of repulsive interaction corresponding to a hard-core plus a screened coulombic electrostatic potential. These α -crystallins being polydisperse and dynamic can self-assemble and depending on their surrounding environment rearrange and/or accommodate subunits. Therefore, the charges on these proteins are distributed such that it leads to a repulsive interaction which could prevent their aggregation.

Similar X-ray scattering and osmotic pressure studies on concentrated β - and γ -crystallins indicated that repulsive coulombic interactions are dominant in β -crystallin with an increase in overall osmotic pressure. On the contrary, a decrease in scattering intensity in X-ray was observed for γ -crystallin, indicating dominance of an attractive interaction between them (Tardieu et al. 1992). This attractive interaction may be the cause of the cold cataract phenomenon observed for γ -crystallins. The major contribution to the lens transparency therefore comes from the repulsive interactions that is favored by high charge, low molecular weight and a high ϕ/c ratio (ϕ – excluded volume), although all of these parameters do not necessarily have to act simultaneously. Consequently, the authors hypothesize that these interactions (i.e. repulsive) helps conserve the transparency by distributing the crystallin evenly throughout the lens, while the attractive interactions contribute to the refractive index by allowing a close packing of the crystallins. These intermolecular interactions therefore are responsible in maintaining the supramolecular structure and the lens translucent. The formation of HMW (high molecular weight) aggregates due to disruption of its surface hydrophobicity can affect these protein interactions and their structure.

Intermediate (mobile) and slow (solid-like) motions in bovine lens homogenate were investigated using ^{13}C NMR spectroscopy. Here, the more mobile phase was characterized by spin lattice relaxation off resonance and dipolar decoupling and cross polarization was employed to detect the presence of a solid-like phase for both cortical and nuclear lens homogenate. In the nuclear part of the lens both mobile and solid-like phases were observed, while only mobile phases were detected in the cortical region. This indicated that the protein homogenate within the lens nucleus might be in a gel-like phase (Morgan et al. 1989). ^1H NMR was used to investigate the role of flexible terminal extension of α -, $\beta\text{B}2$ -, γS and γB crystallins in maintaining the supramolecular order within the lens nucleus and cortex (Cooper et al. 1994). It was found that the C-terminal end of β - and γ - are involved in inter crystallin interactions, although γ -crystallin does not interact with other γ -crystallin, while $\beta\text{B}2$ does interact with other β -crystallin. They observed only the flexible side chains from N-terminal γS and $\beta\text{B}2$ and C-terminal α -crystallins indicating that these are not involved in crystallin-crystallin interactions, but possibly act as spacers or interact with non-crystallin components of the lens.

Light scattering studies on α -crystallin solutions were used to investigate the thermodynamics involved in the crystallin interactions. They found that the thermodynamic stability of α -crystallin is enhanced by its interaction with the other crystallin protein present together, as it enables best solvation property as well as best packing when compared to individual crystallin (Bettelheim and Chen 1998). Using FTIR and near UV Circular dichroism (CD) the changes in the interaction between crystallin proteins at higher concentrations were probed individually. The near UV CD showed an increase in CD intensity with increase in concentration indicating that the aromatic side chains are in a more rigid environment. Therefore higher concentrations of proteins make them structurally more immobile and excluded volume effects tends to lead the protein to form a more compact structure (Liang and Chakrabarti 1998)

1.4 Macromolecular crowding in biological systems

Macromolecules such as proteins, nucleic acid and polysaccharides frequently exist and function in a crowded surrounding, where they are constantly interacting. These macromolecules in fact amounts to about 5 % - 40 % of the total cytoplasmic volume in a cell (Ellis and Minton 2003; Ellis 2001). Proteins are generally present in such a physiological media, at a concentration of several hundreds of grams per liter, for instance erythrocyte cytosol comprises 33 % (w/v) or 300 g/L of hemoglobin (Ralston 1990). In most of the biochemical and biophysical studies this effect of high concentration has been neglected by employing protein concentrations of several ten to hundreds lower than generally found in their physiological conditions. This high macromolecular content per volume is thus generally characterized as ‘macromolecular crowding’.

Several studies have therefore tried to mimic this crowding condition by either using inert macromolecules or in some cases also other proteins (Miklos et al. 2011) in order to understand the effect it has on the biological functions of these proteins. One of the major consequences of this high total macromolecular volume occupancy comes from the fact that the molecules are mutually impenetrable, i.e. excluded-volume effects (Minton 2001) play a central role in this concept of molecular crowding. This volume exclusion phenomenon leads to a decrease in entropy and simultaneous increase in free energy, thus the major consequence of such a molecular crowding is to promote processes that decrease the excluded volume. This is facilitated by protein compaction or assembly as well as possible protein aggregation, wherein the crowding influences the reaction kinetics and equilibria (Minton 2000; Ellis 2001). In certain cases like for hemoglobin, crowding can promote spatial ordering, such that they can spontaneously align and form bundles of self-assembled filaments (Herzfeld 1996). Furthermore the crowding-induced changes can have significant effect on the protein folding reactions which can either stabilize the protein native state (Cheung et al. 2005; Minton 2005) or could have a destabilizing effect (Mittal et al. 2015; Miklos et al. 2011).

The stability of native protein in a highly concentrated environment is promoted by the balance between volume exclusion and hydrodynamic interactions i.e. hard-core steric repulsion and chemical interaction (soft interactions) (Wang et al. 2012; Miklos et al. 2010; Sarkar et al. 2013; Zimmerman and Minton 1993). Some studies have shown that using protein as a crowder can destabilize the protein of interest, due protein-protein interactions (Harada et al. 2013). Crowding can also affect the diffusion of protein, by basically retarding the translation motion, such that the rate of diffusion-limited reactions decreases with increase in concentration. Investigations of crowding effects in our group have already shown that with increasing concentration of protein, the rotational and translational motion is fully coupled for the case of HEWL, while it is strongly decoupled for α B- crystallin protein, in general with increased retardation (Roos et al. 2016).

The eye lens is an example of a such a crowded entity, where all the crystallin proteins co-exist in a very highly concentrated environment. Most of the studies characterizing these proteins

have used dilute conditions rather than its physiologically relevant concentration. Therefore, to obtain a better picture regarding the functionality of these proteins, the study here has considered the use of self-crowding.

1.5 Temperature dependent stability of crystallin protein (γ B and α -crystallin)

Proteins are fully functional in their native folded state. They can under certain environmental conditions tend to aggregate, and lead to a pathogenesis of several disorders like neurodegenerative diseases (Ross and Poirier 2004), cardiovascular myopathies (Kholová and Niessen 2005), Cataract (Graw 2009) etc. These aggregates lead to severe loss of the biological functions of these proteins, which could have a detrimental effect. It is therefore necessary to investigate the protein aggregation to get a better insight into its causes and to develop advanced remedies.

Over the years crystallin aggregation has been investigated by exposing it to various stressors like heat (Borzova et al. 2016), UV radiation (Cetinel et al. 2017) or chemical denaturant (Rasmussen et al. 2011). In certain cases, depending on the environmental factors diverse aggregation pathways can be brought about (Moran et al. 2014; Roskamp et al. 2017). In my work I have specifically studied the heat-induced aggregation of bovine γ B and bovine α -crystallin. Early studies on heat-induced aggregation of crystallins by Steadman et al. using differential scanning calorimetry, showed no/little effect of concentration on thermal stability for γ -crystallin but played a significant role in case of β - and α -crystallin. These lens proteins are generally stable, with a large endothermic transition in temperature range 60 – 90 °C, which indicated a considerable change in their three-dimensional protein structure. While γ - and β -crystallin tends to precipitate at the beginning of the endothermic transition, for α -crystallin it appears only after extensive protein unfolding. Circular dichroism in turn indicated a significant change in the secondary structure for all proteins (Steadman et al. 1989). Kono et al., used far-UV CD and fluorescence measurements to investigate the conformational stability of γ -crystallins, where the increase in temperature from 25 – 78 °C resulted in a loss of β -sheet structure from ~ 70 % to 25 %, and above 80 °C the protein visibly aggregated. This indicated that a small change in tertiary structure of γ -crystallins can influence the conformational stability of the protein significantly (Kono et al. 1990).

Another study using DSC to probe the thermal behavior of γ -crystallins and its fractions revealed two endothermic transitions for γ B, a broad transition at 37 – 57 °C and at 70 °C, which indicated protein unfolding and beyond these temperatures exothermic peak appears that corresponds to irreversible aggregation and precipitation. This was further supported by ANS binding assay (8-anilino-1-naphthalene sulfonate), where the fluorescence intensity follows the thermal denaturation. This indicates that the large enthalpy arises from the protein-protein interactions (i.e. aggregation), is due to the exposure of hydrophobic ends (Sen et al. 1992). More recently γ B crystallin aggregates formed under different stress i.e. heat, cold and UV-induced as well as from refolding from denatured state were investigated using FTIR and EM.

Here the protein was thermally stressed at 70 °C, which resulted into precipitation. The amide I band maximum shifted from 1633 cm⁻¹ to 1620 cm⁻¹ with reduction in band intensity as well as β -sheet structure increased from 50 % to 60 %, indicating a noticeable structural change. Moreover, the ThT assay did not show any increase in fluorescence hinting to no amyloid formation.

Lens crystallins in general have proven to be extremely stable, but this stability also depends on their exposure time in case of thermal stress. Early studies on heat induced stress on α -crystallins revealed that, these proteins are exceptionally stable up to 100 °C, which they probed using far-UV CD (Maiti et al. 1988). Subsequent research based on this thermal stability challenged this finding, where it was found that for α -crystallins, a conformational transition occurs in 40 – 70 °C temperature range. Differential scanning calorimetry studies of bovine α -crystallin indicated a broad endothermic transition with two components in the range of 65 – 77 °C, although at 40 °C these transitions were initiated when compared to other crystallins (Steadman et al. 1989). Similar results were observed using FTIR, where the amide I band broadened at ~ 62 °C as well as CD and DSC showed a structural transition between 60 – 62 °C, indicating a change in secondary structure (Surewicz and Olesen 1995). When probed individually, α A and α B crystallin shows slightly different effect of temperature on their structural stability. At the thermal transition temperature of 62 °C, α B homomultimer is unstable and susceptible to aggregation when compared to α A, as was detected using light scattering (Sun and Liang 1998). Further in FTIR the amide I band broadened for both α A and α B in the 60 - 62 °C and 70 – 72 °C respectively, while ANS binding assay indicated an increased exposure of hydrophobic sites at 59 °C for both (van Boekel et al. 1999). Das et al., showed that at 60 °C the thermal transitions involve conformational structural changes, such that below this temperature, changes mainly occur on the tertiary structure and above this a partial denaturation is involved (Das et al. 1997). Similarly striking effects of increased temperature on quaternary/secondary structure (Farnsworth et al. 1997) were observed above 50 °C with decreasing mobility, which was attributed to the changes in shape, size and organization of α -crystallin aggregates using CD (Burgio et al. 2000) and using Fluorescence emission (Vanhoudt et al. 2000).

Most of the temperature dependent studies described above employed the use of crystallins at much lower concentration than the physiologically relevant state. X-ray scattering studies of concentrated α -crystallin ~ 300 mg/ml, which the authors have classified as ‘gel’, when thermally stress showed a transition at 50 °C. The X-ray scattering indicated a moderate increase in spacing and intensity, which accelerated from 45 – 70 °C, with a major increase in size, shape and size observed above 50 °C (Regini et al. 2004). Early studies using NMR to quantify this effect in α -crystallins showed no change in the ¹H spectra in 25 – 75 °C range, since only the C-terminal extensions are observed. Therefore the temperature induced changes reported by other authors likely arise from effect within the core of α -crystallins that is inaccessible by ¹H NMR (Carver et al. 1993). This is most likely related to the slow tumbling motions. The high thermal stability of α -crystallin observed at 100 °C could therefore be due

to the short exposure to thermal stress (5mins). Regardless, crystallins have shown a phenomenal resistant to temperature in terms of denaturation, although certain secondary, tertiary and quaternary structural changes are inevitable. These changes are known to play a significant role in the chaperoning activity of α -crystallin, by maintaining the structural integrity of the lens over a wide temperature range and prevent aggregation of lens crystallin (Burgio et al. 2000; Hasan et al. 2004; Das et al. 1997).

1.6 Aggregation and gelation of globular protein

Most of the globular proteins tend to aggregate when thermally stressed above or close to its denaturation temperature. Additionally, if present at high protein concentrations, appropriate pH and ionic strength these protein aggregates may form a gel (Ferry 1948). This is mostly characterized by transitioning of a fully folded protein to a partially/fully unfolded protein conformation. Such changes initiated by heating causes the peptide chain to be more mobile, thereby interact and bind to other proteins. Unfolded proteins are random coils that can be modeled as spherical colloidal particles and their aggregation or gelation involves short-range attractive interaction in the form of hydrophobic interactions, hydrogen bonding or electrostatic interactions (Mezzenga and Fischer 2013).

For a protein solution irreversible aggregation could also be characterized by denaturation, where the protein loses its tertiary structure forming permanent bonds for e.g., covalent disulphide bridges as a result of thermal stress. Such an aggregation process can lead to formation of branched, compact or fibrillar aggregate structures, which can be defined by a power law relationship, $M = (R/R_0)^{D_m}$, D_m being the fractal dimension, M average molar mass and radius R (Lazzari et al. 2016). With $D_m = 3$, the particles form a compact structure, while $D_m = 1$ indicates a rod like structure. The fractal dimension can also be used as an indicator of diffusion- and reaction-limited cluster aggregation. In most cases globular proteins follows a reaction limited aggregation process. The aggregate density is additionally dependent on R_0 and D_m such that if $D_m < 3$, with increasing size the density decreases according to $\rho = R^{D_m-3}$ (Nicolai 2007). Therefore, as the aggregation progresses, with decrease in aggregate density the volume occupied by the aggregates increases, eventually leading to percolation and formation of gel network (Zaccarelli 2007). The aggregates are not initially a part of the percolating network but gradually add on until all proteins become a part of the gel (Nicolai 2019). In case of globular protein aggregation, the rate of denaturation and subsequent transformation to reactive species can be different and certain extrinsic factor (e.g., heat) can affect the progression of gelation as well as gel structure. It has been shown for whey proteins that rate of heat induced aggregation and gelation increases with increasing temperature defined by an activation energy (Brodkorb et al. 2016; Nakamura et al. 1978). Since not all the native protein are initially incorporated into the gel network, the storage modulus (G') of the sample solution increases gradually beginning at a percolating threshold and ultimately all the native proteins add into the network (Verheul et al. 1998). Figure 5, is a schematic representation of gel network formation in globular proteins.

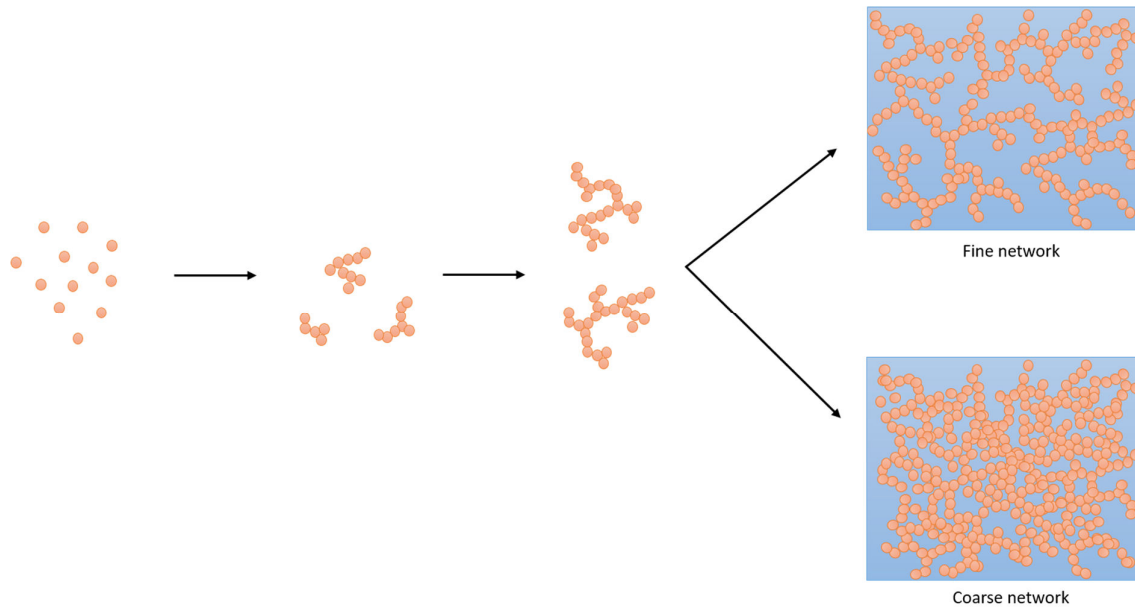


Figure 5: Depending on the type of the globular protein, its native state denatures (completely or partially) to form elementary units, that further aggregate to form self-similar units. These can further associate and form either fine network or coarse network gels which can be distinguished by their fractal dimensions.

1.6.1 What drives the aggregation of globular proteins?

A balance between interparticle forces, the attractive and repulsive interaction helps maintain the structure and functionality of a globular protein at high protein concentrations. For a colloidal system one of the potential model that describes the interparticle forces between the particles is the DeJaguin-Landau-Verwey-Overbeek (DLVO) theory (Hunter 2001, 2009). This theory encompasses both interaction potentials the hard core, repulsive coulombic electrostatic interactions and attractive van der Waals forces. The hard core or hard sphere repulsion/potential implies that the macromolecules cannot interpenetrate at very short distances. The DLVO theory can therefore be applied to native folded protein in order to get a better understanding of protein aggregation. In accordance to the DLVO theory the interaction potential F_{DLVO} for a pair of spherical globular protein with radius R and separated by a distance D , can be given as a sum of screened electrostatic repulsion in Debye-Hückel approximation and van der Waals attractive contribution (Israelachvili 2011), approximated as,

$$\frac{F_{DLVO}}{kT} \approx \left(\frac{\pi \sigma^2}{N_A e^2 I} R e^{-\kappa D} - \frac{3R}{12D} \right)$$

(1)

where, σ is the surface charge density of the protein. As is evident from Equation (1), the size of the particle R had a strong dependency on interaction potential, indicating that smaller the particle size, smaller would be the energy barrier to overcome and hence has a strong protein aggregation tendency (Mezzenga and Fischer 2013). Consequently, by modulating the total potential the aggregation rate can be modified. In the absence of any repulsive forces, the

particles aggregated upon contact leading to a diffusion-limited cluster aggregation. While a non-zero repulsive force tends to a reaction limited cluster aggregation since only certain number of collisions lead to aggregation (Berg 2010). Concerning the network structure, repulsive interactions leads to a formation of connected strands favoring a chain conformation, while attractive interactions forms coarser network structures, where the coarseness is determined by the strength of the attractive potential (Nicolai 2019).

1.6.2 Gelation studies of common globular proteins

Globular proteins mainly β -lactoglobulins, whey proteins, BSA, ovalbumin, Lysozyme etc. have been extensively studied to understand the protein gelation mechanism at higher protein concentration (Doi 1993). A combination of experimental techniques are commonly used to investigate both the gelation and aggregation of these proteins. The change in storage modulus/complex viscosity with time in rheological measurements can indicate the formation of the gel (gel time) (Tobitani and Ross-Murphy 1997) and provide information regarding the gel rigidity (Verheul and Roefs 1998). Electron microscopy and confocal scanning laser can determine the macroscopic structure of the gel (Clark et al. 1981a; Verheul et al. 1998; van Kleef 1986), while conformational or structural changes associated with the protein leading to a gel network can be probed using infrared and Raman spectroscopy (Clark et al. 1981b), far UV CD (Wang and Damodaran 1991) and NMR spectroscopy (van Kleef 1986). Additionally, light scattering can track the protein aggregation (Gimel et al. 1994).

Two major processes contribute to the irreversible gelation of protein that is thermally induced. Firstly, substantial structural change that is initiated by unfolding of native protein. In case of a multi-subunit protein particularly, it could occur after some degree of dissociation. This makes the protein molecule more reactive towards its neighbors. These protein-protein interactions lead to aggregation and the depending on the solvent, gel microstructures are formed (Clark et al. 2001). These denatured proteins unfold either to form random coils or form ordered β -sheet structures with simultaneous decrease in the α helix content. In certain cases such a transconformation is necessary for protein-protein interaction and gel-network formation (Clark et al. 1981b; Doi 1993; Wang and Damodaran 1991). The resulting protein network are held together primarily by non-covalent crosslinks namely hydrophobic interactions, hydrogen bonds, van der Waals or electrostatic interaction, although less frequently covalent disulphide bonds could also be involved (Totosaus et al. 2002; Ikeda et al. 1999). Heat-induced protein coagulation therefore results from the exposure of hydrophobic sites during protein unfolding (Nakai 1983). These heat-set proteins could either form random aggregates as in case of β -lactoglobulin or form string of beads structure as observed for bovine serum albumin, lysozyme and ribonuclease (Doi 1993). Heat-set protein gels are therefore physical gels that can in certain cases associate or dissociate reversibly under thermodynamic and mechanical actions (Djabourov et al. 2013). On the contrary, synthetic polymer gels that are formed by covalent cross-linking of linear or branched macromolecules, swell rather than dissolve in good solvent (Ross-Murphy 1998). Globular protein gels are generally classified as a collection of fractal objects/aggregates closely packed together as a continuous network of

particles resulting in a suspension of high viscosity and finite shear modulus (Shih et al. 1990). It is speculated that a cluster-cluster aggregation is necessary for such a gel formation, where particles diffusing through a medium stick to each other randomly. Such aggregation can be differentiated from their predicted fractal dimensions. The aggregation is reaction-limited (RLCA) when the fractal dimension is in the range 2.0 - 2.2, while it is 1.7 – 1.8 for a diffusion-limited cluster-cluster aggregation (DLCA) (Ikeda et al. 1999).

Eye lens α -crystallin proteins exhibit properties similar to the other globular proteins, i.e., under appropriate conditions these proteins form a gel. From the work of Sun and Liang (1998), the crystallin proteins in their homooligomeric form specifically α B crystallin forms an aggregate at 62 °C although there is no indication of crystallin gel formation, possibly owing the low starting concentration of the protein. Regini et al. (2004), classifies the crystallin protein obtained at a concentration of ~ 300 mg/mL as a gel, which under goes a major transition at 55 °C, that is irreversible. In these studies, the process of protein aggregation or gelation have not been addressed. The studies therefore based on α -crystallin gels are limited, consequently the mechanism of aggregation and gelation of these proteins are still unclear. These proteins could also presumably form physical gels like any other globular proteins where, strong protein-protein interactions after unfolding lead to network formation. Here the storage modulus would increase with time as the gel sets in and G' would be independent of frequency at longer times. On contrary, due to higher concentration subtle changes in the surface can expose the hydrophobic ends and lead to a cluster-cluster aggregation. It would therefore be interesting to look into the changes associated with the α -crystallin protein to get more insight into the dynamics associated with it during gelation.

1.6.3 Solid state NMR and protein structure determination.

To obtain a better understanding of the functional properties of a protein it is crucial to know its structure, which is generally brought about by a range of different biological characterization techniques including X-ray crystallography, cryo-electron microscopy and nuclear magnetic resonance spectroscopy. The most frequently used method of structural determination is X-ray crystallography, where it was used to solve about 89% of all structures in the protein database (PDB). One of the major disadvantages is that crystallography requires a high-quality single crystal of protein and therefore would essentially require large amount of recombinant protein as well as the protein crystal environment could be very different from its native environment and hinder a reliable structural assessment. The progressing technical development with cryo-EM facilitates its use for structural determination, although together with X-ray, is not a suitable method for molecular dynamics study. NMR on contrary, both solution and solid state, can be used to obtain both structural as well as dynamic information which in most cases are complementary. Additionally, the proteins can be studied in their native-like environment.

α -crystallins are the most widely studied crystallin proteins that constitutes major part of the human eye lens (Horwitz 1992). These protein when isolated from the eye lens were obtained

as highly dynamic water-soluble oligomeric assembly of proteins of molecular mass ranging from 200 kDa to 1.2 MDa (Haley et al. 1998; MacRae 2000), this also holds for α A- and α B-crystallins homooligomers (Horwitz 2003). Aside from the hetero-oligomers being widely present in the eye lens, its subunit α B was found in many other tissues; therefore, a lot of research studies were further focused on investigating this subunit of α -crystallin. Since several different theoretical structure model were hypothesized for α -crystallin oligomers (Siezen et al. 1978; Tardieu et al. 1986; Walsh et al. 1991; Wistow 1993; Carver et al. 1994), the development of characterization methods like electron microscopy and NMR-spectroscopy that lead to improved resolution along with recombinant protein production has greatly increased the studies based on α B-crystallin. Although due to its highly polydisperse and dynamic nature the full-length α B-crystallin protein could not be crystallized, a combination of NMR, X-ray crystallography and EM on its short constructs proved to be very beneficial.

In the last decade MAS solid state NMR has evolved as a powerful method to investigate the structural properties of non-soluble and soluble biomolecules like amyloid fibrils (Paravastu et al. 2008; Schütz et al. 2015) and membrane protein (Shahid et al. 2012; Andreas et al. 2015) as well as large protein complexes that are too dynamic to study using X-ray crystallography.

1.6.3.1 Formation of subunits in α B crystallin

As was pointed out in section 1.2.1, α B-crystallin is a sHsps protein, with a conserved central α -crystallin domain (ACD) belted by a variable N-terminal (NTD) and C-terminal (CTD) (Figure 6). Recently, by undertaking a hybrid approach combining information from solid-state NMR, small angle X-ray and electron microscopy has made it possible to obtain pseudoatomic models of these proteins (Jehle et al. 2011; Braun et al. 2011b). The basic building block in α -crystallin are dimers, where the dimer interface is formed by the antiparallel interaction of β 6+7 strands of ACD. These dimers then form a hexameric unit where the IXI motif on the C-terminal from one dimer interacts with the hydrophobic groove formed by β 4/ β 8 strands in the ACD of a neighboring dimer. The basic 24mer unit is then formed by the assembly of four such hexameric unit linked via contacts between the NTR resulting into a tetrahedral symmetry (Delbecq et al. 2015). The NTD being highly variable in length and sequence, and is responsible for sequence variation of α -crystallins within an organism (Haslbeck et al. 2005). The partially resolved crystal structure for the N-terminal region indicates increased flexibility (van Montfort et al. 2001a; van Montfort et al. 2001b) as well as the sites for post translational modifications are situated within this region (Peschek et al. 2013). The C-terminal domain (extension), also has a considerable sequence variation like the NTD. Several studies have shown that the C-terminal region as a whole is flexible (Narberhaus 2002; Kim et al. 1998; van Montfort et al. 2001b; van Montfort et al. 2001a). The highly conserved IXI/V-motif on the CTD, where the X is typically a proline residue (Garrido et al. 2012; Jong et al. 1993) could be important for the chaperone activity (Treweek et al. 2007; Kamei et al. 2000). Even though, the dimer formation is initiated by the α -crystallin domain, the higher order structures are promoted or assembled by the flanking N-terminal and C-terminal regions. Mass spectroscopy

revealed that the α B-crystallins being dynamic forms oligomers with a number of subunits ranging from 24 to 33, with an average of 28 subunits, additionally oligomers with subunits as low as 10 to a maximum of 40 were also found (Aquilina et al. 2003). Haley et al., demonstrated early on that the quaternary structure of human α B-crystallin forms roughly spherical multimers in the range of 8 – 18 nm diameter (Haley et al. 1998).



Figure 6: Domain organization for α B-crystallin protein

2 Scope of the thesis

Aggregation of eye lens crystallin proteins to form large clusters of aggregates occurs gradually throughout the lifespan of an individual. When they are sufficiently large enough it could lead to backscattering of light which increases exponentially with time as a function of age and eventually hampering proper vision (Benedek et al. 1999). In order to have a better understanding of the mechanism of aggregation of protein in the eye lens and the ability of α -crystallin to maintain the lens 'integrity', the effect of thermal stress on these eye lens proteins have been investigated. Albeit it is highly unlikely that heat - induced changes could occur in vivo, it can be used as a model to study the different conformational and structural changes involved when these proteins are physically perturbed.

The thesis aims at getting a clearer picture of effects of thermal stress on the concentrated solutions of eye lens crystallins. Initially the concentration dependence on the heat - induced aggregation of two different crystallins namely bovine γ B and bovine α -crystallin was investigated. Here the feasibility of NMR relaxometry to quantitatively estimate the aggregation of these proteins under crowing conditions was demonstrated (Camilles et al. 2018). A different qualitative aggregation process was observed for both the crystallins, with the bovine α -crystallin forming a transparent gel. It was an interesting observation which indicated that α -crystallin perhaps play a major role in lens transparency. The further work then focused on characterizing the gelation of α -crystallin proteins. Here, the different gelation propensities of α -crystallin, namely homooligomeric h α B and heterooligomeric bovine α -crystallin was investigated. This was achieved by the use of various biophysical characterization techniques, from starting at a globular level and eventually moving down to the molecular level. Firstly, the transparency of the gels were estimated using light transmission, which indicated qualitative differences in the gels formed. The change in particle size during thermal stress was probed via dynamic light scattering studies. Transmission electron microscopy images were recorded in the nm to μ m scale to gain information regarding the structure of the gels. Further on, ATR FTIR was used to directly monitor the changes occurring in the secondary structure throughout the course of heat induced stress. A detailed investigation on the molecular level e.g. changes in molecular interactions or interaction potential in the gels was possible by means of small-angle X-ray scattering, in addition to gaining information regarding the network structure of the gel. And lastly atomic force microscopy for nanoindentation was used to possibly probe the elastic modulus of these gels.

The last part of this thesis focuses on application of solid-state MAS NMR to try and characterize gelation in h α B crystallin with the initial motivation to probe on the atomic (residue) level the possible secondary structure changes on heating. Firstly, the solution and solid-state NMR spectra of α B-crystallin protein were obtained. Here a well resolved solution spectra was obtained for the crystallin protein. But with the solid-state experiments different problems encountered, and the spectra had poor spectral resolution. The aim was then to correlate the resolution of NMR spectra of α B-crystallin with increasing spinning speed and

determine the constraint in the overall slow tumbling motion of the protein as a possible origin of inferior spectral quality. The slower motions that exist were accessed by $T_{1\rho}$ relaxation measurements.

3 Basics of characterization techniques

3.1 Nuclear magnetic resonance spectroscopy (NMR)

The dynamic growth in the field of nuclear magnetic resonance, that still continues today, started back in 1946 when two individual research groups of F. Bloch and E. M Purcell first observed an NMR signal in bulk condensed phase. Further with the development of pulsed Fourier transform NMR spectroscopy by Ernst and Anderson boosted the rise of NMR as one of the most routinely used analytical technique in the field of both material science and protein biochemistry. From structural elucidation of proteins to determining the inherent molecular dynamics of a polymer chain, NMR has been used to characterize a wide range of molecules. Currently NMR spectroscopy, X-ray crystallography and electron microscopy are the only analytical technique capable of determining the 3D structure of macromolecules at the atomic level.

In the following section much of the theoretical description and explanations of fundamental NMR concepts are based on the book by (Levitt 2015), except when indicated otherwise.

Every nucleus has a non-negative nuclear spin quantum number I associated with it which differs from one nuclide to another depending on the interaction of the protons and neutrons in the nucleus. Nuclei can therefore be classified based on their nuclear spin value. Nuclei possessing, $I = \frac{1}{2}$, i.e. ^1H , ^3H , ^{13}C , ^{15}N , ^{19}F , ^{31}P are most commonly used for NMR analysis. There are several nuclei with $I > \frac{1}{2}$ having a nonspherical charge distribution and therefore possesses an electric quadrupole moment $|Q|$. Therefore, every nucleus containing $I \neq 0$ possess a magnetic dipole moment or a magnetic moment μ , which basically means that these nuclei act like a tiny magnet. The spin quantum number I can be written in terms of observable component of angular momentum, which is quantized,

$$|J| = \sqrt{I(I + 1)}\hbar \quad (2)$$

where, $\hbar = h/2\pi$; h = Plank's constant. By convention the measurable Z-component of J is given by the following,

$$J_z = \hbar m_l \quad (3)$$

m_l is the magnetic quantum number which covers the interval from $-I, -I + 1, \dots, I$. Thus J_z has $2I + 1$ possible sub states. In the absence of an external field the quantum states corresponding to the $2I + 1$ values of m are degenerate and the spin angular momentum vector has no preferred orientation. For a nucleus with spin $I = \frac{1}{2}$ in presence of an external magnetic field B_0 , the energy level splits in to two sub states, a low energy level generally denoted as

α ($m_l = +\frac{1}{2}$), which is when the spins are aligned in the direction of magnetic field (z-direction) and β ($m_l = -\frac{1}{2}$) a high energy level, when the spins are opposite to the field. The difference in energy is given as $\Delta E = -\gamma\hbar B_0$. A transition between the states may occur if the energy absorbed or dissipated matches $\hbar\omega_0 = -\gamma\hbar B_0$, where ω_0 is the resonance frequency (Larmor frequency) and γ is the gyromagnetic ratio (a constant for a given type of nucleus). The classical interaction of a particle spin with magnetic field B_0 , attempts to align the magnetic moment in the direction of B_0 field but the angular momentum tends to cause a precessional motion of μ around the field axis. This magnetization precesses at a frequency known as the Larmor frequency $\omega_0 = \gamma B_0$.

The net magnetization arising from the vectorial sum of magnetic moments of all the nuclei in a sample with a nuclear spin I_i is denoted as the bulk magnetization \vec{M} , which is given as $\vec{M} = \Sigma \mu_i = \gamma J$ where $\mu_i = \gamma I_i$. The net polarization is therefore represented as a magnetization vector \vec{M} , pointing along the z-axis. A short radiofrequency pulse (RF) applied by a transmitter coil perpendicular to the B_0 , could perturb this magnetization from its equilibrium state and create a spin coherence by flipping on to the transverse xy-plane. This flip of the magnetization due to the on-resonance rf irradiation is characterized by the flip-angle $\phi_{rf} = \omega_{nut} t_p$, where t_p is the pulse duration and $\omega_{nut} = \gamma B_{rf}$. It is defined as the angle that B_{rf} makes with respect to x-axis and therefore depends on the strength of the B_{rf} field. Once the rf irradiation is switched off, the spin coherence evolves as a transverse magnetization which is time-dependent and precesses with Larmor frequency ω_0 , eventually returning to their equilibrium state. For the simplification of this time dependence and an easier illustration, one uses a framework called rotating frame, where the observer rotates with a frequency ω_{ref} , that is similar to ω_0 , and the magnetization appears static. Therefore, an offset frequency $\Omega_0 = \omega_0 - \omega_{ref}$ is used to describe the Larmor frequency of the system, where the signal offset decays exponentially.

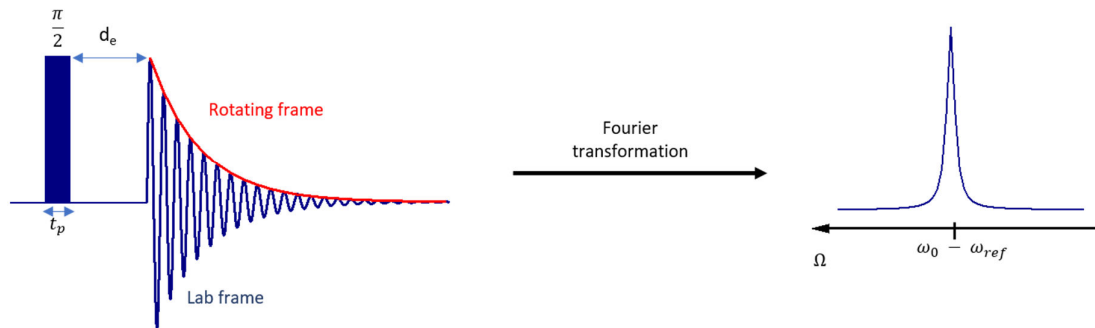


Figure 7: When a $(\pi/2)$ pulse is applied on an ensemble of spins for a duration of t_p , generates transverse magnetization that decays exponentially, where d_e is the dead time. The Fourier transformation of such an exponentially decaying function yields a Lorentzian peak, where the peak width at half height equal to $1/\pi T_2$ (Levitt 2015)

The precession induces a voltage in the same coil which was also used to apply the RF-pulse, lead to a detected signal known as Free Induction Decay (FID). The Fourier transform of the FID gives the individual frequencies resulting into an NMR spectrum as shown in Figure 7

The nuclear spin system can be influenced by factors either being external, like the externally applied static magnetic field B_0 and rf pulses, or internal, where the interactions originate from other nuclei and the surrounding electron. The nuclear spin Hamiltonian \mathcal{H} is thus expressed as follows,

$$\mathcal{H} = \mathcal{H}_{int} + \mathcal{H}_{ext} \quad (4)$$

where,

$$\mathcal{H}_{ext} = \mathcal{H}_0 + \mathcal{H}_1 \quad (5)$$

such that, $\mathcal{H}_0 = -\gamma_I I \cdot B_0$ and $\mathcal{H}_1 = -\gamma_I I \cdot B_1$. Here \mathcal{H}_0 is the nuclear Zeeman interactions, with the static external field B_0 and \mathcal{H}_1 is the interaction between spin and the RF field B_1 . Internal interaction on contrary originates from nucleus and its surrounding environment, either a neighboring spin (e.g., spins I and S) or the electron cloud. It is denoted as

$$\mathcal{H}_{int} = \mathcal{H}_{II} + \mathcal{H}_{SS} + \mathcal{H}_{IS} + \mathcal{H}_S + \mathcal{H}_Q + \mathcal{H}_R \quad (6)$$

Here, the first three terms constitute to dipole-dipole coupling \mathcal{H}_D , where \mathcal{H}_{II} and \mathcal{H}_{SS} are homonuclear and \mathcal{H}_{IS} is heteronuclear coupling as well as to the indirect coupling mediated by bonding electrons, i.e., scalar J coupling (\mathcal{H}_j). \mathcal{H}_S denote the shielding Hamiltonian, specifically chemical shift anisotropy. \mathcal{H}_Q indicates quadrupolar interactions, which arise when nuclei with $I > 1/2$ interacts with electric field gradient that is generated by the surrounding electron cloud. The interaction between rapid molecular rotation and nuclear spin is expressed as \mathcal{H}_R (Liang et al. 2022). Such interactions in general the anisotropic chemical shift, dipolar couplings and J-coupling, along with the relaxation processes play an important role in structural determination as well as elucidating the molecular motions in biological systems.

3.1.1 Internal interactions

1. Chemical shift anisotropy

The electron cloud surrounding the nucleus due to the motion induced by the external field B_0 , also gives rise to a secondary field, thereby the nucleus is shielded from the applied field. The magnetic field therefore experienced by the nucleus is a superposition of the static and the induced magnetic field. The frequency shift, this secondary field interaction causes in the NMR

spectrum is termed as chemical shift. This is therefore the difference in the experienced magnetic field B_0 , given as

$$\delta = \frac{\Omega_0}{\omega_{ref}} = \frac{\omega_0 - \omega_{ref}}{\omega_{ref}} \quad (7)$$

where δ , is the chemical shift which is quite small with values recorded in parts per million (ppm), with the apparent Larmor frequency of nuclei $\omega_0 = \gamma B_0$ and a reference frequency ω_{ref} . Most often, since the molecular environment is not uniform, the induced field can be described as being anisotropic, i.e., the chemical shifts are anisotropic and subsequently depends on the orientation of the molecule with respect to the static magnetic field. In case of liquids the fast-molecular motion averages out anisotropic effects and NMR spectra with a sharp peak is observed. Whereas for solid samples the molecules can adopt several orientations with respect to the magnetic field and one observes a powder pattern, which is a superposition of all individual peaks arising from this different orientation.

2. Dipole-Dipole interactions

The dipole-dipole coupling arises from the interaction of two nuclei in the system, where the magnetic field of one spin is influenced by the other spin and vice versa through space. This can be quantified by dipolar coupling constant D , which is given as

$$D = -\frac{\mu_0}{4\pi} \frac{\gamma_j \gamma_k \hbar}{r_{jk}^3} \quad (8)$$

where, μ_0 is the magnetic moment, γ is the gyromagnetic ratio of the spins j and k , while r_{jk} is the distance between the two spins. For high-field NMR under secular approximation, the Hamiltonian describing the homonuclear and heteronuclear dipolar interactions in the laboratory frame is given as,

$$\mathcal{H}_D^{I_1 I_2} = \frac{1}{2} D_{zz}^L (3I_{1z} I_{2z} - I_1 \cdot I_2) = \frac{1}{2} D_{zz}^L (2I_{1z} I_{2z} - I_{+1} \cdot I_{-2} - I_{-1} \cdot I_{+2})$$

$$\mathcal{H}_D^{IS} = D_{zz}^L I_z S_z \quad (9)$$

respectively, with $D_{zz}^L = -\frac{\mu_0 \hbar}{2\pi} \cdot \frac{\gamma_1 \gamma_2}{r_{12}^3} (3 \cos^2 \theta - 1) = -\frac{\mu_0 \hbar}{2\pi} \cdot \frac{\gamma_1 \gamma_2}{r_{12}^3} P_2(\cos \theta)$.

$$(10)$$

θ here is the angle between the static magnetic field and the vector connecting the two nuclear spins. In liquid sample the isotropic motion causes the reorientation of the molecule and therefore averages out dipolar couplings, although long-range intermolecular couplings remain, which are often small and mostly ignored. For solid samples since local spins are coupled to each other, both inter – and intramolecular dipole-dipole couplings are relevant. In Equation (9), $I_{+1} \cdot I_{-2}$, $I_{-1} \cdot I_{+2}$ are called the flip flop term, which is also responsible for spin diffusion.

3. *J-coupling*

The indirect interactions between spins that occur via the electron cloud of chemically bonded spins are termed as J-coupling. Therefore, these indirect couplings give information regarding the chemical connectivity between different sites. This J-coupling allows the investigation of the local environment in an isotropic liquid, where the dipole couplings are averaged to zero.

3.1.2 Relaxation

When the spins are perturbed from their equilibrium state due to an external force, they tend to return to their initial spin state by the process of relaxation. There are two main relaxation processes. Longitudinal relaxation (spin-lattice), denoted as T_1 , here the system tries to restore the normal Boltzmann distribution and total magnetization returns to z-axis by exchange of energy between the surrounding (lattice) and the spin system. Transverse T_2 relaxation (spin-spin), is related to the x, y-component of the magnetization \vec{M} , which is perpendicular to the B_0 . The energy transfer between the individual spins (that also drives T_1) or additional, possible fluctuating local fields arising from other interactions, lead to fanning out of \vec{M} on the x, y - plane. Transverse relaxation therefore involves gradual loss of coherence with increase in entropy of the spin ensemble. Additionally, the transverse magnetization can be locked at a specific direction in the rotating frame by applying a resonant RF field along this direction i.e. a spin-locking pulse. Such a spin-locked magnetization will decay to zero in the rotating frame, with a characteristic relaxation time $T_{1\rho}$, which is used to access the slow dynamic processes.

Relaxation in NMR occurs due to the fluctuations in the local field at the excited nucleus which is in turn caused by molecular motions. These fluctuations in the local magnetic fields can be characterized by a time correlation function, $G(t)$, that describes the correlation between the average local field at time t and at a time later $t + \tau$. Therefore, for the case of T_1 relaxation,

$$G(t) = \langle B_{x,y}(t) B_{x,y}(t + \tau) \rangle \quad (11)$$

The value of correlation function is large over short time and often decays exponentially with a time constant τ_c , which is the correlation time, so

$$G(t) \propto e^{-t/\tau_c} \quad (12)$$

The proportionality constant here depends on the magnitude of the local field, which has been omitted for simplicity. This indicates that rapid fluctuations lead to fast decay of the autocorrelation function and have small values for τ_c and vice versa. The Fourier transform of the correlation function gives the spectral density $J(\omega)$, which plays a key role in the theory of relaxation and is obtained as,

$$J(\omega) \propto \int_{-\infty}^{\infty} G(t) e^{-i\omega t} dt \quad (13)$$

which can be combined with Equation (12) to obtain,

$$J(\omega) = \frac{2\tau_c}{1 + \omega^2\tau_c^2} \quad (14)$$

This indicates that slow fluctuations correspond to long correlation times and in turn a narrow spectral density.

For protons, different physical interactions give rise to fluctuating local magnetic fields that can lead to spin relaxation, for instance intramolecular magnetic dipolar, anisotropic chemical shift, quadrupolar and scalar coupling interactions. In general, for a biological macromolecule having a spin 1/2 nucleus, magnetic dipolar and anisotropic chemical shift are the primary relaxation sources. In case of proton relaxation for proteins, homo-nuclear dipolar couplings are dominant when compared to hetero-nuclear couplings and although CSA contributes to the relaxation, its effect is usually negligible in comparison to dipole-dipole coupling. The relaxation rate or relaxation time can be expressed as,

$$R_1 = T_1^{-1} = \frac{2}{3} \cdot D (J(\omega_0) + 4J(2\omega_0)) \quad (15)$$

$$R_2 = T_2^{-1} = \frac{1}{3} \cdot D (3J(0) + 5J(\omega_0) + 2J(2\omega_0)) \quad (16)$$

$$R_{1\rho} = T_{1\rho}^{-1} = \frac{1}{3} \cdot D (3J(2\omega_1) + 5J(\omega_0) + 2J(2\omega_0)) \quad (17)$$

Here, D is the effective spin-spin-coupling strength. A larger dipolar coupling constant results in a faster decay of coherences. This is also relevant in the static limit, where the dephasing of the signal occurs due to the dipolar couplings, generally termed as dipolar dephasing. In solids the relaxation decay is a superposition of frequencies that originate from the different orientations of the spins and is represented by a Pake pattern (see Figure 8). The corresponding time domain signal is characterized by a characteristic decay function that is Gaussian initially. This decay is defined by the time constant T_2 spin-spin relaxation time. The short T_2 in this rigid limit is not correctly captured by the BPP theory (Equations (15)(16)(17)) which is generally used to characterize the motions where the relaxation time is longer than the motional correlation time. In the rigid as well as fast-motion pre-averaged limits, the Anderson and Weiss model (Anderson and Weiss 1953) can be used to describe the time signal. The difference between the transverse relaxation times for rigid and mobile regions can be easily distinguished and the fractions can be quantified using the amplitude of relaxation. The relaxation rate constant for nuclei in a protein therefore are characterized by several factors, including overall rotational correlation times, internal motions and strength of the relevant coupling interactions (Cavanagh 2010).

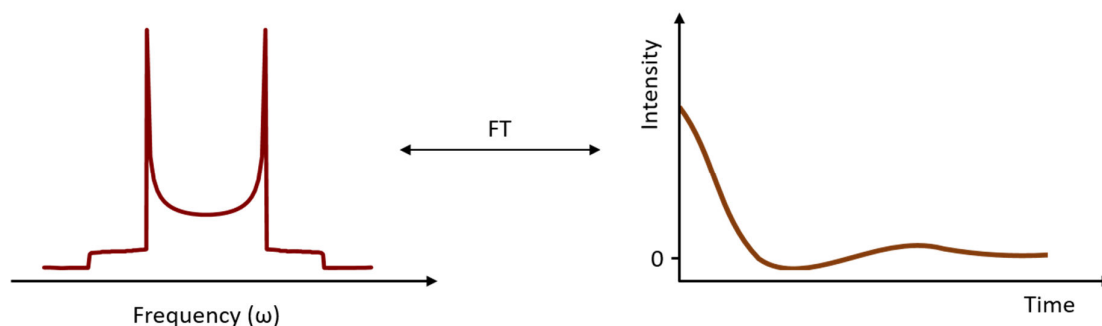


Figure 8: Pake pattern obtained under static rigid limit and the time domain signal obtained after Fourier transformation.

3.1.3 NMR relaxation studies for protein solutions

For a protein the NMR relaxation times depend both on the Brownian tumbling motion as a whole and on the internal conformational mobility. Therefore, in order to precisely determine the internal mobility, one must take into the effects of protein Brownian tumbling. The correlation function of a protein in solution therefore is made up of a product of correlation functions of overall rotation $C_R(t)$ and local motion $C_{int}(t)$ given as,

$$C_0(t) = C_R(t) \cdot C_{int}(t) \quad (18)$$

Consequently, the non-selective proton relaxation data analyzed in this work would depend on the joint action of correlation functions of all protons in the protein. Our aim was to characterize the aggregation kinetics of proteins by probing the proton NMR relaxation at low resonance frequencies. Although at such low resonance frequencies poor spectral resolution is acquired, it is suitable to study the protein tumbling motion as a whole, as the magnetic relaxation is at such frequencies are dominated by overall Brownian rotation (Krushelnitsky 2006). Owing to the low spectral resolution, the integral protein proton signal is evaluated. Protons at different sites in the protein experience different dipolar coupling and hence contribute to different internal dynamics and eventually leads to a spread of relaxation times. The integral protein proton relaxation curve is therefore intrinsically non-exponential, i.e., either Gaussian in the rigid limit, or also multi-exponential where motions are relevant. The transverse relaxation decay curves obtained in this study consisted of two components: a fast component corresponding to protein and a slow one that results from the residual water protons. A pure protein relaxation curve can then be obtained by subtracting the water component. The water component is always single exponential, due to the fast exchange between hydrated and bulk water molecules. As is elaborated in the supporting information of the reference (Krushelnitsky et al. 2014), the mean arithmetic average of the protein relaxation rates equals the initial slope of the relaxation decay. This idea will be elaborated in detail in the results section.

The following section will deal with brief description of the spin relaxation measurements, with particular focus on its technical aspects.

3.1.4 Measuring transverse relaxation

T_2^* and T_2 are time constants that describes the magnetization decay in the xy -plane, that is caused by loss of spin coherence due to a RF-pulse, leading to a simple FID. This transverse relaxation emanates from two prominent sources, i. due to the inhomogeneity of the outer magnetic field B_0 and ii. due to the spin-spin interactions. T_2^* and T_2 are differentiated based on the fact that the latter describes the intrinsic relaxation emerging only from the spin-spin interactions minus the effects of field inhomogeneity. This can be circumvented by the use of a π -pulse (Hahn-Echo) or a train of π -pulses (Carr-Purcell-Meiboom-Gill) applied to the transverse magnetization in the middle of the evolution period τ . For a protein the intrinsic relaxation occurs on a time scale much faster than that of the solvent molecules (water). In order to cover this wide time-scale range and also to precisely obtain the initial slope of the protein relaxation decay a combination of different experiments were used, an FID that characterizes the beginning of T_2 decay and remains unaffected by field inhomogeneities, and the Carr-Purcell-Meiboom-Gill (CPMG) pulse sequence at two delay times, in order to effectively measure both the protein and water components. In contrast to Hahn echo which starts with a two-pulse sequence ($\pi/2 - \tau_1 - \pi - \tau_1$) that gives an echo signal centred at time τ_1 followed by the π -pulse, CPMG consists of the same initial sequence except that it is followed by a train of π -pulses creating a series of echoes, which are then detected. Here, short detection of the integral signal intensity in between pulses makes it possible to detect many points within a single CPMG experiment. The Hahn echo experiment however only provides

information on a single data point, but it can access time scales shorter than CPMG by varying τ_1 before and after the π -pulse. A combination of these experiments gives the complete relaxation decay for a protein solution and after subtracting the water signal, the intrinsically multi-exponential protein relaxation decay can be acquired. In certain cases, if the local environment of the spin changes due to the internal dynamics of the protein or when it interacts with another molecule, a change in chemical shifts is observed which is classified as chemical exchange. Such effects of chemical exchange can be compensated by employing shorter inter-pulse delay between the π -pulses than the characteristic time scale of this effect. Otherwise, the re-focusing by the π -pulses remain incomplete, leading to shortening of the T_2 decay, which may not be related to the Brownian dynamics of the protein.

3.1.5 Magic-Angle Spinning solid state NMR

Unlike for solutions where the molecules tumble randomly and rapidly resulting into their molecular orientation being averaged to an isotropic value, the solid state samples the molecular tumbling might be very slow or even absent in case of rigid solids. In such cases the molecules will be oriented in all possible directions with respect to B_0 , and this random distribution of orientation results in to spectrum that is a sum of several sharp lines superimposed to form a static powder pattern. Such samples can be investigated by employing the concept of Magic Angle Spinning. This involves the complete sample being mechanically rotated at the magic angle $\theta = \arctan\sqrt{2} = 54.74^\circ$. Here the $P_2(\cos\theta) \approx 0$, such that the broadening effects of anisotropic interactions are averaged. Additionally, the presence of a homogeneous (^1H - ^1H dipolar coupling) or inhomogeneous (^{13}C CSA) interaction can have different effect on the averaging due to MAS. One such consequence is the appearance of spinning side bands, that is observed at integral multiple of spinning frequency. For spectra that involves broadening due to inhomogeneous interactions, spin rates greater than the linewidth is required to eliminate the spinning sidebands.

3.1.6 Cross polarization

NMR can be used to obtain structural information via chemical shifts. Although protons are the most abundant atoms in a biomolecule, at moderate spinning speeds the detection of high gyromagnetic ratio (γ) nuclei like protons in solids is not favoured since the homonuclear dipolar interactions may not be accurately averaged out and broaden the NMR lines. A better molecular resolution can be obtained with nuclei having a low γ , but they have very low signal-to-noise ratio, long T_1 relaxation due to absence of homonuclear decoupling and requires high decoupling power during detection. In order to overcome this, and gain information of the spins that are close in space cross polarization can be used. In this technique the dilute spin, in this case ^{15}N derives its magnetization from the neighboring abundant spin like ^1H , which usually has a fast T_1 relaxation. For such a polarization transfer, dipolar coupling between the dilute and abundant spin is necessary. The maximum signal to noise amplification is given as γ_I/γ_S , where γ_I and γ_S are the gyromagnetic ratios of high and low sensitive nuclei respectively, and the maximum enhancement for ^1H to ^{15}N polarization transfer is ~ 10 .

The polarization transfer occurs only if the ^1H and ^{15}N nuclei are coupled and they fulfil the Hartmann-Hahn condition, which is:

$$\omega_1(^{15}\text{N}) = \gamma_{^{15}\text{N}} \cdot B_1(^{15}\text{N}) = \gamma_{^1\text{H}} \cdot B_1(^1\text{H}) = \omega_1(^1\text{H}) \quad (19)$$

Equation (19) is valid for a static sample. The protons are firstly excited with a 90° pulse, creating transverse magnetization, thereafter a spin-lock pulse is applied to both the ^1H and ^{15}N channels, which reintroduces the flip-flop terms in the effective interaction Hamiltonian (see Equation 9). The magnetization is then transferred, when the energy differences caused by the spin-lock match each other, with conservation of energy from the high γ nuclei to the low γ nuclei. The polarization transfer depends on several factors. If the contact time is short, only the closest proton can transfer the magnetization, also the rate of transfer increases when there is strong dipolar coupling. The efficiency of CP can be reduced in case of fast molecular motions. The Hartmann-Hahn match depends strongly on the MAS spinning frequency ω_R , therefore if the spinning rates are on the order of the dipolar coupling dipolar coupling gets averaged out, causing additional reduction of CP efficiency. Under MAS, the matching conditions are given by $\omega_1(^{15}\text{N}) - \omega_1(^1\text{H}) = \pm \omega_R$. To ensure proper matching, usually a ramped amplitude CP is applied on one of the spin-lock pulses (Metz et al. 1994; Duer 2001). A standard pulse program is shown below:

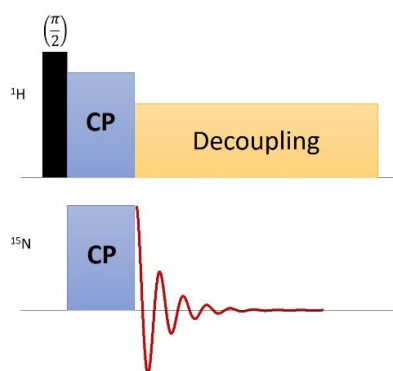


Figure 9: Schematic representation of cross polarization (CP) pulse sequence for a polarization transfer from ^1H to ^{15}N .

3.1.7 Insensitive nuclei enhanced by polarization transfer (INEPT)

In contrast to CP, INEPT exploits the magnetization transfer between spins via the heteronuclear J -couplings, to enhance the intensity of dilute nuclei (S). Here the 90° pulse on the proton (I), leads to the evolution of transverse magnetization, while the 180° on proton refocuses the chemical shift, J_{IS} coupling evolves due to the 180° on S. The transverse magnetization refocused by spin echo, transfers this refocused magnetization on to ^{15}N nuclei. (Roberts 2013)

3.1.8 Measuring relaxation in rotating frame

$T_{1\rho}$ is time constant that characterizes spin-lattice relaxation in the rotating frame in presence of a spin-lock pulse of strength B_1 , with $B_1 \ll B_0$. The RF field is irradiated with the same phase as the spin coherence, such that the spins will be constantly refocused and is held along the axis of the RF pulse. The spin locked magnetization now decays with the characteristic $T_{1\rho}$ relaxation time along B_1 . This allows for the investigation of slow molecular dynamics on the time scale of $1/\omega_0 = 1/\gamma B_1$. Using $T_{1\rho}$ relaxation in terms of obtaining quantitative information on molecular dynamics will be further elaborated in the results section.

3.2 Small-angle X-ray scattering (SAXS)

SAXS is a powerful analytical tool that can be used to deduce structural information from both biological and non- biological samples in the range of 1 to 100 nm. In a typical SAXS experiment the X-ray radiation is elastically scattered by the sample and the scattering intensity curve is the Fourier transform of the autocorrelated electron density contrast associated with the macromolecule (Tardieu et al. 1999). This scattering pattern can be further analyzed to obtain information regarding the particle's size, shape, polydispersity and can be used to reveal the interactions of particles.

The samples are usually investigated in transmission (see. Figure 10). As the monochromatic electromagnetic waves of the X-ray beam are directed into the sample, a small percentage of the X-rays are scattered at the electrons of the atoms. The resulting oscillations lead to local emissions of spherical waves that interfere with each other, resulting into a scattered wave, which is quantified by the q vector $\vec{q} = \vec{k}' - \vec{k}$. The q vector describes the momentum transfer between the incident wavevector, k , and scattered wavevector, k' (see. Figure 10). The absolute value $|\vec{q}|$ is dependent on the scattering angle, 2θ , the refractive index, n , and the wavelength of the incident wave, λ , and is given by:

$$|\vec{q}| = \left(\frac{4\pi n}{\lambda} \right) \sin \frac{\theta}{2} \quad (20)$$

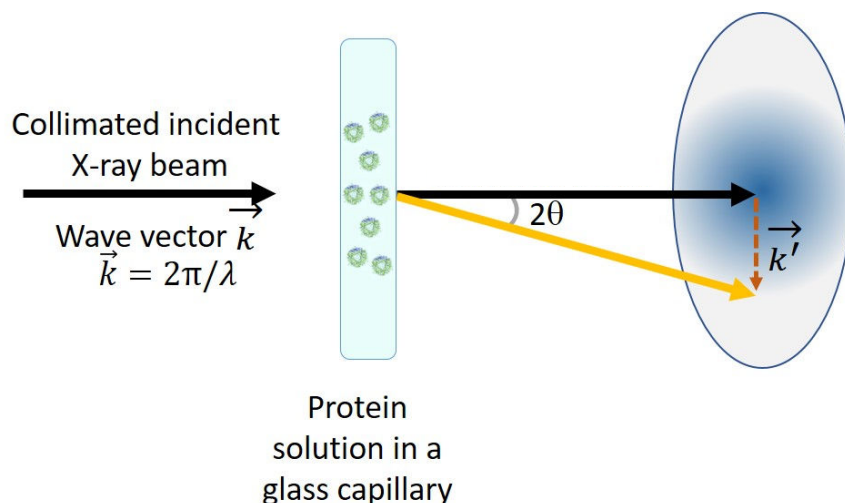


Figure 10: Schematic representation of small angle X-ray scattering experiment.

Further details about the SAXS experiments and data analysis are found in the Material and Methods section.

3.3 Dynamic light scattering (DLS)

Dynamic light scattering is a technique generally used to determine the particle size. Here a monochromatic beam of light directed on to a macromolecular solution would scatter the incoming light depending its size and shape. The molecules undergo always undergo a Brownian motion in a suspension and the intensity of fluctuations of scattered light due to this motion is analyzed. This gives information regarding the diffusion coefficient D that is related to hydrodynamic radius of the molecule. Such motion generally depends on the particle size, temperature and solvent viscosity. The scattered light is then recorded by the detector. In a typical DLS experiment, a normalized intensity correlation function $g_2(t)$ that describes the motion of the molecule and $g_1(t)$ a normalized electric field correlation function, that correlates the motion of particle relative to each other is measured. $g_1(t)$ is expressed as $g_1(t) = \exp(-q^2Dt)$, where q is the scattering vector, D is the diffusion coefficient and t is the time, specifically the time difference resulting from an intensity autocorrelation procedure. The size of the particle can then be determined using the Stokes-Einstein equation.

$$D = \frac{kT}{6\pi n R_h} \quad (21)$$

with D being the diffusion coefficient, k - Boltzmann's constant, T - temperature, n - solvent viscosity and R_h is the hydrodynamic radius of the particle (Stetefeld et al. 2016; Hoo et al. 2008)

3.4 Attenuated total reflectance FTIR (ATR-FTIR)

Fourier Transform infrared spectroscopy (FTIR) has been one of the most popular techniques used for the structural characterization of proteins and peptides. In this technique the incident infrared radiation is absorbed by the molecules when the frequencies of the light and vibrations are equal. The strength of the vibrating bonds determine the absorption and the vibrational frequency and are influenced by the intra- and inter-molecular effects (Barth 2007). In attenuated total reflectance FTIR the sample is placed on an ATR crystal. The incident infrared beam is totally internally reflected and creates an evanescent wave that penetrates the sample. These waves can be absorbed by the sample and the attenuated or residual energy is transferred back to the detector. An infrared spectrum is then generated by the system.

The changes in the secondary structure and its content can be determined using this vibrational spectroscopy technique. The characteristic protein IR bands are amide I ($\sim 1700 - 1600\text{cm}^{-1}$) due to the stretching vibration of C=O and amide II ($\sim 1600 - 1500\text{ cm}^{-1}$) which is the bending vibrations of N-H. These bands are sensitive to changes associated with the secondary structure. This method therefore can be conveniently used to track the changes in the structure over a long period of time.

3.5 Electron Microscopy

Electron Microscopy has been conventionally used to obtain high-resolution images of a specimen both biological and non-biological. In combination with other accessory techniques like thin sectioning, immuno-labeling, negative staining and resin embedding certain specific questions can be clarified. There are two main types of electron microscopy techniques, transmission EM (TEM) and scanning EM (SEM). TEM is used generally used to get information on the structural integrity of the specimen, which was used in this study. SEM on contrary is used to obtain surface information. Here, a beam of electrons having a very short wavelength that acts a source of scattered e^- that are detected. In TEM, the electrons are directed on to a thin specimen. The unscattered electron beam passing through the specimen on to the detector gives rise to a shadow image of the specimen. These are then imaged by appropriate lenses to obtain structural information of the specimen (Goodhew 2011).

4 Material and Methods

4.1 Lens material and recombinantly synthesized protein

For this work eye lens crystallin proteins were procured either by recombinant methods or by purification from the eye lens. Bovine eye lenses used for purification of α -crystallin were obtained from an organic farm Biohof-Barthel in Greudnitz, Germany. b γ B and h α B crystallins were recombinantly synthesized using the below-mentioned bacterial strands and plasmids.

Table 1: Bacterial strand and plasmids used.

Bacterial strand	Plasmid
<i>E. coli</i> TOP 10	Invitrogen (Karlsruhe)
<i>E. coli</i> BL21(DE3)	Novagen (Darmstadt)
pET16b	Innoprofile-NWG
pET23d	Innoprofile-NWG

4.1.1 Culture media

All culture media were sterilized at 1 bar pressure and 121 °C for 20 min and then stored at 4 °C. The respective antibiotics were added with a final concentration of 300 μ g/mL (ampicillin) or 30 μ g/mL (kanamycin) directly before use. Heat-unstable components of the media were sterile-filtered using a membrane filter (pore size - 0.22 μ m). The compositions of the media are given in Table 2.

Table 2: The composition of media used

Solution	Composition
Glycerin stock solution	700 ml Glycerol (87 %) autoclaved and 300 ml cell suspension from the over day culture
dYT -media	For 1 L 16 g peptone 10 g yeast extract 5 g NaCl
MSMCHP2 – Mineral salt solution	875 mL dd H ₂ O 100 mL 10x MSMCHP2 5 mL 1M MgSO ₄ 20 mL 40 % (m/V) glucose 500 μ L 200 mg/mL thiamine
10x MSMCHP2	840 mM K ₂ HPO ₄ 261 mM NaH ₂ PO ₄ x H ₂ O* 141 mM Na ₂ SO ₄ 550 mM NH ₄ Cl 20 mL of 1 L trace elements solution

Solution	Composition
Trace elements solution (1 L)	60 mM Na ₂ -EDTA 62 mM FeCl ₃ x H ₂ O* 5 mM CaCl ₂ x H ₂ O* 883 μM CoSO ₂ x H ₂ O* 626 μM ZnCl ₂ x H ₂ O* 400 μM CuCl ₂ x H ₂ O* 722 μM MnCl ₂ x H ₂ O*

For expression of labelled protein distilled H₂O was replaced with D₂O (>99.8%) and additionally ¹⁵NH₄Cl and D-Glucose (d₇) were used so as to be able to measure using solid state NMR measurement.

4.2 Molecular biology - cell transformation

The DNA of h αB (wild-type) crystallin was provided by Dr. Qi Zhang in the pET16b vector. For the transformation of plasmids into competent cells an aliquot of 150 μl CaCl₂-competent cells 1. BL21(DE3) and 2. TOP10 was thawed on ice and 50-100 ng 3 μl and 1.5 μl of plasmid was added respectively. After an incubation of 30 min at 4 °C, the samples were heated at 42 °C for 42 s and then stored on ice. To each of the cell suspensions 600 μl of dYT media were added and incubated at 37 °C for 30 - 60 min in a shaker and then pelleted at 4500 x g for 1 min. The pellet was resuspended in 200 μL medium and plated onto agar plates containing the antibiotic Ampicillin. Colony growth took place overnight at 37 °C in an incubator. All steps were executed under sterile conditions.

Competent cells with the appropriate plasmid were grown in 5 ml dYT with antibiotic overnight. 300 μl of the cell suspension was resuspended in the sterile hood with previously autoclaved 700 μl of glycerol (87 %) and stored at -80 °C. Replication of plasmids Top 10 cells with the appropriate plasmid were grown in 5 ml dYT with antibiotic overnight and pelleted at 6800 x g for 3 min. The DNA was obtained according to the QIAGEN protocol and the QIA prep Spin Miniprep Kit.

4.3 Protein expression and purification

4.3.1 H αB-crystallin

The h αB cDNA was provided by Prof. Wilbert Boelens (Nijmegen Center for Molecular Life Science; Gelderland, Netherlands) and reviewed by Dr. Qi Zhang cloned into a modified His-tag free pET16b vector and transformed into BL21(DE3) cells. This construct could be expressed in the dYT media or isotopically enriched mineral salt solution MSMCHP2 (Zhang 2013) depending on the purpose. Therefore, for unlabeled hαB, the cells were expressed fully in dYT media. For labelled h αB the constructs were first grown in dYT media and the transferred to deuterated MSMCHP2 media with a stepwise increase in the amount of deuterated H₂O. In this case ¹⁵NH₄Cl was used as the sole nitrogen source. In both the cases

cells were overexpressed with antibiotic Ampicillin by incubating at 37°C for four hours or at 20 - 25°C overnight. The cells were induced in dYT and MSMCHP2 medium at an optical density between 0.7 and 1.0 at 600nm wavelength with a final concentration of 1 mM IPTG. The medium containing the cells was centrifuged at 8280 g for 10 min at 4 °C (rotor SLA-3000) and the pellet was stored at -80 °C.

For purification, the cells were resuspended in buffer A with 2 mg lysozyme per 1 g cells, a 1:50 dilution of 1 M MgCl₂, a 1:20000 dilution of DNaseI and 500 µl protease inhibitor cocktail and left stirring at 4 °C for 15 - 30 mins until the cells were completely dissolved. The cells were then disrupted three times at 4°C with a microfluidizer at a pressure of 500 to 1000 bar. After the first centrifugation step at 47810 g for 30 min x 2 times and 4 °C (SS34 rotor), 2 mg protamine sulfate per 2 ml cell lysate was added and incubated with stirring for several hours at room temperature until a homogeneous suspension had formed. The second centrifugation step then took place under identical conditions. To the supernatant obtained, a calculated amount of 4 M (NH₄)₂SO₄ (pH 8.5) was added so as to achieve a final concentration of 1.4 M (NH₄)₂SO₄. In order to prevent the contamination by DNA the supernatant obtained was applied initially to a HIC column previously equilibrated with buffer B and h αB was eluted at a gradient of 100% Buffer A. The target protein fraction was eluted, which was then dialyzed 3 times against 5 L 20 mM TRIS, 1 mM EDTA pH 8.5 at RT for at least 90 mins. This dialyzed fraction was loaded onto QHP Anion exchange column equilibrated with buffer A and using a gradient of 0 – 100% Buffer C protein was eluted. Pure h αB was obtained with a gradient of 75 % Buffer C.

Table 3: List of buffers used for the purification of h αB-crystallin

Buffer	Composition	pH
Buffer A Lysis Elution HIC Binding IEX	20 mM Tris 1 mM EDTA	8.5
Buffer B Binding HIC	20 mM Tris 1 mM EDTA 1.4M (NH ₄) ₂ SO ₄	8.5
Buffer C IEX elution	20 mM Tris 1 mM EDTA 1 M NaCl	8.5
SEC buffer	50 mM sodium phosphate 50 mM NaCl 1 mM EDTA	7.5
Dialysis buffer	50 mM ammonium hydrogen carbonate	7.0

The pre-cleaned h αB was then applied to a gel filtration column equilibrated with SEC buffer (Hi Load Superdex 200 prep grade) and the degree of purity of the protein obtained was checked using an SDS gel (Schägger and Jagow 1987). For storage purposes, the h αB

previously concentrated (with addition of 0.02% NaN₃ to the buffer) with centrifuge filter units was repeatedly dialyzed against dialysis buffer, freeze-dried and the lyophilized protein was stored at 4 °C. The buffers used can be found in Table 3.

4.3.2 Bovine γ B crystallin

Recombinant bovine γ B-crystallin was expressed from a pET23d plasmid in *Escherichia coli* BL21(DE3). The cells were grown in DYT media. The growth of cells was monitored by optical density at a wavelength of 600 nm and after the cell density reached an O.D of 0.7 - 1.0, IPTG (0.1% v/v 1M) was added to induce protein expression. The temperature was reduced to 22 °C and cells were left overnight (12 - 16 h) for expression. The cells were then harvested at 8280 g for 10 min in SLA-3000 rotor at 4 °C. The pellets formed were stored at -80 °C.

The pellets were resuspended in NPI₂₀ buffer, subsequently 2mg lysozyme per 1 g cells, a 1: 100 dilution of 0.5 mM MgCl₂, a 1: 20000 dilutions of DNaseI and 500 μ l protease inhibitor per 3 L cell culture was added. The cell solution was first homogenized using Ultra Turrax and then digested three times at 4 °C with a microfluidizer at pressure from 500 to 1000 bar. After centrifuging twice at 20000 rpm (47810 g) for 30 min and 4 °C (SS34 rotor), the supernatant was purified by metal ion affinity chromatography (Ni Sepharose High performance). The suspension was transferred on to the nickel metal ion affinity column previously equilibrated with NPI₂₀ buffer and eluted at a gradient of 30 % - 100 % NPI₅₀₀ buffer. The eluate obtained at 30 % gradient corresponded to the γ B-crystallin protein, confirmed by SDS-page. It was then further purified by loading on to a gel filtration column (GELFI) Hi Load Superdex 75 prep grade initially equilibrated with GELFI buffer. The eluate was pooled and concentrated with Amicon and stored at 4 °C after addition of 0.02 % NaN₃ to the buffer. The concentrated protein was dialyzed against the dialysis buffer (Table 3), which was then lyophilized and the protein obtained was stored at 4 °C. The list of buffers used are given in Table 4.

Table 4: List of buffers used for the purification of bovine γ B-crystallin

Buffer	Composition	pH
NPI ₂₀ buffer	50 mM sodium phosphate 150 mM NaCl 20 mM imidazole	7.5
NPI ₅₀₀ buffer	50 mM sodium phosphate 150 mM NaCl 500 mM imidazole	7.5
GELFI buffer	50 mM sodium phosphate 50 mM NaCl	7.5

4.4 α -crystallin from bovine lens

The bovine eyes obtained from cattle less than 6 months old, were stored at -20 °C and partially thawed to obtain the lens. By making a long incision above the lens, this could be detached from the eye by applying pressure to the cornea. The lens was briefly swung several times in

GELFI buffer (Table 4) and stored at $-80\text{ }^{\circ}\text{C}$. The lens preparation was already performed and the lenses stored at $-80\text{ }^{\circ}\text{C}$ was directly used for this work.

The bovine lens homogenate or bovine α -crystallin was obtained by dissolving the individual lenses in GELFI Buffer with addition of NaN_3 . For this purpose, the lens buffer mixture was stored at $4\text{ }^{\circ}\text{C}$ with stirring for several hours until the lenses dissolved. Depending on the desired final concentration of the lens homogenate, the initial volume of the buffer added was approximately adjusted i.e., for a final concentration of approximately 120 mg/ml , 1 g lens in 1.85 ml buffer is required. The insoluble lens components were separated, by centrifuging the mixture several times at $14,000\text{ g}$ for $30 - 60\text{ min}$ and after complete dissolution of the lens and the pellet was discarded. To obtain pure bovine α -crystallin, the soluble lens homogenate was loaded onto a size exclusion chromatography column (Superdex 200 HiLoad 16/600), the collected α -crystallin fractions were combined and concentrated using centrifuge filter units. For storage purposes, the α -crystallin was dialyzed against the dialysis buffer (Table 3), lyophilized and stored at 4°C .

4.5 Sample preparation

In general, for all the experiments the sample preparation involved the dissolution of weighed lyophilized protein in 50 mM Na-phosphate buffer and 50 mM NaCl at pH 7.5. For highly concentrated crystallin samples the powdered protein was dissolved at 20 mg/ml concentration and concentrated down to the required final 200 mg/ml using a Millipore ultracentrifuge falcon tube of 10 kDa molecular weight cutoff. The samples prepared were stored at 4°C . For the studies using low concentration, the 20 mg/ml sample was used as is.

4.5.1 Solution state NMR

4.5.1.1 Relaxation experiments

The crystallin powder was initially dissolved in 50 mM Na-phosphate buffer, 50 mM NaCl and 0.002% NaN_3 which was then lyophilized and subsequently dissolved in D_2O at pD 7.6. The lyophilization cycle with D_2O was repeated thrice to ensure maximum exchange so as to minimize water proton signal. The final protein concentration as determined by absorption at 280 nm was $\gamma\text{B-crystallin}$: 60 mg/mL and 135 mg/mL ; α -crystallin: 60 mg/mL and 200 mg/mL . The use of 5 mm NMR tubes, at high temperatures lead to the solvent evaporation and condensed on the inner walls of the tube. This significantly altered the protein concentration. To overcome this, inserts for 4 mm magic angle spinning (MAS) rotors were used (Bruker, catalogue number: B4493). This ensured tight sealing of the sample and only required $\sim 26\text{ }\mu\text{L}$ of the protein solution.

4.5.1.2 ^1H - ^{15}N HSQC

For solution state ^1H - ^{15}N HSQC the lyophilized labeled αB crystallin was dissolved in 50 mM Na-phosphate buffer, 100 mM NaCl at pH 7.5 containing 10% D_2O . A concentration of

20 mg/ml was used. The concentration of the solution was determined using the intrinsic absorption at 280 nm.

4.5.1.3 *Solid-state NMR – Rotor packing*

The purified ^2H , ^{15}N labeled αB crystallin was subjected to three lyophilization cycles by initially dissolving it in 50 mM Na-phosphate buffer, 100 mM NaCl at pH 7.5 with 15% H_2O and 85% D_2O , to ensure homogeneous degree of protonation of exchangeable sites. After determining the concentration of the diluted solution with the intrinsic absorption at 280 nm, it was passed through a filter of 22 μM to get rid of any unwanted particles. The solution was concentrated down to $\sim 600 \mu\text{L}$ using Millipore ultracentrifugation falcon having a molecular weight cut-off of 100 kDa, this ensured homogenous particle size. The samples were packed into a 1.3 mm thin wall ZrO_2 rotor, using a SpiNpack ultracentrifugal device kit from Giotto Biotech, an Optimal-100 XP ultracentrifuge and a SW32 Ti swinging rotor (Beckman Coulter GmbH). The protein was sedimented into the NMR rotor over 20 h at 4°C at a rotation frequency of the 28000 rpm and the supernatant was removed afterwards. The samples were stored at 4°C until it was used (Mainz et al. 2015).

5 Characterization techniques

5.1 NMR relaxation

Transverse proton relaxation experiments were performed on a 200 MHz Bruker Avance III spectrometer with a static 5mm Bruker probe. These relaxation measurements were conducted at two different temperatures, 30 °C and 60 °C, with an accuracy of about ± 1 with a gradient of approximately 0.5 K. In order to cover a wide range of transverse relaxation time to include solid-like protein aggregates, soluble proteins and residual water, a combination of three experiments were employed: free induction decay (FID) 10 μ s to 0.2 ms and two Carr-Purcell-Meiboom-Gill (CPMG) with different time delays between the π -pulses: 30 μ s (covering 60 μ s to \sim 60 ms) and 0.5 ms (1 to 600 ms). In all the above cases a 90° excitation pulse of 2 μ s and a recycle delay of 3 - 4 s was applied, acquiring 8 scans.

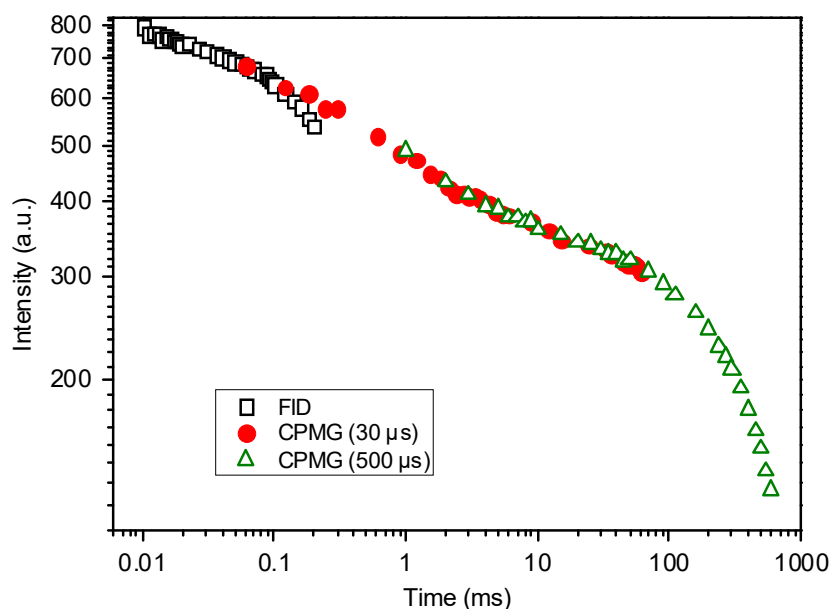


Figure 11: Combining FID and CPMG-based relaxometry curves of bovine α -crystallin, 60 mg/mL (Camilles et al. 2018), reused according to CCC RightsLink agreement.

Figure 11 shows a T_2 -decay curve obtained by combining the three different experiments FID and CPMG at two inter-pulse delays. To obtain a perfect overlap of the three decays, in some cases a multiplication factor in the range of 1.00 -1.02 was used for adjusting the amplitudes of the decay. The FID and CPMG decays could be well overlapped at time delays shorter than 0.1 ms. The FID points after 0.1 ms were not used for plotting the overall T_2 -decay as it is affected by the B_0 field inhomogeneity. It should be noted that the CPMG decays at two different inter pulse delay overlaps perfectly, indicating that the shortening of T_2 curve due to the chemical exchange is negligible at inter-pulse delays and proton resonance frequency (Luz and Meiboom 1963). Therefore, for all the cases, the total integral proton signal was detected without any spectroscopic separation (Camilles et al. 2018).

5.2 Easy NMR relaxation method

Elimination of Artifacts in NMR Spectroscopy (EASY), is a simple NMR FID experiment that cancels out artefacts or background signals (Jaeger and Hemmann 2014). This consists of acquiring two FIDs sequentially with a 90° pulse, here $2 \mu\text{s}$ after the normal waiting time $\sim 3 \text{ s}$ (T_1 delay). The first FID therefore would consist of both the real NMR signal from the protein solution as well as the artefact. The following FID with the second pulse immediately after, with the exact same rf pulse phase and length now contains only the artefact signal. The concept here is that, the first 90° pulse would cause the background protons to experience a very small flip angle, while it primarily acts on the protein sample. Since the background experiences only a small flip the second pulse leads to an identical background signal. Thus, the artefact free-NMR is obtained as a difference of these two FIDs.

5.3 Heteronuclear Single Quantum Coherence (HSQC)

HSQC experiments are generally used to analyze complex protein structure. It is a 2D experiment where the chemical shift of a ^{15}N or ^{13}C is correlated to an attached ^1H and such that each residue of the protein is indicated as a peak in the NMR spectra. Solution state NMR spectroscopy measurements were carried out on a Bruker Avance II 800 with a cryogenically cooled probehead and a magnetic field strength of 18.8 T. Shimming was performed automatically before every measurement. Using a watergate sequence the water signal was efficiently suppressed. For the measurements the temperature was set to 295.15 K. A recycle delay of 1.0 s was used. To obtain a good signal to noise ratio the offset and pulses were optimized. The 90° pulse length of ^1H was $11.5 \mu\text{s}$ at a power level of 9.3W and for ^{15}N $38.0 \mu\text{s}$ at a power level of 132 W. The number of scans taken for this measurement was 16 and a relatively well resolved spectra was obtained. The multi-dimensional spectrum was processed with a line broadening (LB) value 0.3 with a square sine-bell apodization function having a sine bell shift (SSB) value of 2 to 3. The spectrum was processed using TopSpin and the data was analyzed using Sparky NMR.

5.4 Solid-state NMR

The initial solid-state NMR experiments were performed at the Technical University Munich (TUM), in the group of Prof. Bernd Reif where they had already successfully acquired solid-state NMR spectra of αB crystallin (Mainz et al. 2015). Here, I was also trained in the sample preparation for solid-state NMR. The goal was to reproduce the same at Martin Luther University, Halle-Wittenberg (MLU), which was rather unsuccessfully. The experimental details will be discussed in the following sections.

5.4.1 TUM parameters (Structural determination)

MAS solid state measurements were carried out in a wide-bore Bruker Avance III 800 MHz spectrometer with a magnetic field strength of 18.8 T and 1.9 mm E-free triple resonance probe head. The magic angle was calibrated using KBr and the shimming was adjusted using

adamantane. The MAS frequency was set to 30 kHz and the temperature was set according to the probe specific calibration curve to result into a real temperature of 278 K. As an internal chemical shift reference 4,4-dimethyl-4-silapentane-1-sulfonic acid (DSS) was added to the sample. The recycle delay was set to 5 s. The 90 ° pulse lengths were set to 3.1 μ s and 8.9 μ s for ^1H and ^{15}N respectively. The number scans taken were 80 for this measurement. The spectra were processed in order to obtain best outcome in terms of signal-to-noise and resolution.

5.4.2 MLU parameters

MAS solid state measurements were carried out in a widebore Bruker Avance III 600 MHz spectrometer with a magnetic field strength of 14.1 T. An E-free double resonance probe head for 1.3 mm rotor was used. The MAS parameter calibration was done using labelled glycine and temperature calibration was performed using lead nitrate with the shimming being manually adjusted. The solid-state spectra were obtained at a spinning frequency of 20, 30, 40 and 50 kHz at set temperatures of 288.2 K, 278.2 K, 266.2 K and 251.5 K. The 90 ° pulse lengths were set to 1.8 μ s and 4.5 μ s for ^1H and ^{15}N at power levels of 25W and 40W respectively. The recycle delay was set to 2 s. The contact time for ^1H - ^{15}N was chosen to be 1.5 ms. The number scans taken were 1152 for these measurements. All the spectra were processed using the same parameters in order to obtain best outcome in terms of signal-to-noise and resolution.

The $T_{1\rho}$ relaxation was probed at increasing spinning speed from 20, 30, 40 and 50 kHz at ^{15}N spinlock power that was carefully calibrated before every measurement. The ^1H CP power increased with each increasing spinning speed. A long recycle delay of 4.5 s was used. The contact time for ^1H - ^{15}N was chosen to be 1.5 ms.

In all the cases the NMR spectra obtained were processed in Bruker TopSpin and the 2D spectra was processed using Sparky and NMR ViewJ.

5.5 Absorption spectroscopy for concentration determination

Proteins absorb light in different wavelength ranges. UV-C radiation (100 – 280 nm) is mainly absorbed by groups of the peptide backbone, while the three aromatic amino acids phenylalanine (Phe), tyrosine (Tyr) and tryptophan (Trp) absorb UV-B radiation (280 – 315 nm). The protein concentration is determined by the Lambert-Beer law $A = \lg\left(\frac{I_0}{I}\right) = \epsilon cd$, with A : Absorbance, ϵ : theoretically determined extinction coefficient, which is made up of the number and thus sum of the extinction coefficients of Tyr and Trp in a protein and d : layer thickness of the cuvette at a wavelength $\lambda = 280$ nm, can be used. The extinction coefficient was determined using the ExPASy-ProtParam program and was estimated to be 38940 $\text{M}^{-1}\text{cm}^{-1}$ for γ B-crystallin, 14325 $\text{M}^{-1}\text{cm}^{-1}$ for α -crystallin and 13980 $\text{M}^{-1}\text{cm}^{-1}$ for α B-crystallin. The measurements were carried out on the Jasco V-650 UV/Vis spectrometer.

5.6 Small Angle X-ray scattering (SAXS)

SAXS experiments were conducted using Mark tubes with an outer diameter of 1 mm and wall thickness 0.01 mm (Hilgenberg GmbH) and performed in transmission mode using a SAXSLAB laboratory setup (Retro-F) equipped with an AXO microfocus X-ray source. The AXO multilayer X-ray optic (AXO Dresden GmbH, Dresden, Germany) was used as monochromator for Cu-K α radiation ($\lambda = 0.154$ nm). A two-dimensional detector (PILATUS3 R 300K; DECTRIS, Baden, Switzerland) was used to record the 2D scattering patterns. The capillaries were placed inside a heating block of a temperature stage (HFSX350V, Linkam Scientific Instruments Ltd.) and positioned on a second stage for x-y-z positioning inside the measurement chamber (see Figure 12) The intensities were angular-averaged and plotted versus the scattering angle q . The scattering intensities for all the samples were corrected for transmission and measurement geometry. The measurements were performed at 20 °C and 60 °C, as well as corrected for background, transmission, and sample geometry. Bovine α and h α B were measured at concentrations of 20 and 200 mg/ml for at least 45 h each.

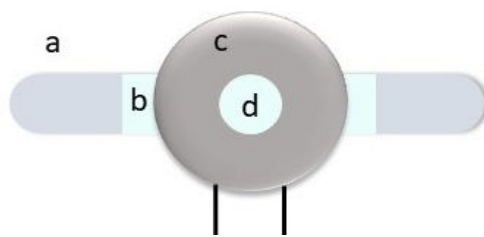


Figure 12: A simplified schematic representation of a sample within the Linkam stage. a. Glass capillary, b. Sample of interest, c. heating stage connected to a thermocouple and d. window with a diameter of 1 mm.

5.6.1 Basic analysis

For a system of monodisperse particles, the total scattering intensity $I(q)$ is given as:

$$I(q) = n \Delta\rho^2 V^2 F(q) S(q) = c M \Delta\rho_m^2 F(q) S(q) \quad (22)$$

where, n is the number density of the particles ($n = c/M$), $\Delta\rho$ is the contrast given by the difference in electron density of the particle and background, V the volume of the particles ($V \propto M$), $F(q)$ is the form factor, that describes the macromolecular scatterer ($F(q = 0) = 1$) and $S(q)$ is the particle structure factor, which includes the contribution from interacting neighboring particles ($S(q \rightarrow \infty) = 1$). q is the scattering vector given by $2 \sin\theta/\lambda$, with the θ being scattering angle and λ is the wavelength of the X - ray.

At low concentrations, $S(q)$ can be assumed to be equal to 1. Hence, a scattering curve at a sufficiently low concentration allows to obtain the cumulative scattering intensity $F(q)$ of the ‘individual’ protein molecule (Guinier A. 1955) as the interparticle interference effects can be neglected. Subsequently, a background correction was applied by subtraction of the scattering

profile of the NaP-buffer. Figure 13, depicts a scattering curve obtained for low concentration of 20 mg/ml BSA, h α B crystallin and bovine α -crystallin at 20 °C. The characteristic parameters that can be obtained from such a scattering intensity curve will be discussed in the following.

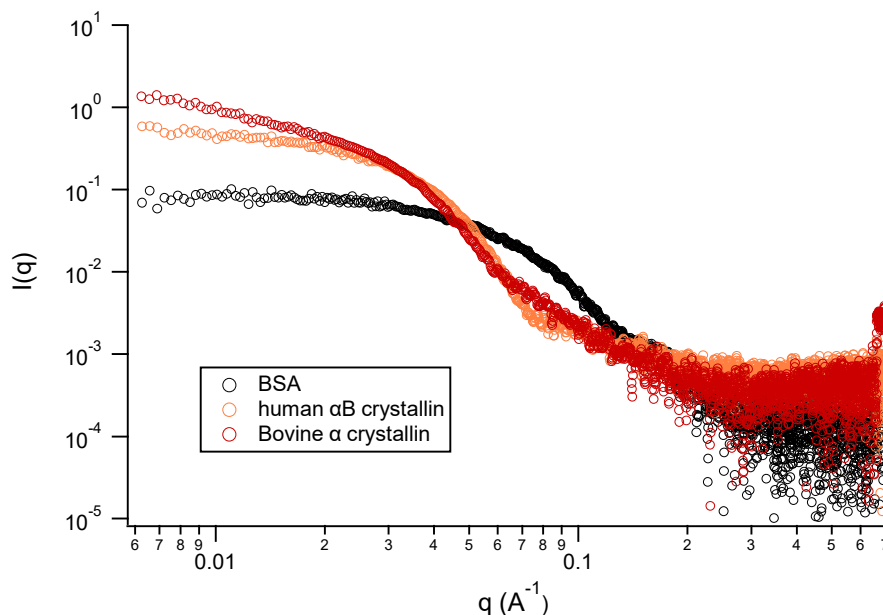


Figure 13: Scattering intensity curve of BSA, h α B crystallin and bovine α -crystallin at 20mg/ml at 20 °C.

5.6.1.1 Guinier Law

The data analysis for all measurements included at first the determination of the radius of gyration, R_g , using the Guinier approximation such that at low q – range, $qR_g < 1.3$ the intensity is derived as:

$$\ln(I(q)) \approx R_g^2/3 \cdot q^2 \quad (23)$$

R_g is used as a measure for the orientational averaged size of a protein molecule. Figure 14, depicts the Guinier Plot ($\ln(I(q))$ vs. q^2) which is a linear function for non-interacting particles, independently of its individual shape. The linear fit of the slope provides the R_g according to Equation (23) (Guinier A. 1955). Here, the R_g value obtained for low concentrated BSA at 20 °C is 32.23 ± 1.35 Å.

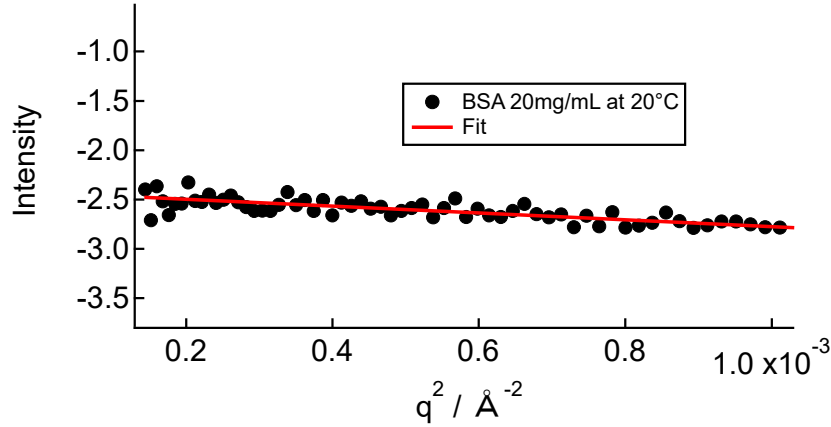


Figure 14: R_g obtained for BSA 20mg/ml using Guinier approximation at 20 °C.

5.6.1.2 Scattering characteristics of ellipsoidal and spherical particles

The proteins investigated in this study could be satisfactorily represented either by a system of ellipsoidal particles or polydisperse spheres. The function describing an ellipsoidal shape is shown in Equation (24), (25) and was used as the fitting function in this study.

$$F(q) \propto \frac{A}{V_{ell}} \int_0^1 f^2 \left[q r_b (1 + x^2 (v^2 - 1))^{1/2} \right] dx \quad (24)$$

$$f(z) = 3V_{ell} \frac{(\sin z - z \cos z)}{z^3}$$

$$V_{ell} = \frac{4\pi}{3} r_a r_b^2 \text{ and } v = \frac{r_a}{r_b} \quad (25)$$

A is the scaling factor that includes particle concentration and density, $f(z)$ is the scattering amplitude for a sphere, r_a and r_b are the radius of the ellipsoid (Feigin and Svergun 1987). For a polydisperse population of spheres with uniform scattering length density, the scattering intensity is given as depicted by equation

$$I(q) = \left(\frac{4\pi}{3}\right)^2 N_0 \Delta\rho^2 \int_0^\infty f(R) R^6 F^2(qR) dR \quad (26)$$

R being the radius of the sphere, $F(qR)$ as depicted in Equation (24) and $f(R)$ a function describing the normalized distribution function of sizes. In case of the Schulz distribution $f(R)$ writes as

$$f(R) = (z + 1)^{z+1} x^z \frac{\exp [-(z + 1)x]}{R_{avg} \Gamma(z + 1)} \quad (27)$$

R_{avg} is the mean radius, $x = R/R_{avg}$, Γ is the Gamma function and z is related to the relative distribution such that $z = 1/p^2 - 1$, where $p = \sigma/R_{avg}$ where, σ is the root mean square deviation from the mean size and p is referred to as polydispersity. (Kotlarchyk et al. 1988).

Figure 15, displays the scattering intensity curve obtained for BSA at low concentration 20 mg/mL at 20 °C and the ellipsoidal fitting function of Equation (24)(25). From the fit, the following values for the radius was obtained, R_a (rotational axis) = $15.30 \pm 1 \text{ \AA}$ and $R_b = 49.27 \pm 0.32 \text{ \AA}$. The average R_g therefore would be $32.86 \pm 0.605 \text{ \AA}$ which is in a good agreement with the result of the Guinier Fit.

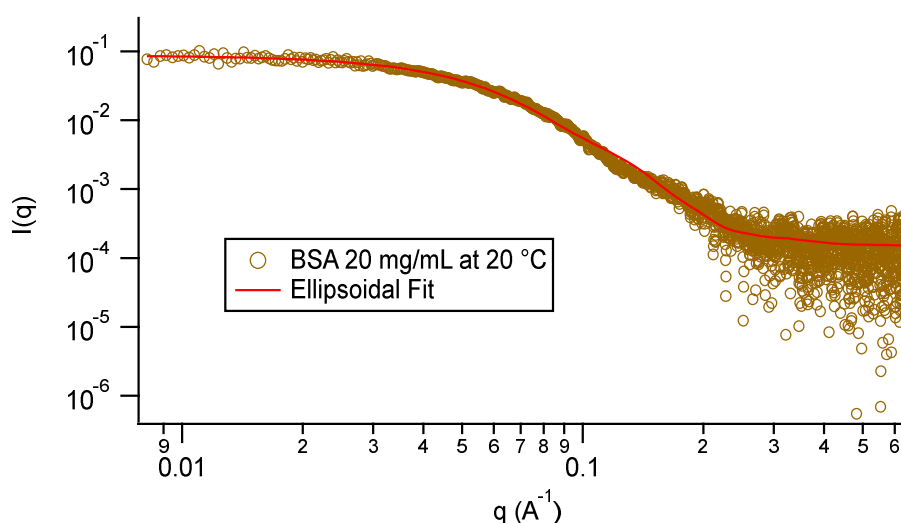


Figure 15: Scattering intensity of BSA at 20 mg/ml at 20 °C.

5.6.1.3 Scattering of monodisperse interacting systems

The interactions of a monodisperse system is given by $S(q)$ and can be studied at increased concentrations. Figure 16 displays the scattering intensity curve obtained for BSA at 20 mg/ml and 200mg/ml at 22 °C. A direct comparison of the intensity curves imply that the shape of the scattering curves is dependent on the protein concentration. For 20 mg/ml BSA a Guinier fit resulted in an average R_g of $32.23 \pm 1.35 \text{ \AA}$ (see Section 5.6.1.1) which is in close agreement with the literature value (Mylonas and Svergun 2007). Hence, at 20 mg/ml the protein-protein interactions are negligible ($S(q) \approx 1$) and the scattering intensity corresponds to the form factor $F(q)$ (Figure 16, grey curve). At higher concentrations e.g., 200 mg/ml, the interactions add to the scattering signal and the scattering intensity is decreased at small q values, indicative of repulsive inter-particle interactions, ($S(0) < 1$) (Figure 16 red curve). An increased

attractive interaction is displayed as a slight increase in the scattering intensity at low q values, which is indicative of unspecific aggregation of the sample.

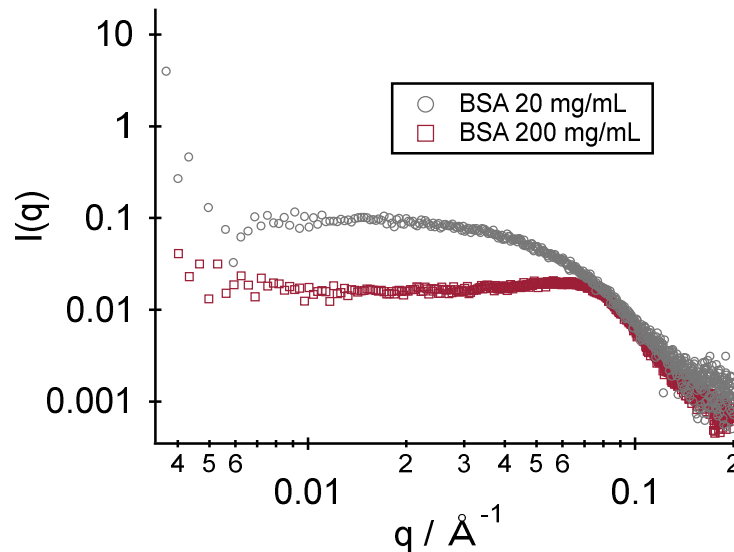


Figure 16: Comparison of X-ray scattering intensity of BSA at 20 mg/ml (grey) and 200 mg/ml (red) at room temperature.

5.6.1.4 Structure factors obtained from interaction potential

Until now the analyses dealt with dilute solutions, where the interactions between the suspended particles are considered to be negligible. With increase in concentration the particles would feel the presence of neighboring particles and the distribution of these particles in space would be determined by the interactions between them. This is quantified by the structure factor $S(q)$ which contains information regarding the arrangement of the particle. $S(q) = 1$ indicates that the protein molecules are farther apart. At increased concentrations, especially at low q -range $S(q)$ strongly depends on the interaction potential between the particles. When $S(0)$ is less than unity the particles are uniformly distributed due to dominant repulsive interaction while $S(0)$ greater than unity indicates prevalent attractive interactions (Tardieu et al. 1999). A detailed analysis of $S(q)$ can therefore provide insights into the nature of interaction potentials. Sticky hard sphere interaction potential is one of the many relevant interaction potentials that can be used to describe a system of particles. This will be further elaborated in section 6.2.2.5.2.3 Structure factor analysis.

5.6.1.5 Fractal dimensions of the gel network

The transient structure or network formed by globular proteins can be further investigated to gain information about the connectivity of these new structures. This can be quantified using the fractal dimension of the evolved structure D_m . The fractal dimension D_m , describes how the mass fractal structure scales with distance ($M \sim r^{D_m}$). For example, the fractal dimension of an aggregated structure/network forming a rod like or linear chain arrangement, with a few

branching points only was found to be between 1 - 1.2. More branched networks would have a fractal dimension in the range of 1.6 - 1.8. A very high fractal dimension of $D_m > 2$ is indicative of a clustered network (Lazzari et al. 2016; Liao et al. 2005). The nature of the network structure formed during aggregation and the corresponding fractal dimension has been shown in Figure 17. The fractal dimensions of the gel networks studied in this work were obtained from the fit of the scattering intensity using the following equation:

$$S(q) = 1 + \frac{\sin[(D_m - 1)\tan^{-1}(q\xi)]}{(qR_0)^{D_m}} \frac{D_m \Gamma(D_m - 1)}{[1 + 1/(q^2 \xi^2)]^{(D_m - 1)/2}} \quad (28)$$

In the simplest approximation the mass fractal can be estimated by the exponent of the power-law dependence $I(q) \approx S(q) \sim q^{-D_m}$ for $1/l < q < 1/l_{min}$, where l is the size of the fractal, l_{min} is the minimum distance between scattering units (Anitas 2019). $S(q)$ was determined using Equation (22) with the experimentally determined from factor $F(q)$ at low concentrations (as discussed above)

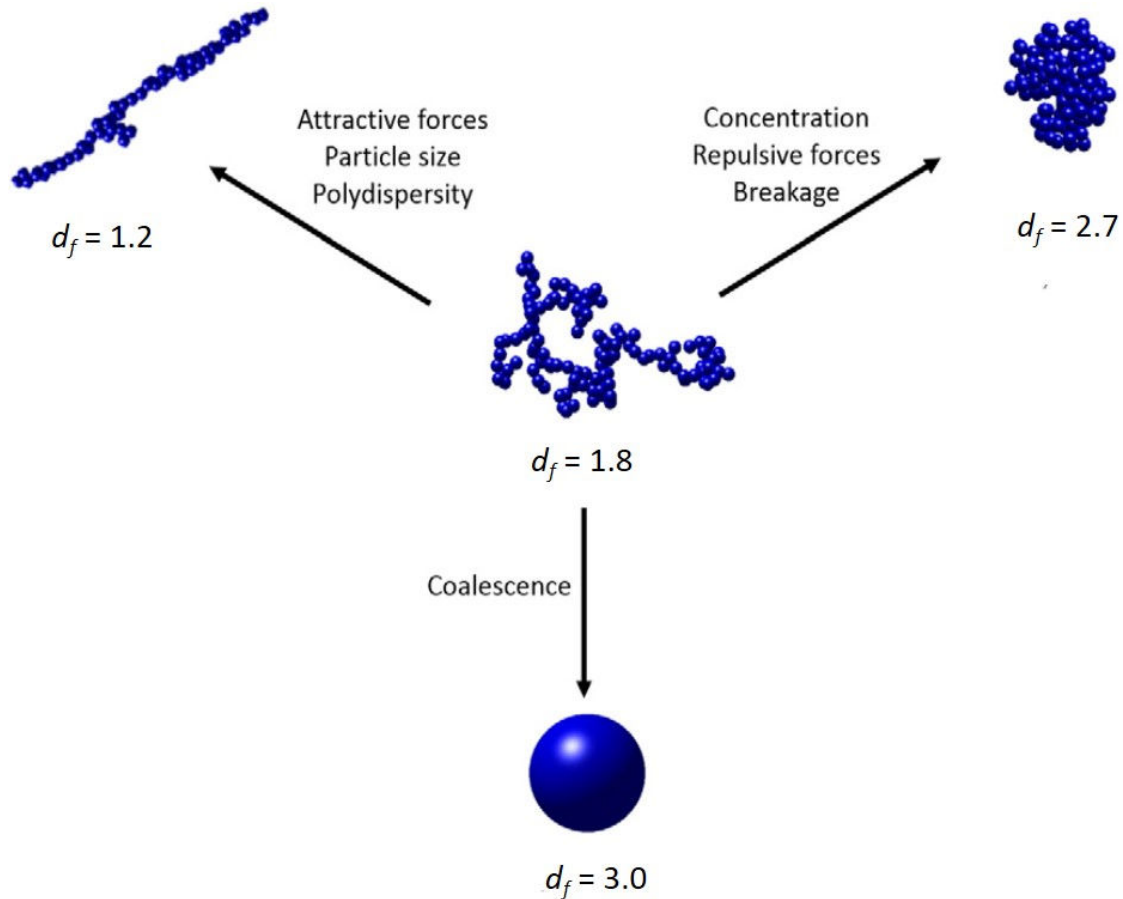


Figure 17: The nature of network structure formed during aggregation and its corresponding fractal dimension (Lazzari et al. 2016) reused with permission (Copyright Clearance Center, Inc, License ID – 5735820829138)

5.6.1.6 Kratky plot

Once we obtained the information regarding the fractal dimensions, additional information with respect to protein native structure can be obtained at higher q ranges. A qualitative estimate of the disordered, unfolded, or globular state of the protein can be deduced from the Kratky plots ($q^2I(q)$ vs q) obtained from its scattering profile. These plots allow to identify the degree of folding or disorder of the protein. For globular proteins the scattered intensity decays at higher q values approximately $I(q) \sim 1/q^4$, resulting into a bell-shaped Kratky plot (Uversky and Dunker 2010). By normalizing with respect to scattering and R_g , the information regarding the shape is obtained while eliminating the size information. This enables the direct comparison of folding states of the protein (Kikhney and Svergun 2015). A normalized Kratky plot for globular proteins would have a maximum at $qR_g = \sqrt{3} \approx 1.7$ (see Figure 18). This will be further discussed with respect to different proteins in the results section.

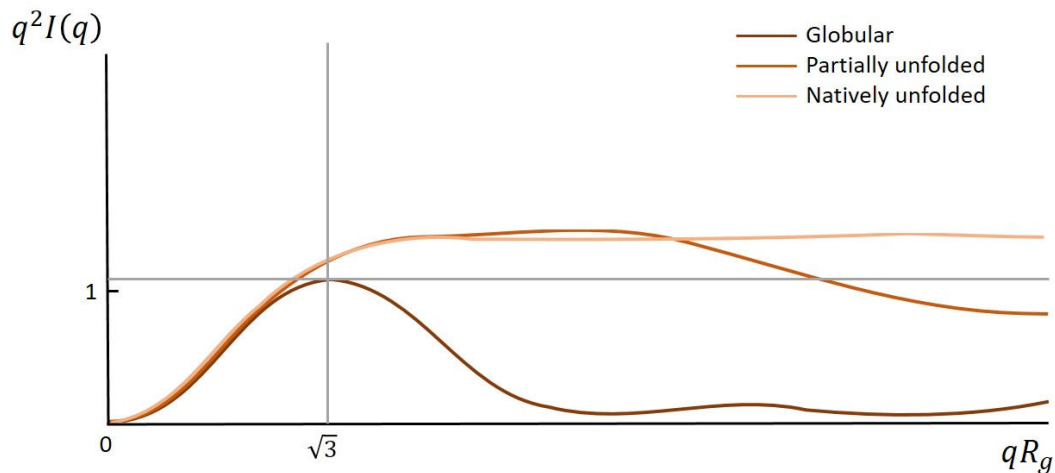


Figure 18: Schematic of Kratky plot adapted from Kikhney and Svergun (2015).

5.7 ATR FTIR spectroscopy

Attenuated total reflection (ATR) FTIR was used to characterize the change in secondary structure of Bovine α -crystallin (200 mg/ml) and Human α B-crystallin (200 mg/ml) during gelation. For these experiments a Bruker Tensor 27 FT-IR spectrometer equipped with BioATRCell II, a LN-MCT photovoltaic detector as well as OPUS data collection program (Bruker, Ettlingen, Germany) was used. Around 20 μ L of the protein solution was pipetted on to the Si-crystal surface before heating. In the first temperature dependent experiment, the temperature was gradually increased from 20 $^{\circ}$ C to 85 $^{\circ}$ C with a step of 5 $^{\circ}$ C and an equilibration time of about 15 mins. In the second temperature dependent kinetics study, the samples were initially heated to 20 $^{\circ}$ C, and once the spectrum was recorded, the temperature was increased to 60 $^{\circ}$ C. Once the temperature is reached the spectral recording was started with an equilibration time of 60 mins between each measurement. The desired temperature (20 $^{\circ}$ C and 60 $^{\circ}$ C) was obtained using a circulating water bath HAAKE C25P thermostat. The spectra

were obtained with a resolution of 4 cm^{-1} , with a scanning range of $4000\text{ to }900\text{ cm}^{-1}$, scanning velocity of 20 kHz , zero-filling factor of 4 and number of scans 256. The spectrometer and ATR cell were purged using N_2 . The recorded spectra were corrected for water/buffer contribution by subtracting the spectrum obtained of the buffer at the same temperature and pH.

The data was further treated to obtain a better baseline corrected data by Dr. Christian Schwieger (Institute of Chemistry, MLU). This pretreatment involved choosing the spectra in the range from $1800\text{ -}1475\text{ cm}^{-1}$, then applying rubber band baseline in the spectrometer software with 1 iteration and 64 baseline points. The spectra range was then cut from $1730\text{ -}1475\text{ cm}^{-1}$ and exported as txt file. This data was further used for the analysis in this thesis.

5.8 Electron microscopy

The negatively stained samples for TEM were prepared by Dr. Annette Meister at the Biozentrum, Martin Luther Universität, Halle. The samples were prepared by spreading $5\text{ }\mu\text{l}$ of the α -crystallin protein A dispersion (10 mg/ml) onto a Cu grid coated with a Formvar-film (PLANO, Wetzlar). After 1 min excess liquid was blotted off with filter paper and $5\text{ }\mu\text{l}$ of 1% aqueous uranyl acetate solution were placed onto the grid and drained off after 1 min. The dried specimens were examined with an EM 900 transmission electron microscope (Carl Zeiss Microscopy GmbH, Oberkochen, Germany). Micrographs were taken with a SSCCD SM-1k-120 camera (TRS Moorenweis, Germany).

In this work, to obtain TEM images of concentrated gels, resin embedded sample preparation technique was used. EM was performed by Prof. Gerd Hause at the Biozentrum, Martin Luther Universität, Halle. For transmission electron microscopy (TEM) protein gels were fixed with 3 % glutaraldehyde (Sigma, Taufkirchen, Germany) in 0.1 M sodium cacodylate buffer (SCB) for 3 h, washed 4 times with SCB and postfixed with 1% osmium (VIII) tetroxide in SCB for 1 h. After washing with H_2O samples were dehydrated in a graded ethanol series (10-30-50-70-90-100%), which included a 1% (w/v) uranyl acetate staining step at 70% ethanol (1 h). Thereafter the samples were infiltrated with epoxy resin according to Spurr (Spurr 1969) and polymerized at 70°C . Subsequent ultrathin sections of 80 nm and 300 nm were cut with an Ultracut R ultramicrotome (Leica, Wetzlar, Germany). The 80 nm ultrathin sections were placed on copper grids and observed with an EM900 transmission electron microscope (Carl Zeiss Microscopy, Jena, Germany) operating at 80 kV. The images were recorded using a Variospeed SSCCD camera SM-1k-120 (TRS, Moorenweis, Germany).

5.9 Dynamic Light scattering

DLS experiments were conducted on a Litesizer 500 (Anton Paar) disposable cuvettes of $500\text{ }\mu\text{L}$. The irradiation wavelength was $\lambda = 658\text{ nm}$, while the detection angle was maintained at 90° (side scattering). Crystallin proteins at a concentration of 20 mg/ml were investigated. The hydrodynamic radius was initially obtained at $20\text{ }^\circ\text{C}$ and for the kinetic studies a constant temperature of $60\text{ }^\circ\text{C}$ was used. Prior to each measurement, the sample was allowed to

equilibrate for at least 10 min. The viscosity of the buffer at 20 °C and 60 °C was determined prior to the measurements using a viscosimeter. The background corrected data obtained from DLS measurements were evaluated directly using Kalliope software (Anton Paar).

5.10 Transmission Experiments

Transmission studies were carried out on a FLUOstar Omega (BMG Labtech GmbH, Ortenberg, Germany) reader using Greiner 96 F-bottom well plates (Greiner Bio-One GmbH, Frickenhausen, Germany). The transmission was monitored at an excitation wavelength of 800 nm. The experiments were performed with h α B and bovine α -crystallins at protein concentrations of 20 and 200 mg/ml at 60 °C, pH 7.4 and final sample volume of 50 μ L. The transmission data was collected every 1800 s, with a number of cycle 136 and 20 flashes per well and cycle.

6 Results and Discussion

6.1 A quantitative study of heat-induced aggregation of eye-lens crystallin proteins under crowding conditions using low-resolution NMR.

The results discussed here have been published in, **Camilles *et al.* BBA - Protein and Proteomics, 1866 (2018):1055-1061** (<https://doi.org/10.1016/j.bbapap.2018.07.007> and <https://doi.org/10.1016/j.bbapap.2019.02.00> (Corrigendum)) and the figures are reused in this section according to CCC RightsLink agreement.

A fully functional structured protein tends to remain folded in its native state, and certain genetic mutations or external factors can lead to its unfolding or misfolding resulting in protein aggregation. In most cases the aggregate formed are simply non-functional and, in some cases, they can be toxic and disrupts its proper functioning. The protein aggregate might follow several different aggregation mechanisms and eventually form various aggregate structures depending on its environmental and stress conditions (Moran et al. 2014; Roskamp et al. 2017). Several different analytical techniques have been employed to investigate the change in structure and thermal stability of proteins during aggregation. To elucidate the change in structure or heat capacity accompanying the denaturation or aggregation process, differential scanning calorimetry (DSC), FTIR spectroscopy, circular dichroism (CD), and UV absorbance have been routinely used (Kumar et al. 2011; Matheus et al. 2006; Ghosh et al. 2016; Vermeer and Norde 2000; Harn et al. 2007; Borzova et al. 2016; Joshi et al. 2014). While dynamic light scattering (DLS), size-exclusion chromatography (SEC) and fluorescence spectroscopy can distinguish the aggregated and non-aggregated proteins based on their size (Kumar et al. 2011; Ghosh et al. 2016; Hofmann et al. 2016; Matheus et al. 2006; Le Bon et al. 1999). Most of these characterization techniques used to follow the aggregation kinetics of protein require dilution of samples for analysis because at higher concentrations spectroscopic techniques could provide erroneous results. For instance, under concentrated conditions DLS, CD, UV absorbance, and fluorescence spectroscopy can alter its refractive index, cause changes in its absorbance, inner filter effects could arise or for light scattering, multiple scattering can occur. Additionally, extrapolating the data obtained under dilute conditions to higher concentrations could provide imprecise results and / or even may tend to be faulty. Most of these techniques cannot precisely estimate quantitatively the amount of aggregated protein. Therefore, investigation of protein aggregation under their physiologically relevant ‘crowding conditions’ e.g., those that resemble the interior of a living cell are important and necessary, but methodological problems in quantitative estimation persist.

Nuclear magnetic resonance (NMR) is one of the most powerful techniques available for studying protein structure and dynamics, although it is rarely used to investigate the kinetics of protein aggregation owing to it being complex, expensive, and time-consuming, and due to its inherently low sensitivity. Most of the NMR-based protein aggregation studies enable indirect observation of the aggregation of proteins and information regarding its aggregating state is

rather limited. These NMR - based aggregation studies involved observation of the disappearance of signal of dissolved monomers using high resolution spectra (Suzuki et al. 2012; Xu et al. 2017; Mishra et al. 2009), monitoring the behavior of the solvent (Oakes 1976a, 1976b; Taraban et al. 2017; Indrawati et al. 2007) or certain indirect NMR methods (Dalvit et al. 2017).

The aggregation of eye lens crystallin is one important example of pathogenic protein aggregation which leads to a clinically known condition called cataract. These proteins, owing to their lack of protein turnover, in the unfortunate event of mutation, post-translational modification or UV exposure these proteins denature and aggregate, without the option of regeneration. The crystallin proteins therefore have to remain stable and soluble for a lifetime. In the human eye lens these proteins exist as a highly polydisperse colloidal dispersion, with the protein concentration ranging from 200 mg/ml at the periphery i.e. the cortex to ~ 400 mg/ml at the lens nucleus (Fagerholm et al. 1981). Under such highly crowded conditions the properties of these proteins are significantly affected due different inter-molecular interactions. It is therefore important to investigate and understand the proteins stability and aggregation kinetics under its relevant high concentration.

The study of lens crystallins have been prevalent with respect to its stability, denaturation and aggregation. In this work the protein behavior under thermally stressed condition is probed for two individual crystallins namely recombinant bovine γ B- and native bovine α -crystallin. A detailed account of effect of temperature on these crystallin protein can be found in the section 1.5. The studies reported here, dealt mainly with investigating the stability of the crystallin protein and does not directly probe the kinetics of aggregation. Accordingly, the heat induced study here is undertaken at a temperature of 60 °C, which is well below the denaturation temperature of these proteins, so as to gradually follow its aggregation kinetics. More importantly, the aggregation kinetics of individual crystallin proteins at high concentrations have not yet been investigated to the best of my knowledge.

The aim of this study is to follow the protein aggregation kinetics of α - and γ B - crystallins when thermally stressed at two different concentrations. This kinetics was investigated using proton NMR transverse relaxation measurements. As opposed to earlier studies here the protein signal could be directly measured in a wide range of relaxation delays, aggregation of protein under crowding condition was feasible as well as the aggregation could be monitored in real time. A new insight into the aggregation of α - and γ B -crystallin at high concentration was obtained, wherein it turns out to be quantitatively different for each of them.

6.1.1 Transverse relaxation at high protein concentration

The feasibility of using NMR relaxometry experiments to investigate concentrated bovine crystallin solutions were initially tested. These solutions at two different concentrations were compared and quantitatively interpreted, before and after aggregation at 60 °C.

For these experiments' concentrations of 60 mg/ml and 135 – 200 mg/ml were chosen, in order to mimic the conditions closer to the crowding in the eye lens. At a temperature of 60 °C, the NMR-detected aggregation of proteins was possible on a reasonable time scale, such that the crystallin monomer does not undergo extensive temperature induced unfolding. The raw transverse relaxation decay curves obtained for the two different α - and γ B-crystallins are shown in Figure 19. The relaxation curve here consists of two distinct components, one corresponding to protein and other to residual water proton having different relaxation time/rates. The water residual proton due its long relaxation time can be separated from the overall relaxation decay. Since it is impractical to prepare proteins sample without appreciable amount of water protons, this property of the water component allowed its unambiguous subtraction and pure protein relaxation decay curve was obtained as shown in Figure 20.

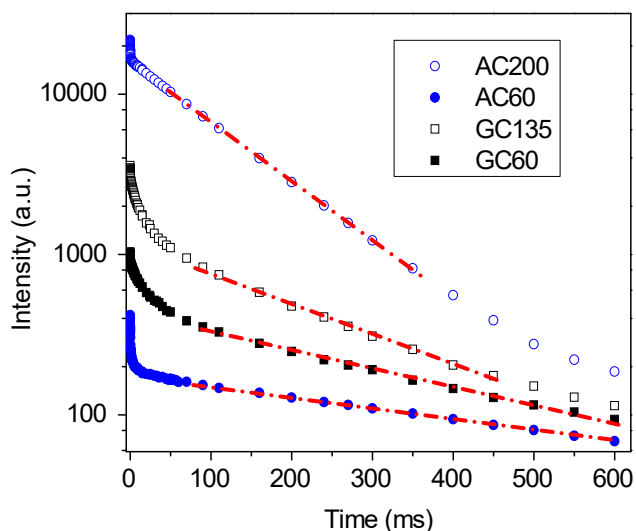


Figure 19: Transverse relaxation decays of bovine α -crystallin at 60 mg/ml (AC60) and 200 mg/ml (AC200), recombinant bovine γ B-crystallin at 60 mg/ml (GC60) and at 135 mg/ml (GC135) at the first point of aggregation kinetics measurements. The dashed red lines here depict the long exponential relaxation component of the residual water protons, which was subtracted from the integral signal

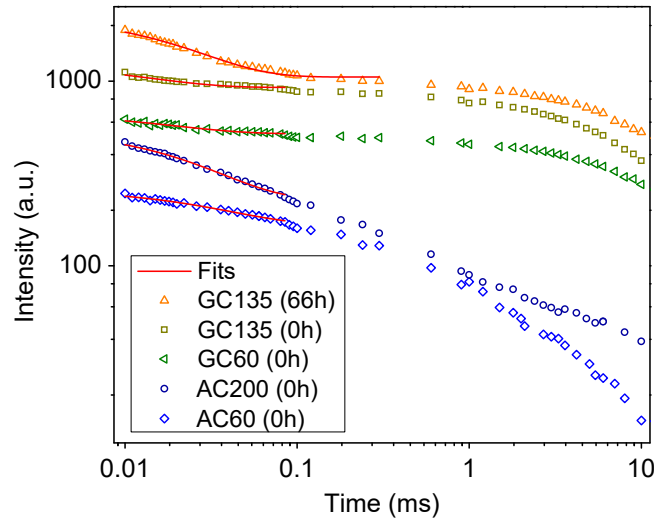


Figure 20: Protein transverse relaxation decays obtained after the subtraction of water component from Figure 19, of bovine α -crystallin at 60 mg/ml (AC60) and 200 mg/ml (AC200), recombinant bovine γ B-crystallin at 60 mg/ml (GC60) and at 135 mg/ml (GC135) at the first point of aggregation kinetics measurements (at 0 h). For a comparison, the relaxation decay of GC135 after 66 h at 60 °C is also shown, along with the fits to the initial parts (Equation (29)) are depicted by solid line.

6.1.2 Data analysis approach

This section explains in detail the approach to derive parameters that would allow the systematic study and interpretation of results from the measured data. A direct quantitative analysis of the shape of the relaxation decay is impractical, due to the proteins' complex structure, their overall and internal dynamics and due to certain changes, they might undergo during the aggregation process. Therefore, a relevant quantitative parameter, that would be an indicator of protein conditions and behavior, had to be defined which is characterized by these transverse relaxation decays. Hence a mean relaxation rate was used as an integral parameter to characterize the protein dynamics, as has been previously shown (Roos et al. 2015b; Roos et al. 2015a). Although this single parameter does not give a detailed information regarding the state of protein during the aggregation process, since it is dependent the different molecular parameters involved, it can be readily used for investigating the rate of aggregation process. The mean relaxation rate is obtained from the initial slope of the decay curves (Roos et al. 2015a; Roos et al. 2015b), determined by a bi-exponential fit of the initial part according to the formula

$$I(t) = p_a \exp(-t \cdot R_a) + p_b \exp(-t \cdot R_b) \quad (29)$$

and the mean relaxation rate is calculated as

$$T_{2avg}^{-1} = \langle R_2 \rangle = \frac{p_a R_a + p_b R_b}{p_a + p_b} \quad (30)$$

where, $p_{a,b}$ and $R_{a,b}$ are the intensities and rates of two components ('a' and 'b') respectively. These fits are shown in Figure 20.

6.1.3 Average T_2 values and aggregation kinetics

The NMR relaxometry data recorded during the thermally stressed aggregation of crystallins at different concentrations were analyzed according to the approach outlined above. This allowed the quantification of time course of dissolved monomer and aggregated protein states, which is explained in details in the following section.

The transverse relaxation decays of γ B and α - crystallins during the process of thermally induced denaturation and aggregation at two different concentrations are shown in Figure 21 and Figure 22 respectively.

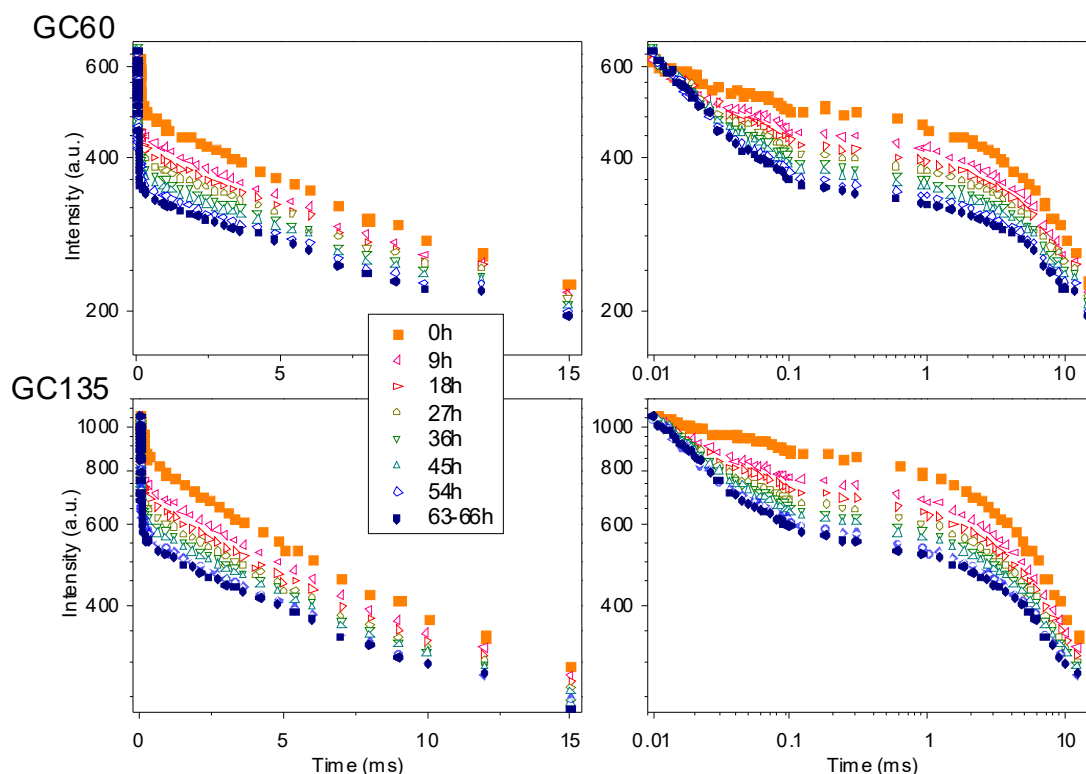


Figure 21: Protein transverse relaxation decay curves for recombinant γ B-crystallin during thermally induced aggregation at 60 °C at 60 mg/ml (GC60) and 135 mg/ml (GC135) (left panel: log-linear plots; right panel: log-log plots)

A compilation of the mean inverse relaxation rates, which is the mean T_2 relaxation time extracted using Equation (30) from these data (Figure 21 and Figure 22) are shown in Figure 23. These constitute the major results of this work, with two interesting and relevant

features. First, is the difference in the shape of the transverse relaxation decay curves and second, is the dependence of concentration on the thermally induced aggregation kinetics of the α – and γ B– crystallin (Figure 23, a and b).

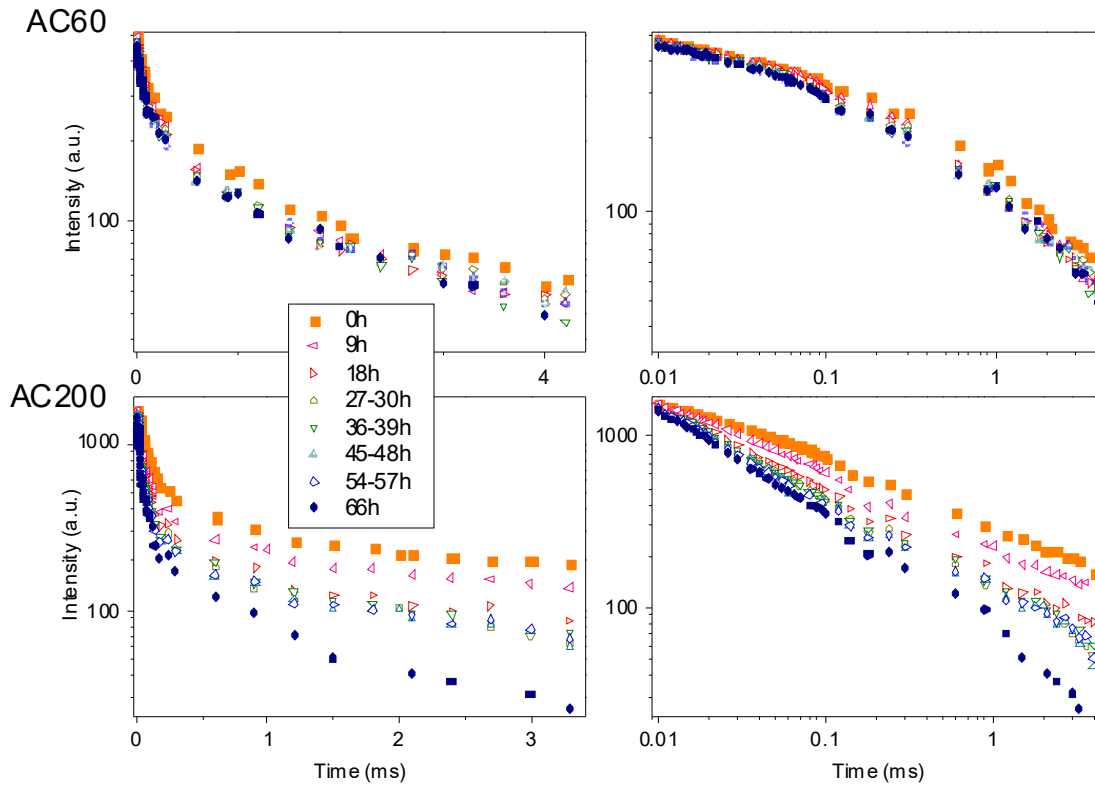


Figure 22: Protein transverse relaxation decay curves for bovine α -crystallin during thermally induced aggregation at 60°C at 60 mg/ml (AC60) and 200mg/ml (AC200) (Left panel: log-linear plots; right panel: log-log plots)

It was observed that for both the proteins at high concentration, with increasing time of experiment, the mean T_2 decreases. This is an expected result, since the aggregation process would slow down the overall protein tumbling which eventually leads to speed up of transverse relaxation. But for the two different protein the shape of the relaxation decay curves are rather different. γ B-crystallin decays curves clearly exhibit two components with distinctly different T_2 ; the short component corresponds to the precipitated aggregates i.e., solid like fraction of the protein and a long component corresponding to dissolved unaggregated protein (native). This two-component curve clearly indicate that in the protein solution two fractions co-exist, the immobilized precipitate which could be swollen and still be internally mobile and the dissolved protein, as well as an overall negligible amount of protein oligomers. On the contrary, the relaxation decay curves of α -crystallin does not feature such a two-component shape rather it simply becomes shorter with increasing experimental time (for AC200). This is due to the high molecular weight of α -crystallin, that even without aggregation, the Brownian tumbling of such large protein is rather slow, on a time scale of roughly 1 μ s (Roos et al. 2015b). This ensures a fast relaxation decay already before the aggregation starts. Although the change in

T_2 is not as pronounced for α -crystallin as for γ B, i.e., the two separate components cannot be distinguished, rather the fast decay is characterized by the slow-down of protein tumbling due to aggregation.

6.1.4 Aggregation kinetics vs concentration

This section focuses on the different concentration dependence of these crystallin on their aggregation kinetics. One of the remarkable features of the data presented here is the qualitatively different dependence of concentration on aggregation of α - and γ B-crystallin.

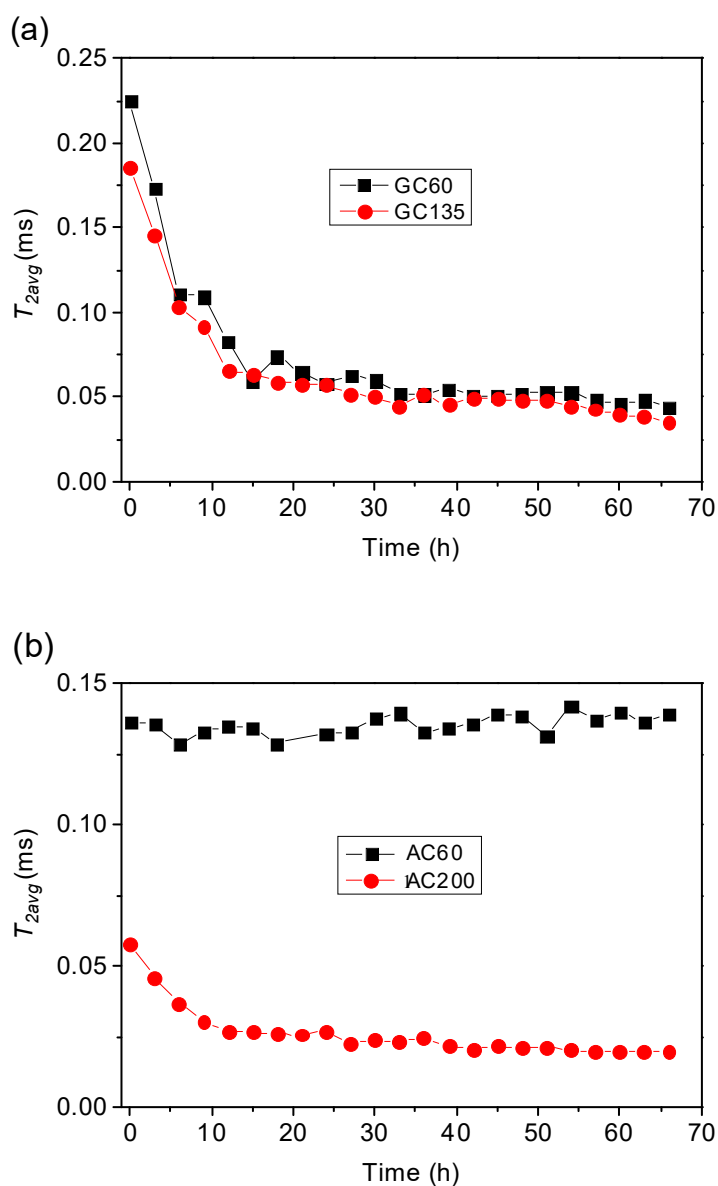


Figure 23: Time dependence of mean transverse T_2 relaxation time for (a) bovine γ B-crystallin and (b) bovine α -crystallin.

As illustrated in Figure 23 a, γ B-crystallin aggregation is hardly concentration dependent, while α -crystallin aggregates only at 200mg/ml and not significant change is observed for the 60 mg/ml solution (Figure 23 b). A qualitative difference can also be easily recognized by visual inspection. The photographs of aggregated α - and γ B-crystallin solutions have been shown in Figure 24; where γ B-crystallin forms a white precipitate, as opposed to α -crystallin which forms a transparent gel without visible precipitation.

It has to be noted that the aggregation of γ B-crystallin studied here is not directly related to the thermal denaturation of these proteins, since its 'melting point' is markedly higher than 60 °C but certain subtle structural alteration could have led to their aggregation (Steadman et al. 1989; Sen et al. 1992). Similarly, the thermally induced unfolding of α -crystallin is at a temperature much higher than 60 °C (Maiti et al. 1988; Carver et al. 1993). Although there are some indications of conformational changes associated with α -crystallin at 60 °C (Surewicz and Olesen 1995), no experimental evidence of aggregation at this temperature is known to the best of my knowledge, especially at such high concentration. The non - selective proton NMR relaxometry approach employed here cannot provide the information on the internal structural changes, because such changes might overlap with the aggregation process and a clear separation of these is practically impossible. And therefore, it is speculated that these proteins might retain the native fold and the process of aggregation involves the certain inter-molecular physical links formed possibly by the unstructured C-termini, eventually leading to immobilization and gel formation.

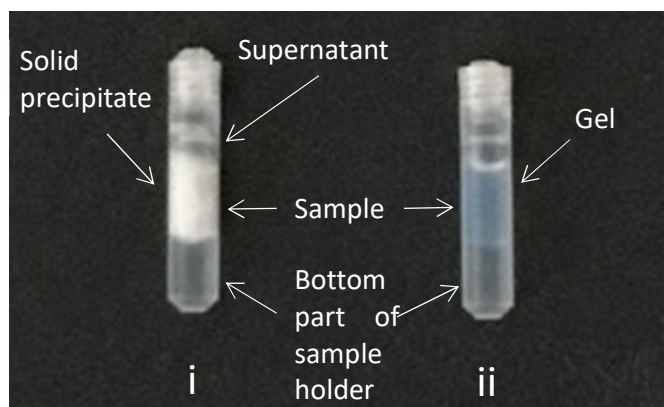


Figure 24: Aggregated (i) γ B-crystallin at 135 mg/ml and (ii) α -crystallin at 200 mg/ml

6.1.5 Quantitative estimation of aggregated protein (γ B-crystallin)

The two-component relaxation decay curve of γ B crystallin (Figure 21) facilitated the quantitative estimation of the amount/fraction of aggregated protein, which is obtained by ratio of intensities of the two components. The time dependence of the amount/percentage of aggregated proteins in the solution at two different concentrations are depicted in Figure 25, which basically yielded aggregation time constant of 43 h and 32 h for 60 mg/ml (GC60) and

135 mg/ml (GC135) respectively. This fraction of aggregated protein was determined from the bi-component fit as $p_a/(p_a + p_b)$, where 'a' corresponds to the fast decaying component (Equations (29), (30)). Therefore, one of the important advantages of NMR relaxometry technique compared to other characterization approaches is that, NMR allows for a direct and uncomplicated determination of the amount of aggregated molecules in solution at any given concentration.

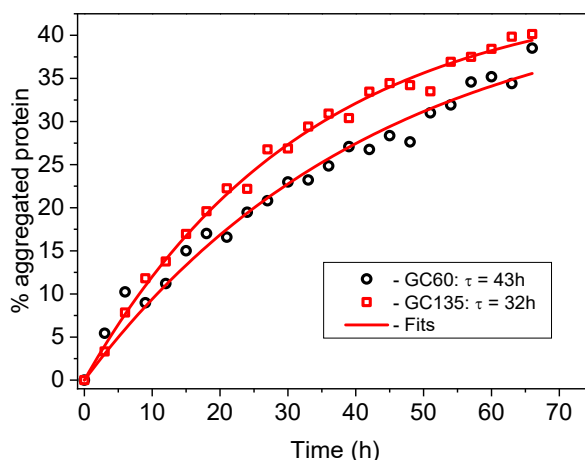


Figure 25: The time dependence of the percentage of aggregated γ B-crystallin at 60 mg/ml (GC60) and 135 mg/ml (GC135) are shown, which have been fitted with an exponential growth function $I(t)=A \cdot (1-\exp(-t/\tau))$, where $I(t)$ is the intensity at time t , and A is the amplitude of the slowly aggregating species. The aggregation time constant can be derived from the main fit result i.e. τ .

6.1.6 Transverse relaxation of the solvent

The time dependence of the T_2 relaxation time of residual water protons is another important source of information. This time dependence of residual water proton T_2 relaxation is shown in Figure 26. For α -crystallin a significant change is only observed at high concentration 200 mg/ml, where the T_2 decreases by 30 - 35 %, while at low concentration 60 mg/ml it essentially remains constant. Here, this decrease is attributed to the restricted water mobility due to the gel formation. This directly correlates to the observation from the protein signal. On contrary for γ B-crystallin such a correlation between the solvent relaxation and protein relaxation during aggregation was absent. This is clearly evident from the decrease in effective protein concentration in the supernatant due the precipitation and thus longer relaxation times are observed for the water proton (a weak trend for γ B crystallin at 60 mg/ml). It can therefore be ascertained that indirect observation of protein aggregation by monitoring the water proton relaxation could provide highly dubious results.

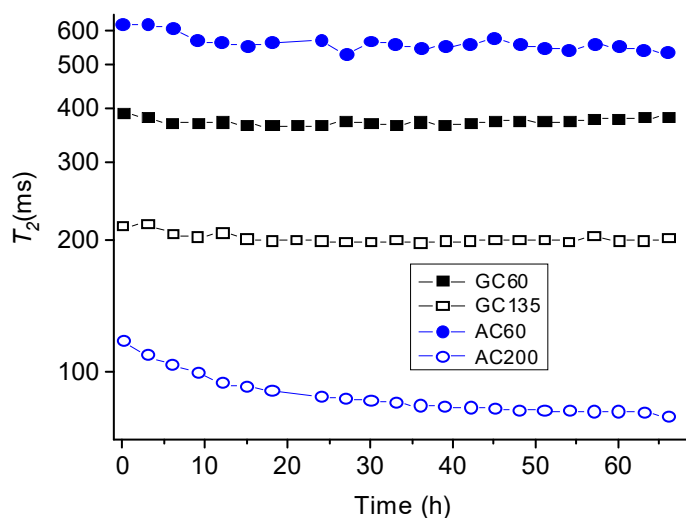


Figure 26: The time dependence of residual water proton T_2 relaxation time during the aggregation of bovine α -crystallin (AC60 and AC200) and γ B-crystallin (GC60 and GC135).

6.1.7 Conclusion

NMR relaxometry can be used as a simple and robust tool for monitoring the protein aggregation. The key feature of this technique is the direct observation of the protein contribution to the proton NMR signal, by monitoring the integral proton transverse relaxation, over a wide time scale from microseconds to hundreds of milliseconds. This technique proved to work well for proteins at several different concentrations, especially under crowded condition, that mimics the interior of a living cell or even the eye lens. Although not in all cases, transverse relaxometry can be used for a direct and straightforward estimation of the ratio between the aggregated and non-aggregated fractions of protein during their course of aggregation. One of its main disadvantages is the time resolution for real time monitoring of the protein aggregation kinetics due to the time scale of conducting different experiments. Additionally, the solvent transverse relaxation as an indicator of protein aggregation can be rather misleading in some cases.

The current study demonstrated firstly a qualitative difference in the aggregation mechanism, of α - and γ B crystallins under crowding conditions and at a temperature of 60°C where the monomers are essentially in their native folded state. A concentration- independent aggregation was observed for γ B-crystallin, with an aggregation constant of $\sim 30\text{h} - 42\text{h}$, while α -crystallin remained soluble at 60°C and forms a gel network at 200 mg/ml. This is a first experimental demonstration of thermally induced gelation of α -crystallin at such a high concentration well below its actually unfolding transition temperature. Further studies focus on characterizing the gelation in α -crystallin proteins to get a better insight into its gel network formation and correlate it to the lens transparency.

6.2 Investigation and characterization of gelation of α -crystallin eye-lens protein

This chapter focuses on investigating the gelation and gel properties of one of the prominent eye lens globular proteins i.e., the α -crystallins. In the previous chapter, the heat-induced aggregation kinetics study of crystallins revealed that α -crystallin undergoes a concentration-dependent aggregation, where at a relatively high concentration the α -crystallin forms a gel. In this section, a comprehensive analysis of the gel structure development of these proteins and their interactions is undertaken.

In general, for globular proteins it is well known that certain conformational changes due to changes in solvent conditions (acid induced, change in pH or ionic strength) or rise in temperature (heat-induced), lead to aggregation and at sufficiently high concentration to gelation. The gels investigated in this study are specifically heat-induced and therefore could be speculated to originate from aggregation of the protein. As stated in the introduction, heat-induced gel formation follows a three-step process: unfolding or partial denaturation, aggregation and network formation. Primarily, the aqueous solutions of native protein are stabilized by the long ranged repulsive interactions, which are compensated by the weak attractive interactions. Heating, therefore, helps overcome the strong repulsive interaction between the native protein, thereby exposing the hydrophobic and cysteine residues located within the protein and subsequently leading to the aggregation and gelation (Boye et al. 1996). Additionally, depending on the balance between the attractive and repulsive interactions, the process and kinetics of the aggregation the structure as well as the properties of the gel formed could differ (Pouzot et al. 2005; Weijers et al. 2002); (Totosaus et al. 2002; Nakamura et al. 1978).

6.2.1 Aggregation and gelation in globular proteins

For globular proteins, aggregation and gelation is mostly characterized by transitioning of a fully folded protein to a partially unfolded protein conformation, initiated by heating that causes the peptide chain to be more mobile and thereby interact and bind to other proteins. These proteins resemble a spherical colloidal particle with a short-range attractive interaction in the form of hydrophobic interactions, hydrogen bonding or electrostatic interactions (Mezzenga and Fischer 2013). In the case of β -lactoglobulin (β -lg), electrostatic attractive interactions drive the protein phase separation and aggregation, which could be controlled by the addition of salt (Parker et al. 2005). The strength of such an attractive interaction influences the phase separation kinetics i.e., if the interaction is confined and short ranged compared to the size of the particle, the phase separation would lead to a reversible aggregation and if net attraction exceeds a critical value the phase separated aggregates densify and merge to form a protein dense phase. Additionally, if the protein concentration is high this leads to irreversible aggregation with the aggregates slowly growing and adding to a percolating gel network (Nicolai 2019).

6.2.2 Gelation in eye lens α -crystallin protein

A vertebrate eye lens is composed of a concentrated aqueous mix of eye lens crystallin proteins, and owing to its short range ordered arrangement makes the lens highly refractive and most importantly transparent (Bloemendal et al. 2004). The major contribution towards this lens transparency is from α -crystallin protein, due to its relatively high concentration in the lens cytoplasm ($\sim 50\%$ of the total lens protein mass) and highest molecular mass (Xia et al. 1994). Such a highly concentrated system although essential for imparting high refractive index, can also act as a driving force for protein aggregation (Ciryam et al. 2015; Moreau and King 2012).

In this section the aggregation and gelation of bovine α -crystallin, which is a heterooligomeric mix of $\alpha A : \alpha B$ (3:1) and h αB crystallin have been investigated when thermally stressed at 60 °C. To get a better insight into the change in molecular interactions, secondary structural conformation and size associated with the gelation process small angle X-ray scattering, ATR-FTIR, TEM and DLS have been implemented. While the transparency of the gel is characterized by turbidity tests. The major questions that would be addressed here are (i) Does gelation of these globular proteins involve an overall structural change or partial unfolding? (ii) How does the gelation differ for h αB crystallin subunit and bovine α -crystallin? and (iii) Can the gelation be correlated to transparency in the eye lens? To the best of our knowledge such a detailed investigation on the heat induced 'gel' of α -crystallin has not yet been implemented.

6.2.2.1 Transparency of the gels investigated using light transmission

The main functionality of the crystallin proteins are to maintain the lens transparency by maintaining the short-range ordered arrangement and its high concentration contributing to high refractive index of the lens. Any perturbation in the crystallin conformation or arrangement can lead to formation of aggregates that act as light scatterers and thereby impair vision. α -crystallin are the major contributors to this lens transparency. In this section the percentage of light transmitted, when a beam of incident light of wavelength 800 nm is directed on to α -crystallin solutions is discussed. This can be directly used as measure of transparency of the crystallin solutions. Here the time course of change in % transmission of h αB and bovine α -crystallin when heated at 60 °C is probed at two different concentrations namely 20 mg/ml and 200 mg/ml. At high concentrations both h αB and bovine α crystallins have the propensity to form gel. Figure 27 shows the evolution of transmittance over time for h αB and bovine α -crystallin at a wavelength of 800 nm. As a reference the % transmittance of NaP buffer used to prepare the crystallin solution was also measured. In general, the turbidity measurements are conducted in the near-infrared region 700 - 1000 nm range, in order to avoid influence of any colored substances. Therefore, in this study turbidity was investigated at the wavelength of 800 nm.

Over the course of heating, a decreasing trend in the % transmission for the crystallin solutions were observed. As can be clearly interpreted, h αB crystallin at 20 mg/ml (h αB 20) over the

course of time gradually forms larger aggregates that eventually render 0 % transmittance, indicating a turbid system. The highly concentrated h α B (haB200) although tends to form aggregates, but after 47h still can transmit 30 % of incident light. Both the h α B crystallin samples were visually turbid. In contrast to h α B, bovine α crystallin samples remained relatively visually transparent. The lowly concentrated bovine α -crystallin (Bovine a20) remained transparent throughout the heating course. This transparency was comparable to that of the buffer. Moreover, bovine a20 was still soluble, while haB20 had formed a gel. A transmittance of about 73 % was detected for bovine a20. The highly concentrated bovine α crystallin (Bovine a200) had an initial transmittance value of 72 %. With increase in exposure time at 60 °C the decrease in transmittance was gradual and after 46h the transmittance was about 61 %. Although both the Bovine a200 and haB200 at high concentration ultimately formed gels interestingly, the former was relatively more transparent. Bovine a200 had an initially reduced % transmittance presumably due to the concentration effects, but the gels ultimately formed were relatively transparent. Additionally, it was observed that the % transmittance value for buffer was at 84% which is 100% transparent solution. This could be an artefact of the experimental method, where the unavoidable evaporation of the solvent made the coverslips used for the well-plate foggy. But results show a qualitative difference in the aggregation processes of these crystallin proteins.

Except for Bovine a20, all the others formed gels, i.e., possibly the formation of a 3D cross-linked network. However, the decrease in transmittance is an implication of heterogeneity on the length scales that is comparable to the wavelength of the visual light. Bovine α -crystallin, which is a heterooligomer, is more resistant to temperature-induced ageing, even though at high concentrations it forms a gel, it remains relatively transparent. This indicates that the gelation does not considerably affect the transparency.

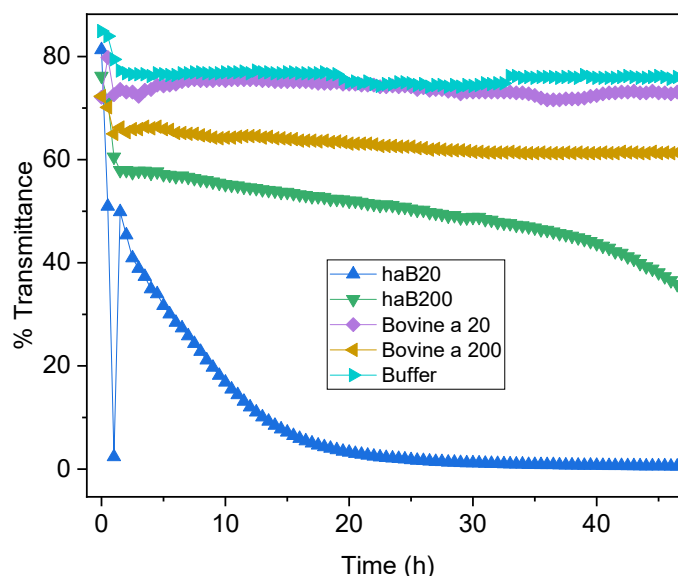


Figure 27: The change in % transmission of h α B crystallin haB20 (20 mg/ml), haB200 (200 mg/ml), bovine α -crystallin Bovine a20 (20 mg/ml), Bovine a200 (200mg/ml) and NaP-buffer when thermally stressed at 60 °C at 800 nm.

6.2.2.2 Change in particle size determined using dynamic light scattering (DLS)

One of the most common techniques used to determine the particle size of a macromolecule is dynamic light scattering, being based on the Brownian motion of the dispersed particles. In this method the diffusion coefficient (D) of the dispersed particles is measured and the molecular weight (M_w) and hydrodynamic radius (R_h) is estimated using the Stokes – Einstein equation (Equation (21)). One of the advantages of using DLS is that it enables the analysis of samples containing a wide distribution of particles with different molecular masses. Here, the measurements of time-dependent changes on the hydrodynamic radius of h α B and bovine α crystallin were performed at 60 °C. Since highly concentrated samples can produce multiple scattering events by scattering off of several particles sequentially before reaching the detector, DLS measurements requires the use of low concentrations. Therefore, a concentration of 20mg/ml was employed for these measurements. The hydrodynamic radii obtained at 20 °C for h α B and bovine α crystallin were 8.99 nm and 12.48 nm respectively, which is in agreement with earlier studies (Peschek et al. 2009; Ryazantsev et al. 2018; Burgio et al. 2000).

The kinetics of changes in the size of these proteins at 60 °C is shown in Figure 28. H α B crystallins (Figure 28, red), after an equilibration time of 10 mins at 60 °C, showed an initial increase in size to 11.16 nm. Further on, the size increased strongly up to 5h, eventually forming larger aggregates that can no longer be detected. Visibly the solution becomes turbid and ‘gel-like’ indicating protein aggregation.

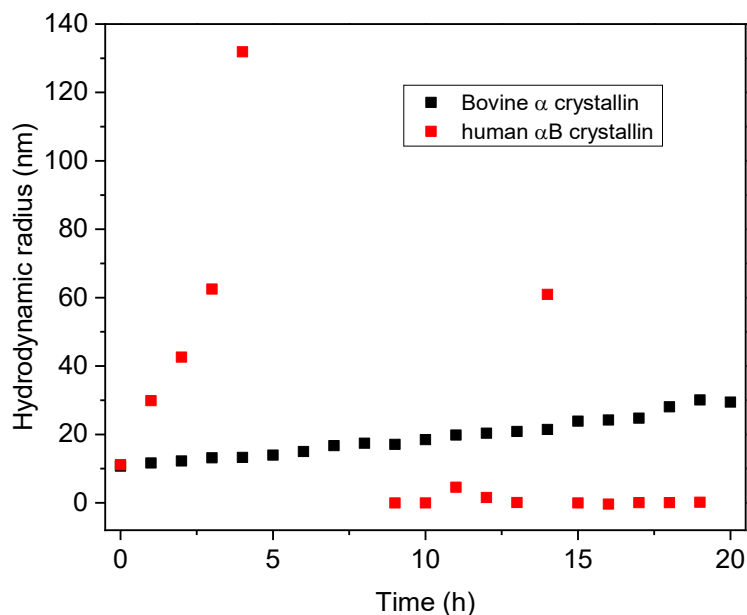


Figure 28: The time dependent changes in the hydrodynamic radii of h α B and Bovine α crystallin at 20 mg/ml when thermally stressed at 60°C

On contrary for bovine α -crystallin (Figure 28, black), immediately after equilibration at 60 °C, the size becomes smaller i.e., 10.74 nm compared to its initial state. The size of the protein then consistently increases weakly over time, indicating the formation of somewhat

larger oligomers. Although as opposed to h α B, visibly bovine α is still soluble and does not aggregate.

Light scattering therefore is a direct indicator of the change in the size of the particle with the progression of thermal stress. h α B-crystallin clearly forms larger oligomers with time, while bovine α crystallin remains in a homogeneous state. The heterooligomers thus demonstrate remarkable stability towards thermal stress.

6.2.2.3 *Transmission electron microscopy study of human α B- and bovine α -crystallin*

To get further information regarding the structural integrity of the protein in this study TEM images were recorded. The TEM image of a low-concentration negatively stained bovine α -crystallin sample is shown in Figure 29. The protein, as expected, appeared as roughly spherical oligomers i.e., being an overall globular structure. The data obtained revealed that the α -crystallin has a distribution of size indicating heterogenous oligomeric complexes and the size range varied from 9 - 12 nm in diameter. These oligomeric proteins either tend to assemble into an aggregate or form some elongated particles contributing to the polydispersity of the protein complex formation. A similar observation was reported by Selivanova and Galzitskaya (2020).

In general, to obtain a TEM image of a negatively stained sample with a good resolution requires small concentrations. In our case the gels only formed at a relatively higher concentration of 200 mg/ml for both human α B- and bovine α -crystallin. Therefore, here the gel samples were first embedded in an epoxy resin using the procedure described in the methods section. The images were then acquired from the thin sections of this resin embedded gels as shown in Figure 30. Although this only provides lower resolution images, it can be ascertained that these proteins, when they form a gel, still retain their globular structure. Both the crystallin proteins seems to have similar gel structures. The gels formed appears to be long-chain networks of these globular protein. The experimental procedure used to obtain these images can albeit lead to an ambiguous result regarding the network structure (that could be a preparation artefact), as a first approximation it could be established that the crystallin proteins maintain their globular structure even after forming a gel.

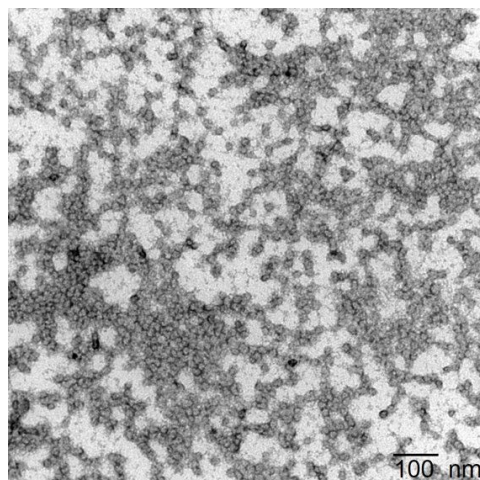


Figure 29: Transmission electron microscopy image of negatively stained α crystallin from bovine eye lens at 10mg/ml at RT in 50mM NaP-buffer at pH 7.5

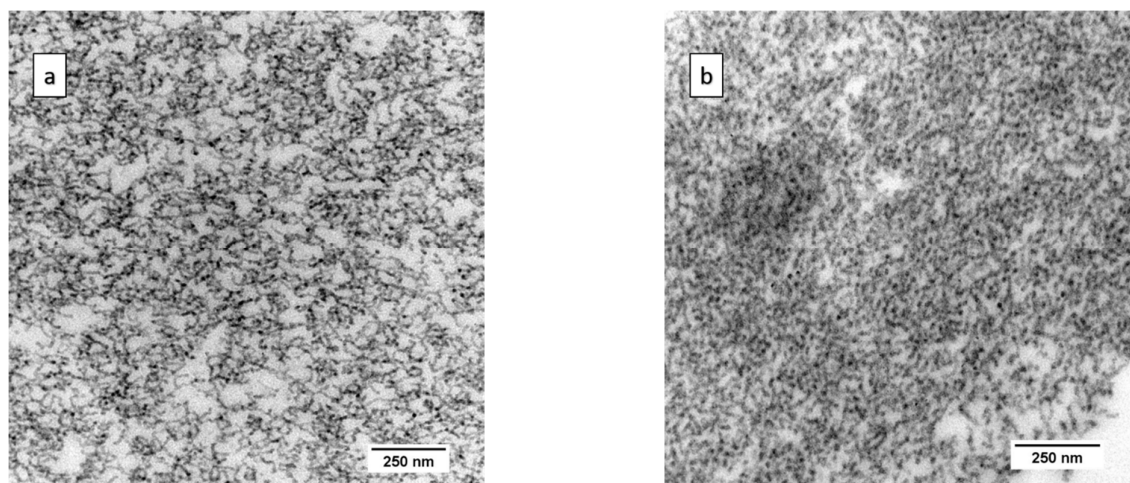


Figure 30: Transmission electron microscopy image of a. human α B-crystallin and b. bovine α -crystallin gels embedded in epoxy resin

6.2.2.4 Secondary structural changes probed using Fourier transform infrared spectroscopy (FTIR)

Vibrational spectroscopy has been routinely used to characterize the secondary structure content of a protein sample. The characteristic IR bands of protein are the amide I and amide II, where amide I arises due to the stretching vibration of C=O bonds of the peptide group and amide II due to the bending vibrations of N-H bonds with a contribution from C-N stretching vibrations (Barth 2007; Haris and Severcan 1999). The amide I band in the range from 1600 cm^{-1} to 1700 cm^{-1} , is most sensitive to the changes in protein secondary structure. Therefore, the bands within this region have been considered for this study. Table 5 summarizes the band positions in the amide I and amide II region that corresponds to the protein secondary structures. Additionally, the peak positions obtained from fitting the raw data (see section 6.2.2.4.3) is presented in Table 5.

Table 5: Amide I and amide II band position assignments

Amide band	Corresponding secondary structure	Band / peak position expected (cm ⁻¹) ^[Ref]	Fitted band / peak positions (cm ⁻¹)
Amide II	α – helix	1540	1540
Amide I	α – helix	1648 – 1658	1660 / 1663
	β – sheet	Parallel	1623 – 1641
		Antiparallel	1674 – 1695
		Turns	1655 – 1685
disordered / random structure	1642 – 1657	1650	

Ref: (Barth 2007; Tatulian 2019; Haris and Severcan 1999; Barth and Zscherp 2002), (Kumosinski and Farrell 1993)

In general, there was a good agreement between the peak positions obtained from the literature and the fitted data, especially for the β -sheet structure. Although, peak position of the α -helix in the amide I region is not within the expected range, Barth et.al. (Barth and Zscherp 2002) states that shorter α – helix tends to show weaker bands at ~ 1660 cm⁻¹ and 1670 cm⁻¹. The peak at 1540 cm⁻¹, in the amide II region corresponds primarily to the α – helix secondary structure. Amide II contains contribution from other secondary structures as well, but are rather poorly resolved, and are seldom used for the quantitative estimation of protein secondary structure.

6.2.2.4.1 Temperature dependent changes on h α B and bovine α crystallin secondary structure

The temperature dependent changes in the amide I region of the h α B and bovine α -crystallin at a concentration of 200 mg/mL are depicted in Figure 31, with increasing temperature from 20 °C to 85 °C. Since the samples were equilibrated only for 15 mins at each temperature step, the it is unclear if the structural transitions were completed at each step. Several works have stated that for α -crystallins, the maximum absorbance peak appearing in the range 1629 – 1632 cm⁻¹, is an indication of the predominantly β -sheet structure. The disordered or random structure appear as a weaker band at 1645 cm⁻¹, while α -helices resonate at 1658 cm⁻¹ (Surewicz and Olesen 1995; Lamba et al. 1993). At 20 °C the maximum at 1632 cm⁻¹ and 1630 cm⁻¹ in the amide I band for h α B and bovine α - crystallin respectively, with minor features at around 1686 cm⁻¹ implies the presence of primarily β -sheet secondary structure. With increasing temperature, the amide I band remained unaffected up to approximately 50 °C for h α B and 60 °C for bovine α crystallin, indicating that the proteins retain their secondary native structure in this temperature range. Further temperature increase caused more significant changes in the amide I band.

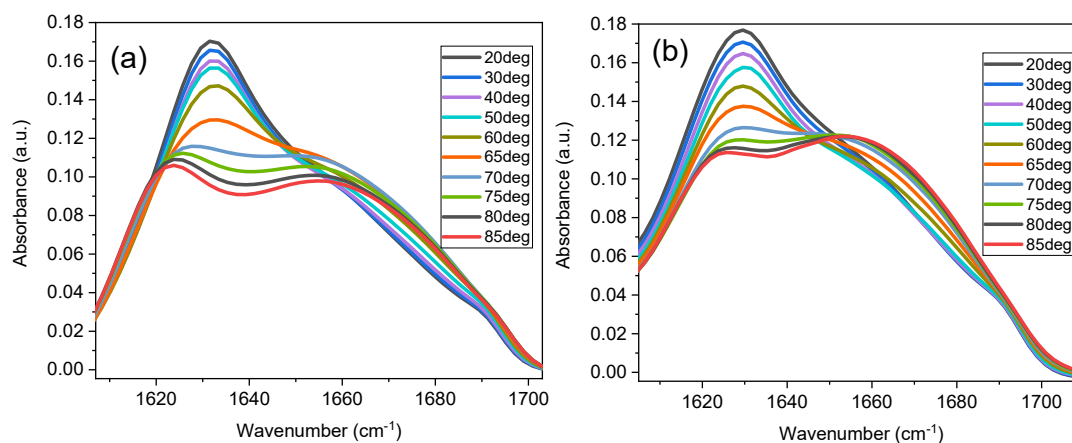


Figure 31: The temperature dependent changes in FTIR spectra of a. h α B and b. bovine α -crystallin at 200 mg/ml

6.2.2.4.2 Changes in the secondary structure of h α B and bovine α crystallin at 60 °C (kinetics)

Further on, the time dependent changes in the secondary structure when the crystallins are exposed to thermal stress at 60 °C was probed. The concentration of the proteins were 200 mg/mL. Figure 32 depicts the change in amide I band contour of h α B and bovine α -crystallin over 50 h. The rescaled corresponding spectral data obtained by scaling all the spectra to constant amide II is included in Figure 32 as well. As was observed earlier, the predominant band corresponding to β -sheet secondary structure was initially observed for both the crystallins. But as opposed to the observation in the temperature-dependent study, holding the crystallins at 60 °C lead to a gradual shift in the dominant peak from 1632 cm^{-1} to 1623 cm^{-1} for h α B (Figure 32 a), while for bovine α -crystallin the peak at 1630 cm^{-1} shifted to 1625 cm^{-1} (Figure 32 c). In general, the peaks shift to lower wavenumbers although still residing in the wavelength region corresponding to β -sheet structure. Alperstein et al. showed that the shift of the amide I band 1631 cm^{-1} observed in juvenile eye lens to 1620 cm^{-1} in a cataractous eye lens can be attributed to formation of amyloid β -sheets (Alperstein et al. 2019). Ultimately, by annealing the proteins at 60 °C, bovine α crystallin underwent much less structural changes in comparison to h α B crystallin.

In general, an overall decrease in the absorbance intensity was observed over time for the crystallins. It has to be emphasized here that ATR-FTIR is widely known as a surface layer technique, wherein the evanescent wave that results from the contact with the sample, attenuates exponentially into the bulk of the sample over a length scale determined by the IR wavelength ($\sim 0.5 - 2 \mu\text{m}$) (Glassford et al. 2013). In our case, the decrease in the signal intensity could be attributed to the fact that the proteins moved out of the sensitivity range when the aggregated protein moved to the top of the sample. Consequently, the spectra do not show isosbestic points, however after rescaling, the (at least approximate) observation of isosbestic points provides a consistency check of the amide II based intensity normalization (see Figure 32 b and d).

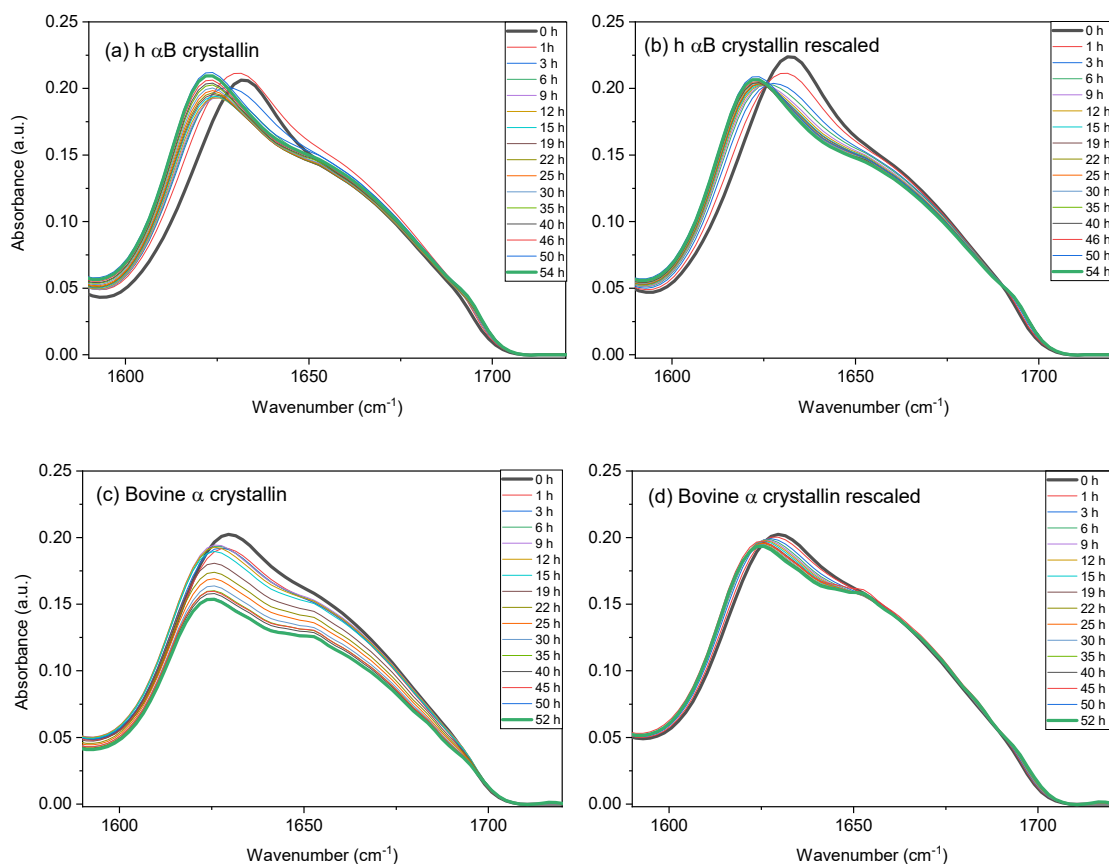


Figure 32: The time dependent changes in the amide I region of the FTIR spectra of a. h α B, b. h α B rescaled, c bovine α -crystallin and d. bovine α -crystallin rescaled at 200mg/ml when thermally stressed at 60 °C

6.2.2.4.3 Deconvolution of the FTIR spectra

The amide I region of the spectra specifically in the range 1580 cm^{-1} to 1720 cm^{-1} was further evaluated for both the α -crystallins. A global fit of the initial and final spectra was simultaneously performed in the range 1520 cm^{-1} to 1720 cm^{-1} which included the amide II component, using a 6-component Voigt fitting function. This led to a precise estimation of 6 peak positions in total (a fit with less bands were not satisfactory). For both the crystallins the peak positions obtained were quite similar. As discussed earlier in Table 5, Peak 1 at 1540 cm^{-1} corresponds to amide II, peak 2 at 1620 cm^{-1} corresponds to amyloid β sheet structure (Alperstein et al. 2019), peaks at 1633 cm^{-1} and 1680 cm^{-1} are two band components from β sheet, peak at 1660 cm^{-1} is assigned to α helix, and disordered / random structures at 1650 cm^{-1} (Lamba et al. 1993). The α helix and disordered structures absorption occurs in the overlapping region within 1647 – 1660 cm^{-1} which makes the precise estimation of these secondary structures rather difficult (Kleinschmidt 2019).

A peak deconvolution of the amide I peak was performed by fixing the peak positions obtained from the global fit at all in-between times. The change in amplitudes for each of the components could therefore be estimated. The peak deconvolution of h α B crystallin spectra at 0 h and after

54 h at 60 °C is shown in Figure 33 (a) and (b). At 0 h the beginning of the kinetics run, all the peaks with a defined width are observed with a dominance of β sheet structure. This is generally the case for crystallin proteins, where the ACD region is typically composed of β sheet structure. After annealing the protein at 60 °C for 54 h, an increase in the peak intensity at 1620 cm^{-1} which is generally observed when hydrogen-bonded extended structures are formed (Alperstein et al. 2019) e.g. amyloid fibrils or ordered intermolecular β -sheets. In addition the shoulder at 1649 cm^{-1} starts to become more prominent, which can be assigned to disordered structures (van Boekel et al. 1999). Additionally, a simultaneous decrease in the β sheet and α helical structure was noted. The β turns remain rather unaffected.

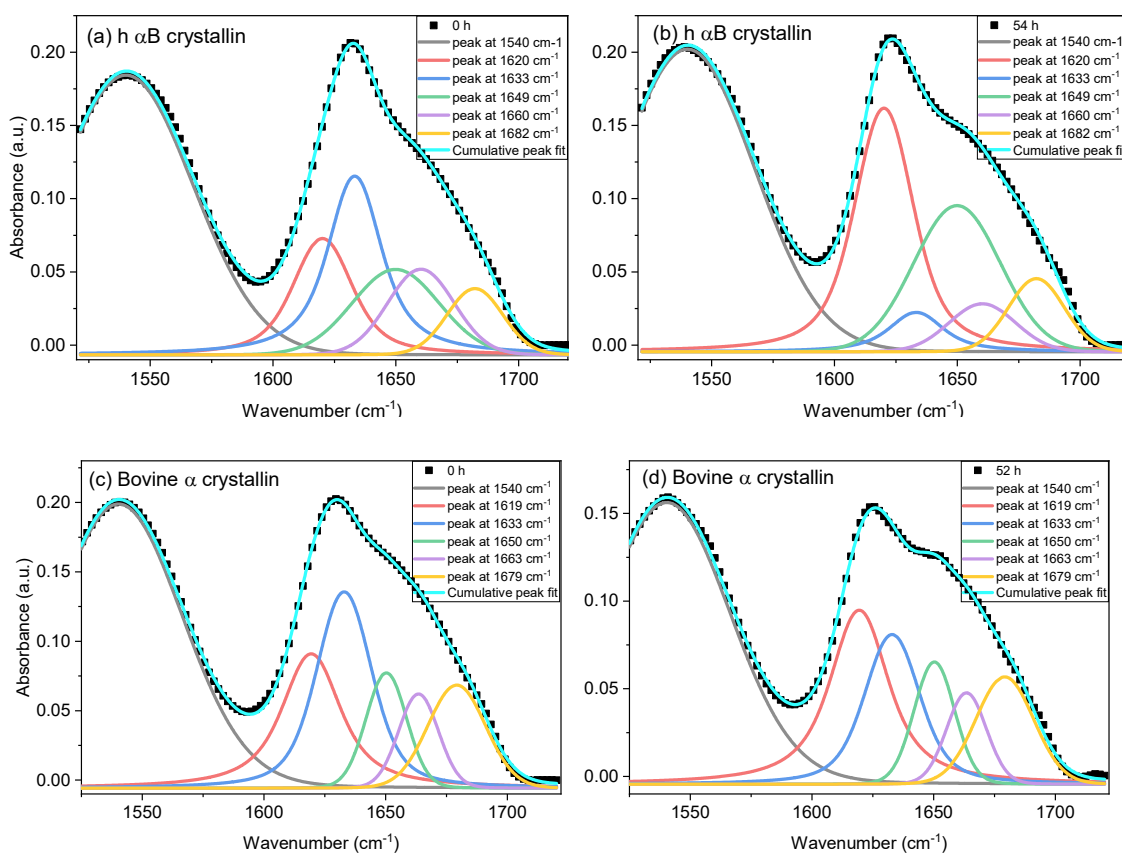


Figure 33: Peak deconvolution of of h α B crystallin spectra at 0 h and 54 h and for bovine α crystallin spectra at 0 h and 52 h.

The peak deconvolution of bovine α crystallin spectra at 0 h and after 52 h at 60 °C is shown in Figure 33 (c) and (d). As observed earlier the crystallins show a prominent peak at 1633 cm^{-1} which is typically attributed to β -sheet structure, owing to its dominance in the ACD region. As opposed to h α B crystallin, a relatively higher proportion of amyloid like β -sheet (1619 cm^{-1}) is observed at 0 h. After 52 h, a noticeable increase in the peak at 1619 cm^{-1} and a decrease in peak at 1633 cm^{-1} is observed, with the peak at 1650 cm^{-1} , 1663 cm^{-1} and 1679 cm^{-1} remaining relatively constant.

Before we turn to a closer inspection of the kinetics, we focus on the changes observed upon further heating. Based upon the now known and fixed band positions, Figure 34 shows the peak deconvolution for spectra obtained at 20 °C and 85 °C for h α B and bovine α crystallin. For both the crystallins at 20 °C the peak at 1633 cm^{-1} corresponding β sheet was prominent, but is significantly reduced at 85 °C. As was already pointed out earlier, crystallins undergoes extensive structural change when annealed at 85 °C, which is well above its denaturing temperature. This was additionally evident from the broadening of the amide I peak.

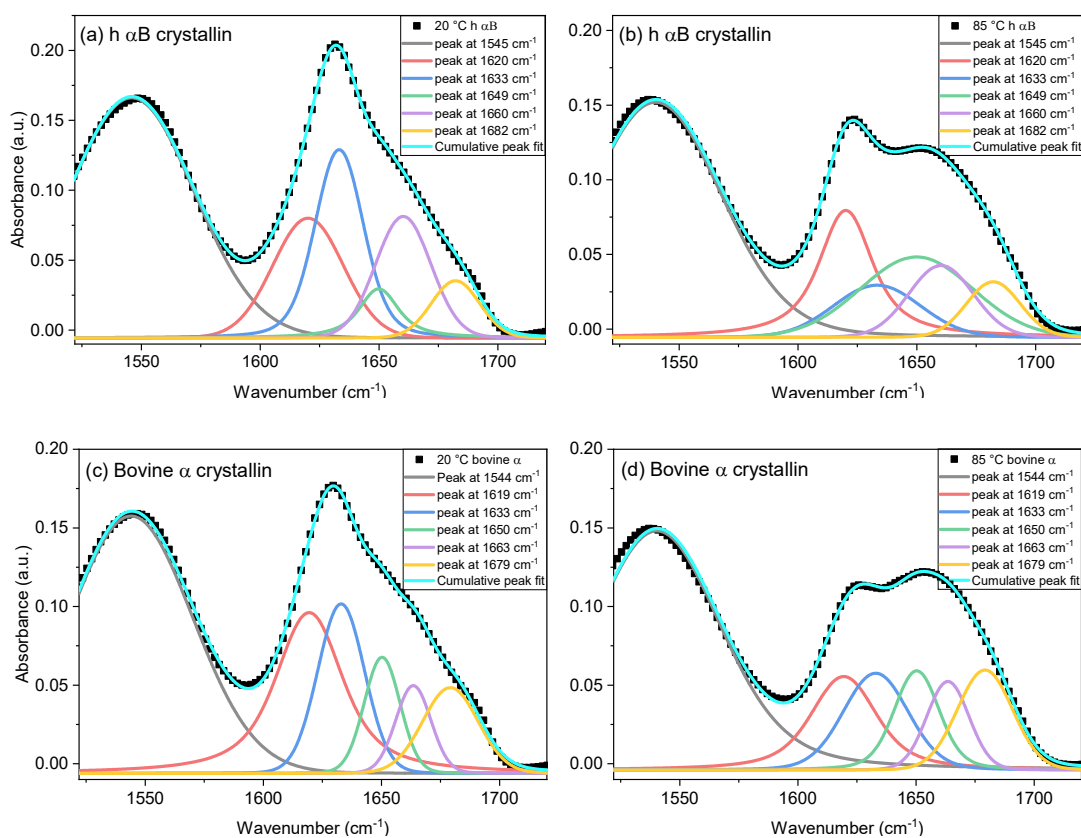


Figure 34: Peak deconvolution of h α B and bovine α crystallin spectra at 20 °C and 85 °C.

Coming back to the more relevant annealing kinetics the change in the amplitude of the 5 major peak positions namely 1620 cm^{-1} , 1633 cm^{-1} , 1650 cm^{-1} , 1660 cm^{-1} and 1680 cm^{-1} at 60 °C over the course of the annealing time is shown in Figure 35. The amplitudes were normalized by considering the amplitude of amide II as a constant internal intensity standard.

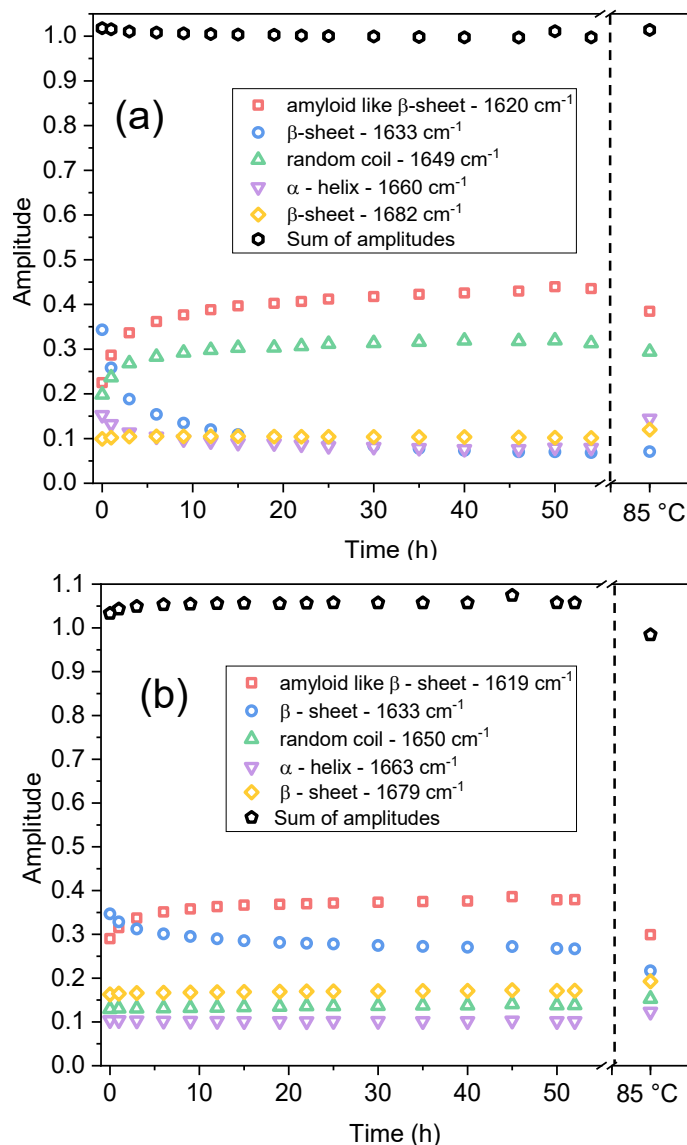


Figure 35: Change in the peak amplitudes for a. h α B crystallin and b. bovine α -crystallin when heated at 60 °C and when heated at 85 °C

Figure 35 illustrates the significant changes in the secondary structure of the crystallin proteins due to the effect of annealing at 60 °C. Additionally, the amplitudes obtained when annealed at 85 °C was introduced for a comparison. Firstly, to check the consistency of the peak deconvolutions, used to estimate the peak amplitude for each of the secondary structure, the sum of amplitudes was included in Figure 35 as well. As expected, the fractional peak areas sum up to unity in all case, providing a consistency check. For the h α B crystallin over time, a sharp decrease in the amplitude of the peak at 1633 cm^{-1} is observed which corresponds to its inherent β sheet, and concomitantly there is an increase in the amyloid β sheet, which is the peak at 1619 cm^{-1} . Interestingly, the fraction of disordered structures (peak at 1650 cm^{-1}) increased as well, although only a small decrease was observed for the α helix structure (peak at 1663 cm^{-1}).

On the contrary, for the bovine α -crystallin the decrease in the β sheet is not as striking as for the h α B crystallin, and an increase in the amyloid β sheet was noticeable. Furthermore, the peaks corresponding to the disordered structure, α - helix and β - turns remained fairly constant, which is an indication that the bovine α -crystallin underwent a rather minimal secondary structural change in comparison to h α B crystallin, when heated at 60 °C over 50 h. Interestingly, the peak corresponding to disordered structures at 1650 cm^{-1} behaved starkly different with a large noticeable increase for the case of h α B crystallins, while remaining rather constant for bovine α crystallin. This could point to the instability of α -crystallin as a homooligomeric protein and the would be more stable as an heterooligomer.

Although the data obtained at 60 °C cannot be directly compared to the spectra at 85 °C, it could be presumed that when left at 60 °C for a longer time, the crystallins could undergo a similar extensive structural transition. H α B crystallin at 85 °C showed an increase in the α -helical (peak at 1660 cm^{-1}) content with a decrease in the predominant β - sheet structure. Similarly, for bovine α -crystallin a rather small increase in the disordered and α -helical contents were observed. It has to be noted here that due to the extensive structural changes, there is a possibility of overlap of the intensities of the different structural components and the estimation here may not be fully accurate.

It could therefore be presumed here that the changes observed in our investigation during the gelation at 60 °C, the β -sheets become more ordered similar to that of an amyloid β -sheet arrangement, without undergoing an extensive structural change. The gelation occurring here could involve reorganization/transformation of intramolecular β -sheets to intermolecular β -sheets, but we note that TEM suggests the globular structure is retained. Thus, the prolonged exposure of these proteins at 60 °C does not substantially affects its secondary structure. At the thermotropic transition temperature, these proteins undergo minor secondary structural changes that eventually lead to gel formation. The gelation possibly leads to the arrest of this state, preventing further structural changes, i.e., once formed, these large aggregates appear to be frozen into their new organization.

6.2.2.5 *Molecular interactions investigated using small angle X-ray scattering (SAXS)*

SAXS has been routinely used to study properties of macromolecule in the nanometer regime especially, changes in molecular interactions, interaction potentials, size and conformation during certain perturbations. One of the advantages of using SAXS, in comparison to other protein characterization techniques like DLS, CD or fluorescence is that with SAXS the protein can be studied under its physiologically relevant concentration conditions. This makes it feasible to get a better understanding of the interactions that exist in the colloidal-like protein environment found for e.g., in the cell's interior or within the eye lens.

In this section, the use of X-ray scattering to investigate the gelation of BSA (as a comparison), h α B and bovine α -crystallin when thermally stressed at 60 °C are discussed. Initially the

proteins were characterized at low concentrations conditions and further on compared to highly concentrated protein solutions.

6.2.2.5.1 Heat-induced structural changes in bovine serum albumin (BSA) solution

Bovine Serum Albumin (BSA) is one of the most commonly investigated globular proteins. The heat-induced changes associated with these globular proteins have been extensively studied with a high emphasis on its gel formation and stability, due to its several significant applications in food industry. In this study the changes associated with it over time at 60 °C at pH 7.5, are compared to those of crystallins under the same conditions. It has already been shown that at 60 °C BSA undergoes thermally induced unfolding and aggregation (Borzova et al. 2016).

Initially, thermally induced aggregation of BSA was investigated as a function of concentration. Figure 36 depicts the scattering intensities of a 20 mg/ml BSA solution at room temperature, at 60 °C and after subsequent cooling. The measurements times were 2 h each. Obviously, an increase in temperature, induced a significant change of the shape of the scattering curve, with a concomitant intensity increase at low scattering angles, indicative for an increase in particle size. This can be attributed to contributions from interparticle interactions. Indeed, fitting the scattering intensity by an ellipsoidal form factor revealed an increased size of the scatterer with R_a (rotational axis) = 24.7 ± 1.2 Å and $R_b = 82.1 \pm 0.7$ Å (avg. R_g of 55 Å) at 60 °C compared to R_a (rotational axis) = 15.3 ± 1.0 Å and $R_b = 49.3 \pm 0.3$ Å (avg. R_g of 33 Å) at 20 °C. This increase is indicative of a heat-induced aggregation of BSA. The irreversibility of this aggregation process is depicted by the scattering curve obtained after cooling (green curve), as the aggregate does not disassemble at low temperatures.

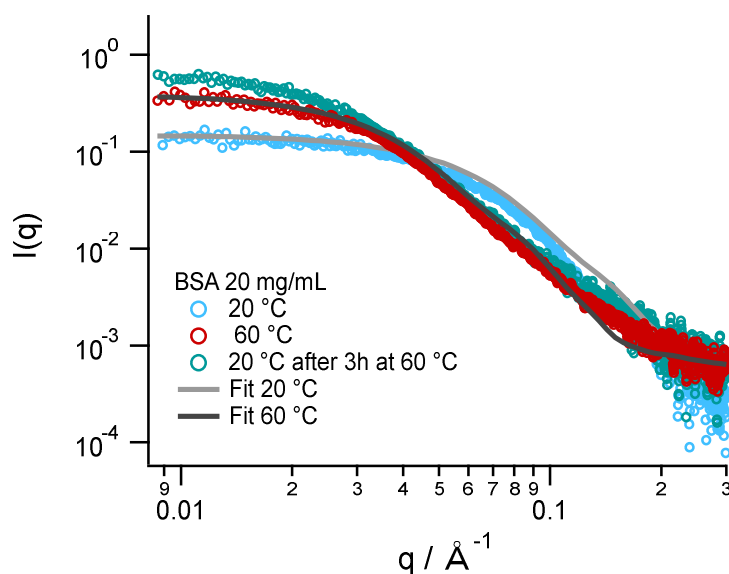


Figure 36: Scattering intensity curves of BSA at 20mg/ml, before heating, at 60°C and after heating at 20°C.

At high concentrations, the repulsive inter-particle interactions add to the scattering signal and the scattering intensity decreases at small q values (see Figure 37 a). In the same manner, a BSA solution with a high concentration (200 mg/ml) was exposed to thermal stress at 60 °C for 15 h, and the scattering curves were recorded after every 60 mins. As is seen in Figure 37 a, with increasing exposure time the scattering intensities increased at low q . The information regarding the spatial arrangement and the interference effects between proteins (with the known form factor), can be accessed by the structure factor. This is readily obtained by calculation of the q – dependent ratio of the experimental scattering intensity and the form factor (Equation (22)). The structure factor can be used to deduce information regarding the interactions between the particles of the superstructure formed during aggregation. The structure factor depicted in Figure 37 b, is obtained by division of the scattering intensities in Figure 37 a by the form factor obtained at 20 mg/mL, 20 °C (grey). The red curve in the Figure 37 b is the structure factor for BSA at high concentration and room temperature. After raising the temperature, the structure factor increased by one order of magnitude at low q . With time, the intensity increases at low q even further, eventually reaching a plateau after 15 h while forming gel. Moreover, the peak at $q = 0.1 \text{ \AA}^{-1}$ in the structure factor seen at the beginning of the experiment reflects the distance of the closest neighbors ($R_{cc} = 62.8 \text{ \AA}$, the distance between the centers of the particles), which eventually vanishes over time as the gelation progresses. The change in the shape of the curve over time demonstrates that the gel formation for BSA involves a slow overall structural change. For the final gel formed by BSA at 200 mg/ml after 15 h, the fractal dimension was found to be 1.2, indicating a linear and slightly branched aggregates.

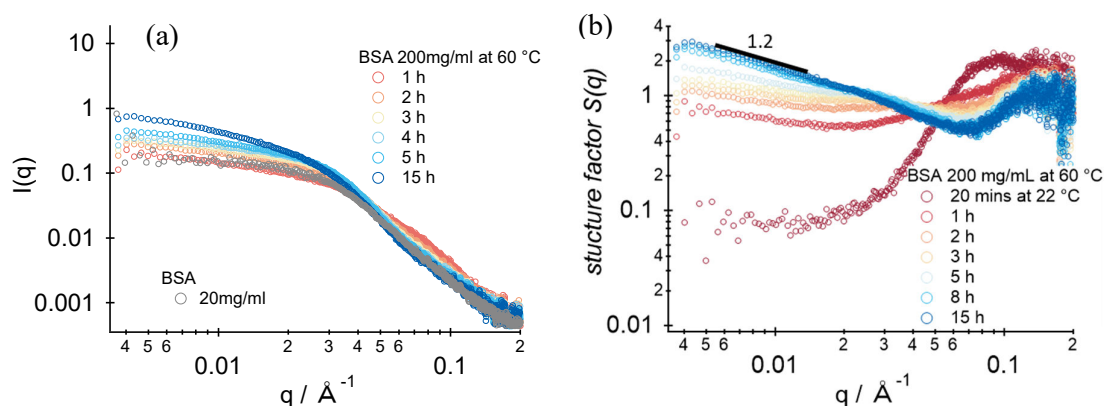


Figure 37: a. Scattering intensity curve obtained over the course of thermal stress at 60°C of BSA at 200mg/ml. b. Structure factor obtained from the data in 'a'.

6.2.2.5.2 Heat-induced structural changes of h α B and bovine α -crystallin: A comparison at different concentrations

In this part we study the concentration dependence of the temperature induced protein-protein interactions and structural rearrangements of the two eye lens crystallins h α B and bovine α .

For this reason, the heat-induced changes associated with the crystallin at a concentration of 20 mg/ml and 200 mg/ml were recorded with increasing exposure time at 60 °C.

6.2.2.5.2.1 H α B crystallin

The X-ray scattering profiles of the heat-induced changes of h α B crystallin a homooligomer, at low concentration is plotted in Figure 38. At 20 °C an initial mean radius of gyration of about 61.0 ± 0.5 Å (relative distribution – 0.11) was obtained using a scattering function of polydisperse spheres for data fitting following Equation (26). After heating at 60 °C, the scattering intensity changed significantly. The size of the scatterers had increased to 75.9 ± 1.2 Å (relative distribution – 0.4). With time, a slow additional increase in the scattering intensity at the low q range was observed, reflecting a slow change in the particle's relative arrangement.

The subtle clustering of proteins was studied using the concept of the fractal dimensions. For h α B crystallin at the low concentration of 20 mg/ml we found after 72 h a fractal dimension of 1.4 using Equation (28) in combination with the form factor of polydisperse spheres (see fit Figure 38). The results indicate that h α B over the course of heating also forms a linear, slightly branched network (see Figure 17)

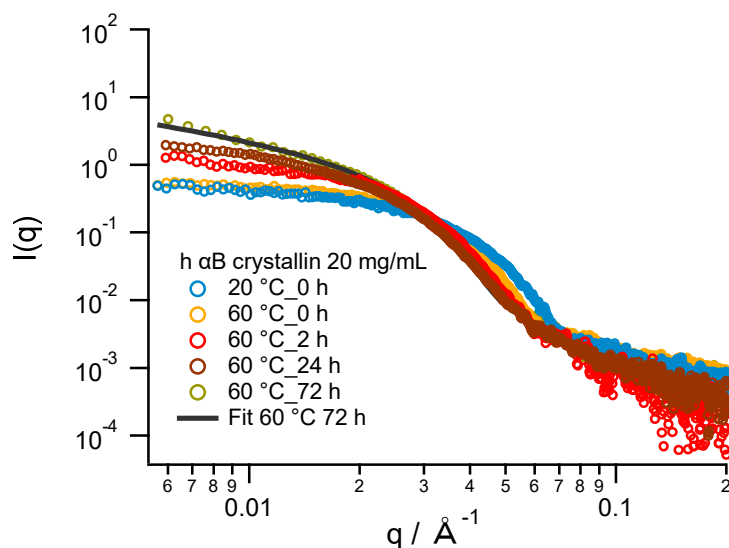


Figure 38: Scattering curves of h α B. low concentration 20 mg/ml when thermally stressed over 72 h at 60 °C.

Moreover, information regarding the change in native folded state can be accessed from normalized Kratky plots i.e., $I \times (qR_g)^2$ vs (qR_g) . The Kratky plots were normalized using the R_g of 75.9 Å and are displayed for different heating times in Figure 39. In its native state, h α B crystallin have an essentially globular structure, which is evident from the maximum at qR_g with a value of 1.7 that was maintained even at elevated temperatures. It was observed that after 2 h the maximum is still located at $qR_g = 1.7$ agreeing well with theoretical expectations. With increasing waiting time, the bell-shape of the Kratky plot remained with a

gradual shift of the peak towards lower values and a concomitant increase. While both changes can be attributed to the structural rearrangements and are of minor importance, the bell shape of the curve confirms a folded state. Partial unfolding would have led to a linear increase of the normalized Kratky plot towards higher values of qR_g (see section 5.6.1.6, Figure 18).

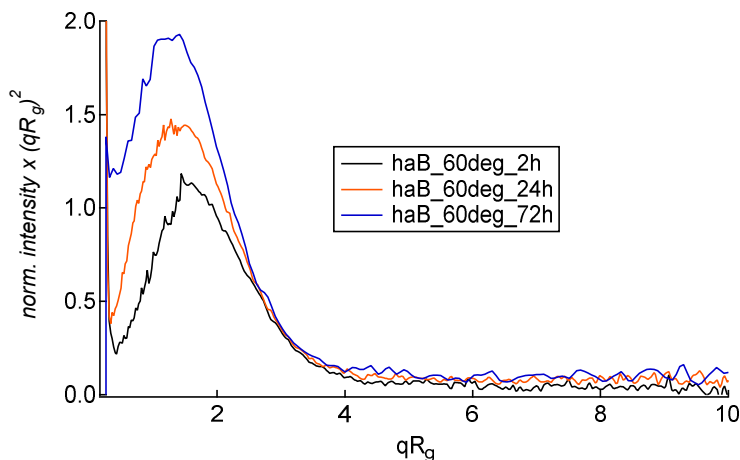


Figure 39: Kratky plot of human α B-crystallin at a concentration of 20 mg/ml, at different waiting times at 60 °C.

To summarize the effect of temperature for lowly concentrated h α B solutions, we found an initial temperature-induced increase in size while there were no indications for temperature-induced unfolding. The proteins, however, formed a linear, slightly branched network structure. This finding should be now compared to the sample at a higher, near-physiological concentration of 200 mg/ml. The initial scattering intensity of 200 mg/ml h α B at 22 °C decreases at small q values compared to the 20 mg/mL sample indicating net repulsive interparticle interactions (Figure 40 a). As it was observed for the lowly concentrated sample (see Figure 38), the heat exposure of 60 °C led to an initial increase in size followed by a gradual increase in the scattering intensity in the low q -range with time (Figure 40 b). The structure factors displayed in Figure 40 c was calculated using the form factor at 60 °C of the lowly concentrated sample in order to discuss the structural changes with time.

With the progression of thermal stress, the repulsive interactions gradually disappeared (0 h - 17 h) and eventually, the formation of a superstructure could be indicated (51 h - 67 h). The last in situ-measurement was compared to the scattering characteristics of gels formed outside the instrument in an oven (gel, 29 h) and in the FTIR microscopy cell (gel, 45 h). As opposed to BSA, the repulsive interaction in h α B disappeared rather slowly and eventually by the end of 67 h a gel is formed, which is suggestive of aggregation. Using the fitting function of Equations (26, 27) the block radius of such an aggregate amount to about 80.0 ± 2.2 Å compared to the initial size of the protein being 57.0 ± 1.0 Å (22 °C) and 75.9 ± 1.2 Å (60 °C). A fractal dimension of 1.1 was obtained which is typical for a newly unbranched 1D aggregated linear chain.

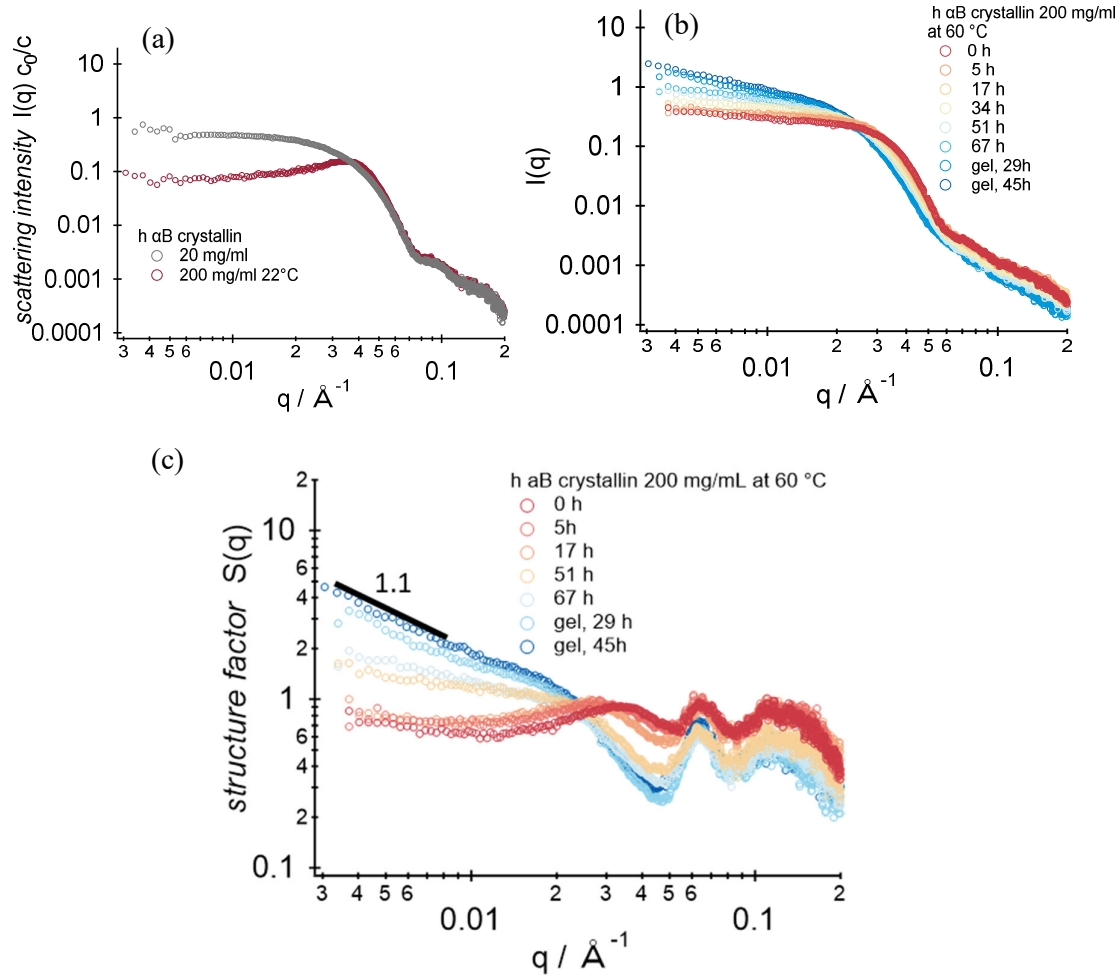


Figure 40: a. Effect of increased concentration on the scattering intensity, b. Scattering curves and c. Structure factor curves of h α B 200 mg/ml when thermally stressed over 67 h at 60 °C.

6.2.2.5.2.2 Bovine α -crystallin

In a similar experimental setup, the X-ray scattering profile for bovine α -crystallin protein, a hetero-oligomer consisting of both α A and α B subunits, were obtained initially at low concentration (Figure 41). In the beginning, at 20 °C the radius of gyration of bovine α -crystallin was found to be $59.0 \pm 0.2 \text{ \AA}$ (relative distribution - 0.3). At elevated temperatures of 60 °C, the intensity of the scattering curve initially decreased at low q values. The radius of the scatterer was about $70 \pm 1.5 \text{ \AA}$ using the Schulz sphere distribution function. With increasing incubation times at 60 °C, however, the intensities at low q values increased again, which was accompanied by a slight left-shift of the scattering decay. Indeed, a fit of the scattering curve at 72 h (Schulz sphere), showed an increase in particle size to $74.0 \pm 1.3 \text{ \AA}$ (relative distribution - 0.3) and a fractal dimension of 1.8 using Equation (28). The latter is indicating a branched network structure. Interestingly, increasing the heating time to 120 h, the mean radius for bovine α -crystallin did not increase further ($75.0 \pm 1.1 \text{ \AA}$), but the network was further maturing. The fractal dimension increased to 2.04 which is an even denser network structure.

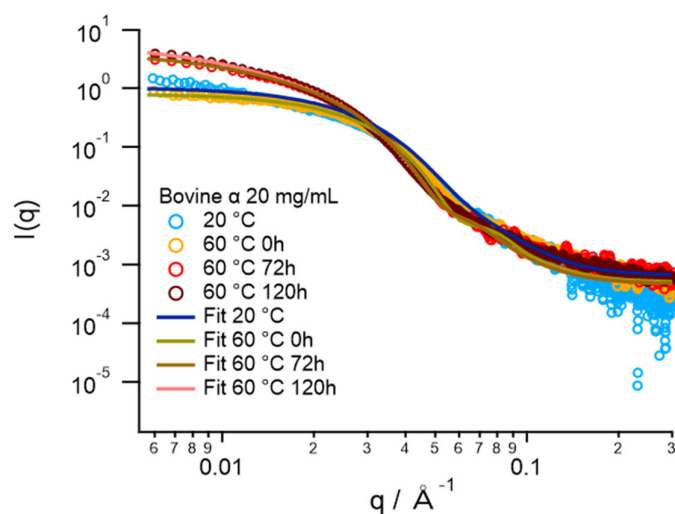


Figure 41: Scattering curve of Bovine α crystallin low concentration 20 mg/ml when thermally stressed over 72 h

The Kratky plots for thermally stressed bovine α crystallin at different incubation times (2 h, 24 h, and 72 h) are represented in Figure 42. The plots revealed a maximum at qR_g that is initially at 1.7 that confirms a globular structure. Similar to α B, bovine α crystallin maintains a defined maximum through the course of thermal stress, which is again an indication that these proteins do not thermally unfold.

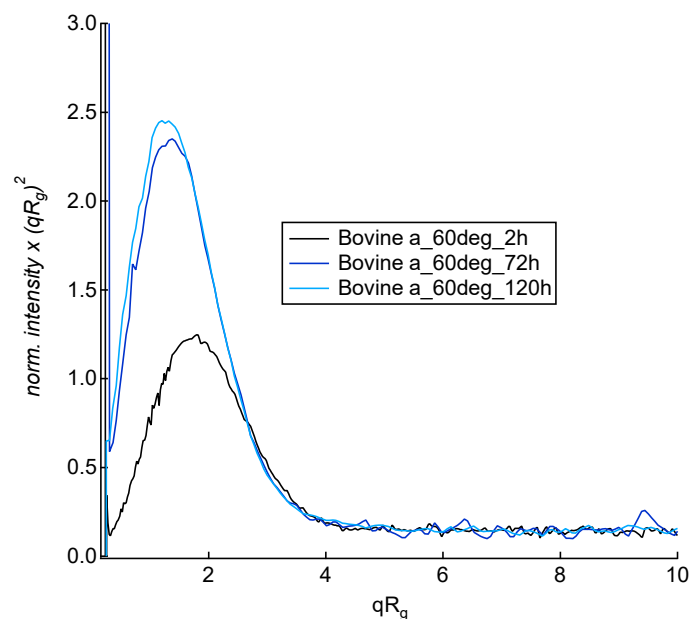


Figure 42: Kratky plots of bovine α -crystallin at a concentration of 20 mg/ml, at different waiting times at 60 °C

6.2.2.5.2.3 Structure factor analysis

The investigation of lowly concentrated bovine α -crystallin revealed that heating to 60 °C did not substantially affect sizes nor folding, despite the observed increased interparticle interactions and contacts. This was also true for the highly concentrated sample as shown in Figure 43 a. The scattering curves showed a rather slow and marginal increase in the scattering intensity at the low q - values. Even the gels that were independently formed by heating in an oven (blue full symbols Figure 43 b) or within the FTIR setup (during FTIR experiment) displayed the same feature (Figure 43 b, black curve).

The structure factor curves (Figure 43 c) were calculated using the form factor obtained for low concentrations at 60 °C. The low q – values <1 of $S(q)$ imply a strong repulsive system that did not change during heating for the observed q - range (up to 45 h). The α -crystallin sample from the FTIR experiments showed at least an onset of a probable inter particle interaction at low q - values. Physically, the sample behaved like a gel, hence it is probable that the interaction related contribution term for the highly concentrated sample might be apparent only at lower q - values.

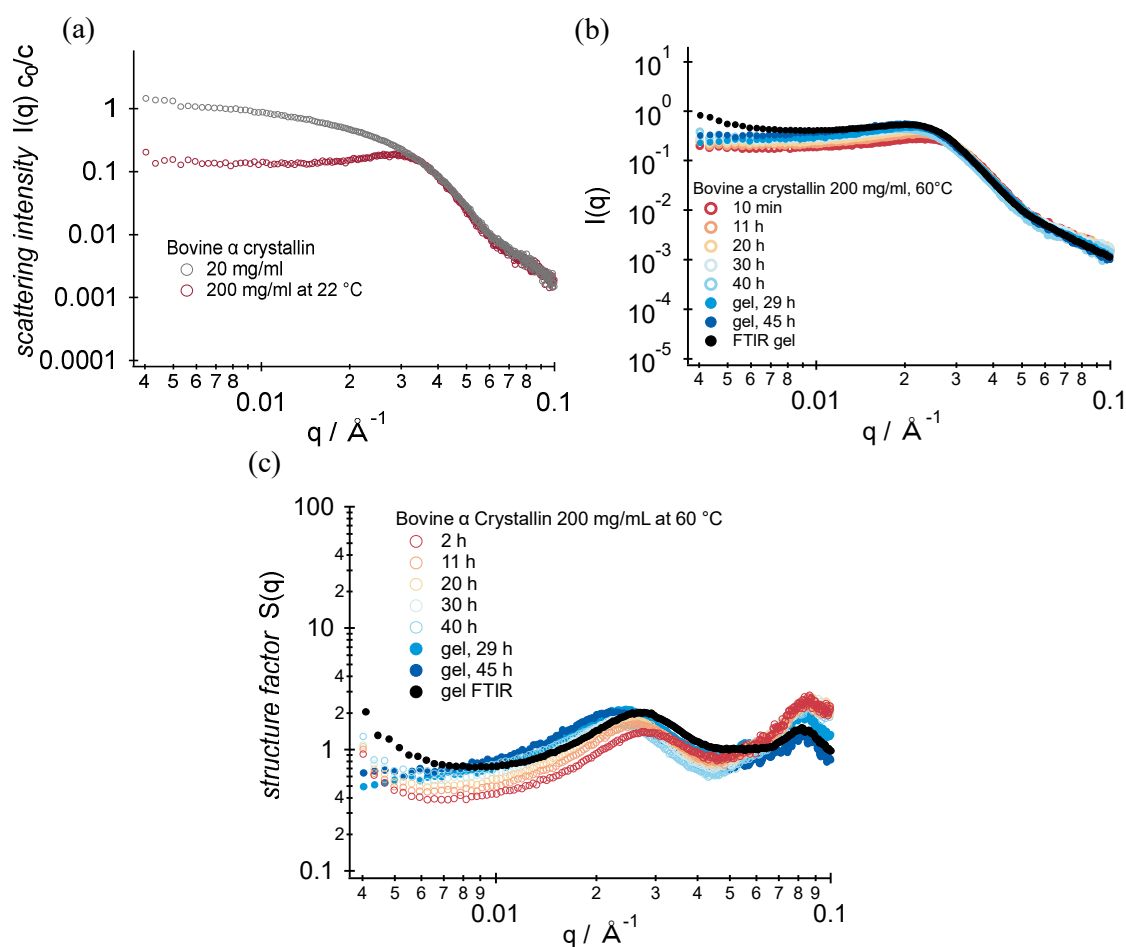


Figure 43: a. Effect of increased concentration on the scattering intensity, b. Scattering curves and c. Structure factor curves of Bovine α 200mg/ml when thermally stressed over 45 h at 60 °C

We examined in more detail the interaction potential using a sticky hard sphere potential, which is used to describe the short-range attraction between protein clusters. The sticky hard sphere potential is defined as,

$$U(r) = \begin{cases} \infty & r \leq \sigma \\ -u_0 & \sigma < r < \sigma + \Delta \\ 0 & r > \sigma + \Delta \end{cases} \quad (31)$$

Here, u_0 is the depth of the potential well. The structure factor therefore, provides information regarding the interaction potential and strength of an attractive well that can be characterized in terms of ‘stickiness’ (Sauter et al. 2016). The stickiness is defined as τ , which is a function of both the interaction strength and perturbation parameter and is given as,

$$\tau = \frac{1}{12\varepsilon} \exp(u_0/kT) \quad (32)$$

where u_0 and ε the perturbation factor describes the range of interaction relative to the particle’s radius. After a heating time of 2 h we found u_0 to be 0.45 ± 0.05 kT and $\varepsilon = 0.24 \pm 0.003$, which would correspond to an interaction range of 5.9 nm (Figure 44). The stickiness parameter τ was about 0.54 ± 0.02 . After about 45 h the stickiness parameter increased to 0.68 ± 0.06 , with the perturbation parameter $\varepsilon = 0.26 \pm 0.01$ and u_0 was found to be 0.77 ± 0.11 kT. α -crystallins are known to show a repulsive hard core interactions that conceivably keeps the crystallins from collapsing and forming an aggregate (Foffi et al. 2014). The repulsion that is persistent in this case after heat stress originate from the hard sphere potential rather than the charges on the protein.

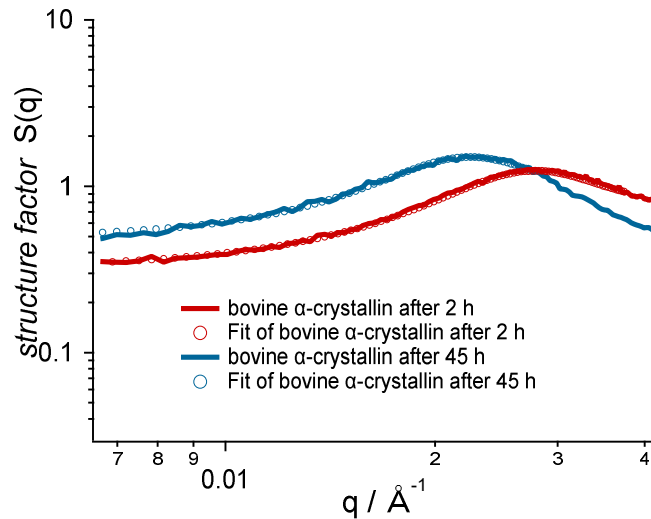


Figure 44: Fits of the structure factor of bovine α -crystallin 200 mg/mL after 10 mins and 45 h

6.2.2.5.2.4 Comparing h α B and bovine α -crystallin gels

A similar analysis was performed for h α B (Figure 45), where the depth of the potential well u_0 after 2 h was 0.006 ± 0.01 kT. Compared to bovine α , h α B crystallin revealed a smaller initial τ value of 0.30 ± 0.02 that vanished with time while forming a long-range network (Figure 45). Contrarily, bovine α -crystallin showed a τ value of 0.68 ± 0.06 even after 45 h, still displaying a sticky sphere with rather transient interactions. Due to the stickiness, the particles are still rather dynamic oligomer and hence a weak dynamic network is formed.

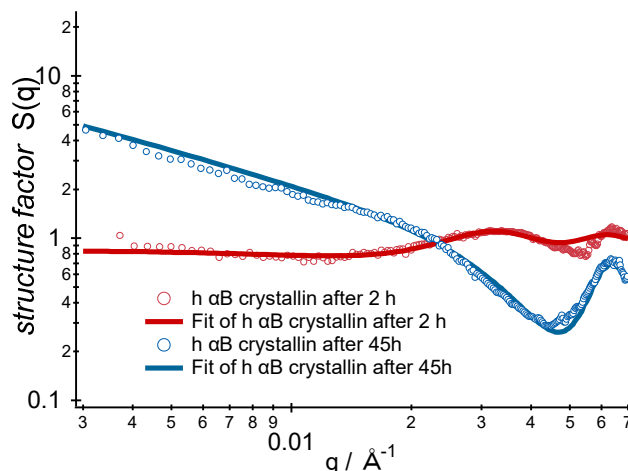


Figure 45: Fits of the structure factor of human α B-crystallin 200 mg/mL after 2 h and 45 h

The X-ray scattering of heat induced crystallins at high concentration showed that over time both of the proteins aggregate and form superstructures. Human α B-crystallin when thermally stressed forms a gel, composed of independent ‘sticky’ sphere leading to an extended network of unbranched linear chains. Bovine α -crystallin maintains its repulsive interaction throughout the course of thermal stress and forms a gel by transient, most probably weak hydrophobic surface-surface interactions.

The structural changes associated with h α B crystallin and bovine α crystallin at 20 mg/ml and 200 mg/ml when subjected to thermal stress at 60 °C was investigated using SAXS and compared to a model protein BSA. In general, for both the crystallins, with increasing annealing time at 60 °C, an aggregation is observed, forming different superstructures. It is important to note here that the change induced by the thermal stress remained irreversible in both the cases. Overall, both the crystallins tend to form larger aggregates/oligomers, by essentially maintaining their globular structural form.

6.2.2.6 Mechanical properties of human α B- and bovine α -crystallin

We further attempted to estimate the mechanical properties of the gels formed by the crystallin proteins using rheology. The initial tests performed using rheometer were unsuccessful, since the preparation of the gels at high-concentrations within the rheological plate-plate setup was

rather challenging. The gelation time was quite long which in turn resulted into evaporation of the solvent causing the samples to dry out. We also attempted to test the mechanical properties using the nanoindentation method using PIUMA nanoindenter, wherein the samples were sent to Optics11 Life, Amsterdam. The attempts were unsuccessful since the gels formed were very sticky and adhered to the probe. The data obtained were therefore unreliable. Finally, the gels were to be tested using the atomic force microscopy at Technical University Darmstadt. Using dynamic indentation, it was tedious to obtain results due to the extremely low moduli of gels in buffer, that almost exceeded the measuring capability. But we were able to obtain the elastic modulus for h α B-crystallin at 200 mg/mL concentration, which was estimated to be 200 Pa, whereas storage modulus was 70 Pa and loss modulus 40 Pa. A force curve obtained for h α B-crystallin is shown in Figure 46. The measurement was unfortunately not reproducible. Further analysis of human α B- and bovine α -crystallins was not possible due to the sample limitations.

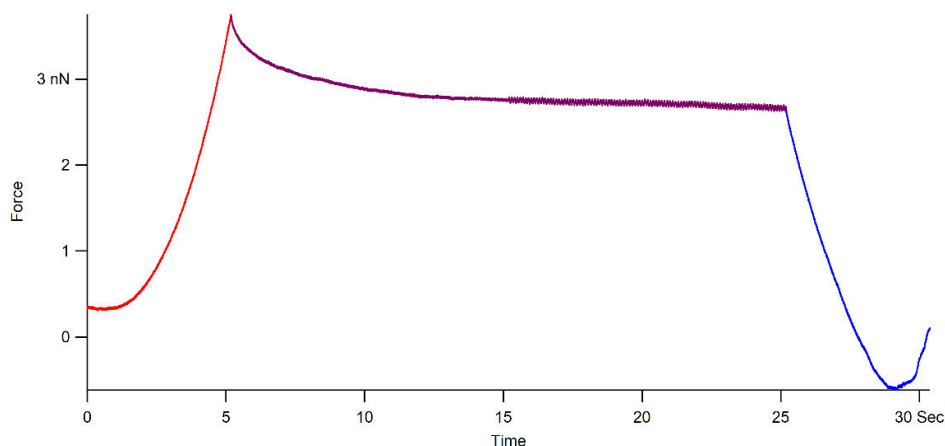


Figure 46: Force curve obtained for h α B-crystallin at 200 mg/mL.

6.2.3 Conclusion

As is generally known globular proteins, under the influence of certain stress of and above a critical concentration, can form a three-dimensional gel network. In this chapter, a detailed examination of gelation of α -crystallins a prominent eye lens globular protein has been conducted. Predominantly, the gelation propensity of human α B-crystallin, a homooligomer and bovine α crystallin, a heterooligomer composed of both α A and α B subunits, have been investigated at physiological pH of 7.5. Both the crystallin proteins formed gels upon prolonged annealing at 60 °C, which is well below its denaturation temperature. This enabled a gradual investigation of changes in the protein conformation and interactions, which in turn in certain aspects mimic the slow ageing process of the eye lens proteins.

The prolonged exposure of these crystallins at temperature well below the denaturation temperature led to the formation of gel network. The turbidity test showed that the gels formed by human α B-crystallin are relatively turbid while those of highly concentrated bovine α crystallin was transparent. Here the lowly concentrated bovine α -crystallin was stable and remained soluble throughout. Further on the change in the particle size was investigated using

dynamic light scattering at low concentrations. The heating caused a general increase in size of the particle, but the rate of change in particle size was higher for human α B-crystallin. Also, it was observed that after 22 h h α B clearly formed larger particles, with the solution being turbid. This is a possible indication of denaturation and aggregation. Bovine α crystallin on contrary showed a gradual increase in size but remained in a homogenous state without undergoing denaturation. TEM images showed that the globular structure of the proteins remains intact after the gel formation. From the ATR FTIR experiments it was observed that heating did not substantially affect the secondary structure of these proteins. The shift in the amide-I peak was still within the β -sheet structure, which could indicate a more ordered structuring of the β -sheets. This further confirms the observation from the TEM images that the protein does not undergo extensive structural modification on heating and the globular structure is intact.

The changes in the protein interactions and aggregate size when the crystallins h α B and bovine α form a gel was firstly investigated using scattering technique. For this study, bovine serum albumin was used as a model protein to get a better insight into globular protein aggregation and gelation. For a comparison, initially the changes associated with BSA were investigated. The kinetics of heat-induced changes probed for both low- and high-concentration BSA, showed that within the first hour the protein aggregated to form larger network structures. For the crystallin proteins the heat-induced formation of larger oligomers was a gradual process. It was interesting to note that the different crystallin proteins have different gelation propensity. At low-concentration (20 mg/mL) the hard-core repulsions are negligible. The h α B crystallins with increasing incubation time gradually increased in size, which was indicated by intensity increase in at low angles. Even though a similar observation for bovine α -crystallin was recorded, the increase in size was marginal. Therefore, the observations can be attributed to the change in particle interaction with time. From Kratky plots it could be confirmed that the formation of larger aggregates proceeded without denaturation, since the overall globular structure remained intact even after longer exposure time. H α B crystallin eventually formed a stable long network structure while bovine α crystallin formed network 'possibly' having a more dynamic network structure. The results obtained from the ATM studies to estimate the mechanical properties of the gel was rather inconclusive. The indentation experiments will therefore be repeated once the materials become available.

6.3 Effect of Magic Angle Spinning (MAS) on solid-state NMR resolution of α B-crystallin protein probed using $T_{1\rho}$ relaxation

Crystallin proteins are water soluble protein which makes it extremely accessible to investigate these proteins using most experimental techniques. As already known from literature (Horwitz 2003), the α B-crystallins generally exist as high-ordered oligomers, with only the flexible parts being accessible by solution state NMR. These large oligomeric assemblies are rather polydisperse and therefore cannot be crystallized. This hampers the well resolved full-length solution NMR spectra of these proteins. Therefore to analyze this complex system a hybrid approach of solution and solid state MAS NMR is generally used (Mainz et al. 2015)..

In this study sedNMR approach was used, where the sample is sedimented and immobilized into an NMR rotor, which is then spun rapidly inclined at an angle of θ_{MA} of 54.74° with respect to the magnetic field. This ensures a narrowing of spectral line, especially for immobilized solid sample, which is brought about when the overall rotational/tumbling correlation time of the protein is larger than the rotor period. For protein complexes like α B-crystallin with a molecular weight of approximately 600 kDa, the tumbling correlation time amounts to only a few μ s without the MAS (Ravera et al. 2013). This method therefore circumvents the limitation of a standard solution state NMR, by overcoming the molecular weight limit imposed by molecular tumbling.

The aim of this study initially was to investigate the structural changes associated with α -crystallin protein upon gelation. This proved to be quite a challenge, since the heating of the sample within the rotor during spinning was not possible, considering the temperature within the rotor could not be estimated accurately, in addition to the increased temperature due to sample rotation. Also filling the rotor with the α -crystallin gel did not provide any reliable results. Therefore, the focus was then to obtain a well resolved NMR spectra of α B-crystallin with respect to increasing spinning speed and correlate it to the overall tumbling motion of the protein. The slower motions that exist are accessed by $T_{1\rho}$ relaxation measurements. In order to get a better understanding of this effect we first look into the solution and solid-state NMR spectra of α B-crystallin protein.

6.3.1 Solution state NMR experiment with α B crystallin (HSQC)

The 1D proton NMR spectra of proteins generally consist of a multitude of superimposed peaks originating from different proton sites (Figure 47). The slow tumbling of proteins additionally causes line broadening due to the short transverse relaxation time (T_2) arising from the spin-spin interactions. To obtain a well resolved protein spectra, a multi-dimensional approach is employed, wherein proton chemical shift is plotted against either ^{15}N or ^{13}C spin chemical shift. One of the most commonly used technique is the hetero-nuclear single quantum coherence (HSQC) experiment (Bodenhausen and Ruben 1980). The basic scheme here involves initially transfer of magnetization from proton to the nuclei of interest (^{15}N) via INEPT and after a delay

time (t_1), the magnetization is transferred back to proton via another INEPT step. The signal recorded is obtained as an FID with evolution time (t_2). Several such experiments with increasing delay time and Fourier transform in both t_1 and t_2 dimensions, gives a 2D NMR spectra, where the proton chemical shift can be correlated to the neighboring ^{15}N nuclei. Such an HSQC spectrum can therefore be considered as a spectral fingerprint of the protein.

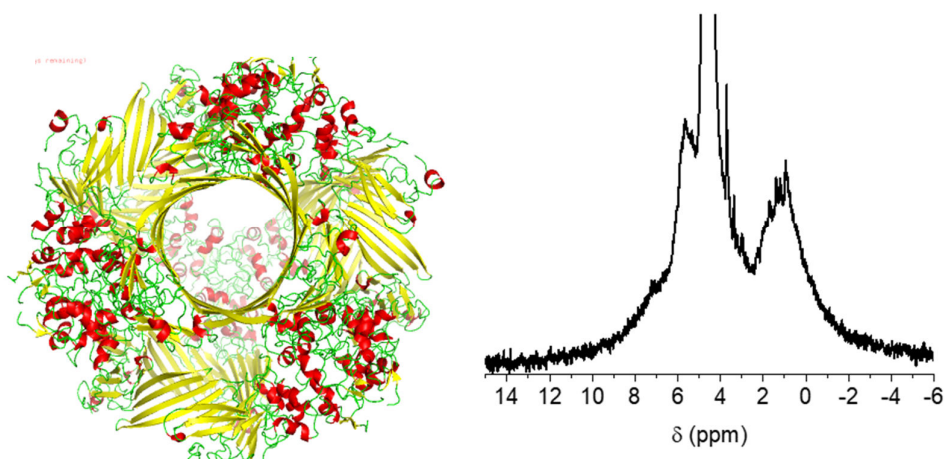


Figure 47: *h* α B crystallin: *pdb* code:2YGD, processed using *pyMol* (Braun et al. 2011a) and 1D proton spectra of *h* α B crystallin at 30°C pH 7.5 in D_2O

The NMR spectra of full-length *h* α B oligomers were recorded. A typical ^1H - ^{15}N HSQC spectra for *h* α B crystallin was obtained as shown in Figure 48, at 22°C pH 7.5. Here the chemical shift assignments corresponds to those published by (Mainz et al. 2015; Mainz and Reif 2015) and was comparable to those observed in this work. Generally, the NMR spectra of particles/proteins having larger size exhibit set of cross peaks that arise from the mobile residues i.e., those which have a faster dynamic compared to the overall particle tumbling motion. This indicates that only the mobile regions of the protein would be observed in the solution state NMR spectra.

For α -crystallin it is quite well know that the C-terminal regions are highly flexible, unstructured, highly polar and has excellent solubility (Delbecq and Klevit 2013; Treweek et al. 2010; Carver 1999). This gives rise to a well resolved solution state NMR spectra, wherein the region starting from S153 to the very end of the C-terminal region which is K175, including the IXI-motif is observed. Apart from the flexible C-terminal region, due to the overall large particle/oligomeric size, complexity and rigidity makes it difficult to obtain the full-length spectra of these protein using solution-state NMR methods.

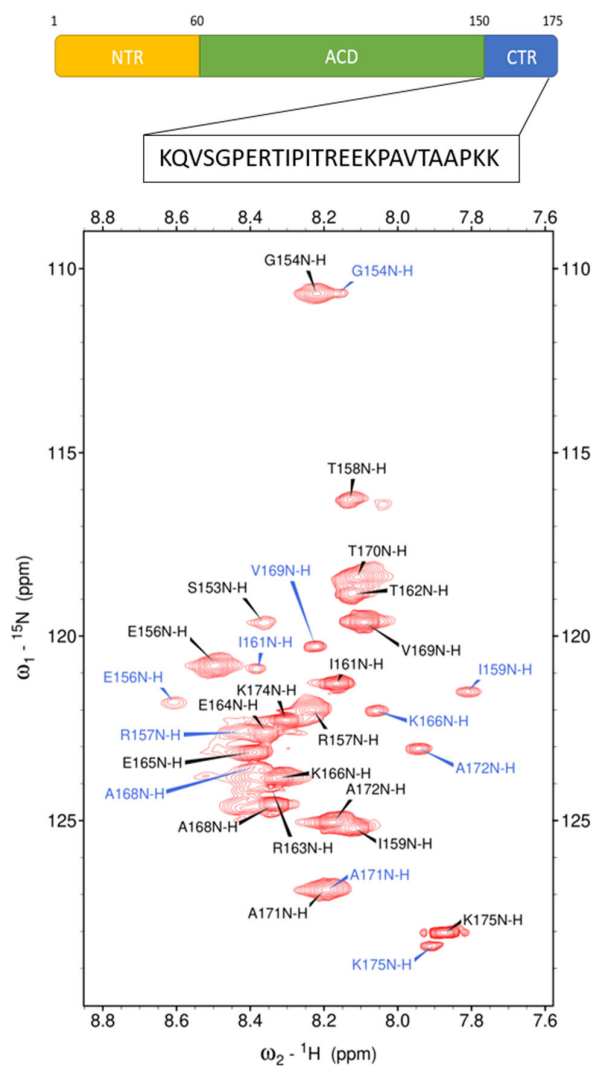


Figure 48: ^1H - ^{15}N HSQC spectra of *h* αB crystallin at 20 °C, *pD* 7.2. Major states indicated in black and minor states in blue.

For almost all the residues in the CTD region a second set of peaks were observed which are in accordance to published data of Mainz (Figure 48). This second set of peaks were classified as minor states having significantly lower intensity. In Figure 48, the assignment for major state is indicated in black and minor state in blue. The minor state could be derived from the same oligomeric species since they were found to have the same translational diffusion, but differed in the dynamics. This indicated that the CTD, exists in two different conformational states that undergoes slow chemical exchange on the time scale of (Mainz et al. 2015)

6.3.2 Solid-state MAS NMR of αB crystallin (TUM Data)

In comparison to solution state NMR studies where only the flexible C-terminal region of αB crystallin are detected, solid state NMR proved to be a better technique to study these proteins at atomic resolution. In general, to obtain a high-quality spectrum the protein has to be rotationally immobilized within the rotor and preparation of such a homogeneous sample is

often a challenge. The MAS NMR experiments were performed here by the sedimentation of the protein into the rotor, where it is investigated in its solution form, as opposed to the conventional SS NMR experiments.

Here, ^{15}N - ^2H labeled h αB synthesized recombinantly in a D_2O based minimal media with exchangeable hydrogens replaced by ^1H , by dissolving in a mixture of H_2O and D_2O -based buffers were used for the experiment. The proton back exchange ratio was about 15 %. Such a predeuteration of the protein yields high resolution spectra in solid state, by suppressing the dipolar interaction between ^1H - ^1H . Figure 49, depicts the ^1H , ^{15}N correlation spectrum of perdeuterated αB -crystallin (this experiment was performed at TUM, by Dr. Riddhiman Sarkar). Here a refocused INEPT approach for solids was used to obtain the correlation spectrum (Elena et al. 2005). The figure shows the characteristic signal pattern of αB -crystallin, which was nearly similar to that observed by (Mainz et al. 2015).

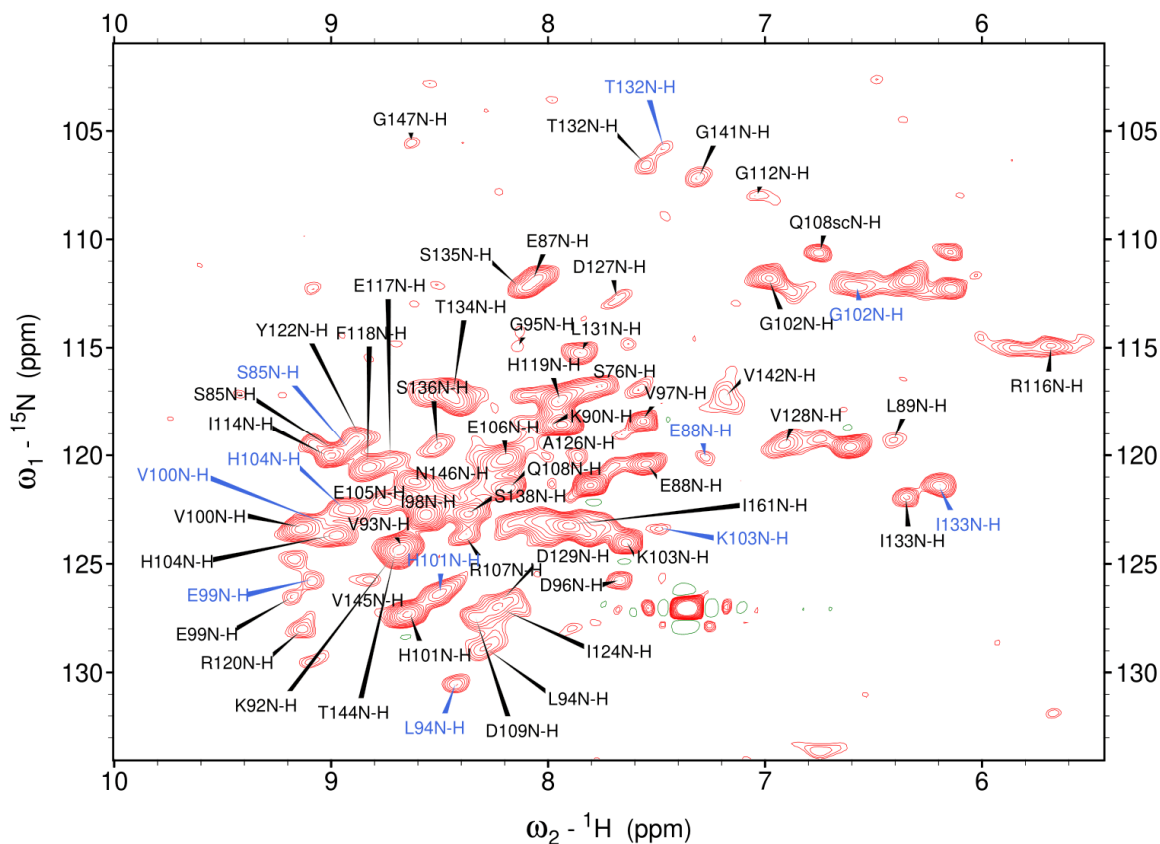


Figure 49: ^1H - ^{15}N solid-state NMR spectra of human αB -crystallin protein (at 4°C , MAS – 30 kHz, in 1.9mm rotor, at magnetic field strength – 18.8T)

Owing to the different experimental setup, where a 1.9 mm rotor at ^1H Larmor frequency of 950 MHz, a well resolved NMR spectra was obtained. Most of the cross peaks obtained corresponded to the amino acid residues from the ACD region. For several residues, a peak doubling was observed which mostly originated from residues close to the loops β_4 , β_5 and β_8 .

This is an indication that in the α B-crystallin oligomers, the ACD region exist in at least two different states, which can be well-resolved (Mainz et al. 2015). In both the cases solid and solution state NMR experiments, the amide resonances of N-terminal residues were not observed. This is an indication that the N-terminal domain is fairly rigid.

6.3.3 Solid-state MAS NMR of α B crystallin (MLU Data)

A similar attempt was made to obtain a solid-state NMR of α -crystallin protein in MLU, Halle (Figure 50). The results obtained showed very broad solid-state spectra with practically unresolved peak intensities. We attributed this to the poor sedimentation of the sample within the rotor and which pointed to the fact that the protein is most likely liquid-like. In general, a narrow line in a high-resolution spectrum is obtained when the spinning at the magic angle, periodically modulates the anisotropic molecular interactions i.e., dipole – dipole and chemical shift anisotropy (CSA). These are eventually averaged out over the sample rotation period in the μ s time range. The averaging is dependent on the correlation time of the motion and the time scale of the rotor period. This means that if the tumbling motion is faster, then the averaging occurs within one rotor period but, if the motions are slower than the rotor period then the system can be considered as rigid during the rotor period and hence, MAS leads to an effective averaging of the anisotropic interactions. However, if during the rotation there is certain motion with a relatively larger amplitude as well as the orientation of the CSA and dipolar tensor changes during the rotation period then the average is no longer zero.

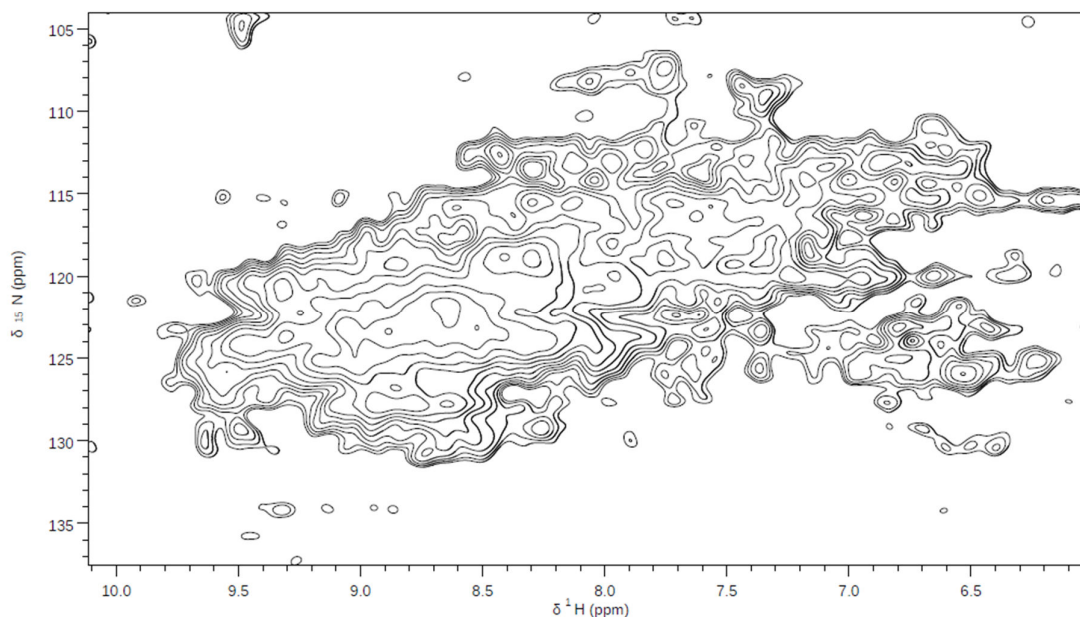


Figure 50: ^1H - ^{15}N solid-state NMR spectra of human α B-crystallin protein (at 13 °C, MAS – 20 kHz, in 1.3 mm rotor, at magnetic field strength – 14.1 T)

In our case we work with sedimented samples which would have protein concentrations much greater than 200 mg/ml, that could lead to an increase in the correlation time but this increase may not be many orders of magnitude. This would mean that the rotation may not be

completely isotropic due to certain restricted motion and the relatively large amplitude of these motions might correspond to the time scale of rotor period. This may have been the case here, where the still liquid-like sediments lead to incomplete averaging of the interactions and eventually lead to bad spectral resolution.

This led to the question if the slower motions within the samples can be restricted with increasing the spinning speed of the rotor. The slower motions were then to be accessed by $T_{1\rho}$ measurements. Within the scope of this study, a solid-state NMR investigation of h α B-crystallin was undertaken. The h α B-crystallins are large globular proteins having rotational correlation time of $\sim 1 \mu\text{s}$ (Roos et al. 2016). Here, the authors showed for α -crystallin that the concentration dependence on the rotational correlation time was the weakest in comparison to that of BSA and HEWL. This weak dependence is due to the spherical and weakly interacting nature of these proteins; they can still undergo smooth rotational motion. The asymmetrical shape of the proteins like BSA and HEWL as well as their strong polar/columbic interactions leads to hinderances in their motion.

This was further investigated in this study where the human α B-crystallin were subjected to increasing magic angle spinning frequency of 20, 30, 40 and 50 kHz. This increase in MAS has two consequences. Firstly, due to increase in centrifugal forces the concentration in the sedimented layers would increase, thereby slowing down the restricted rotational motion. Secondly, as the MAS is increased the rotor period becomes smaller. When the slow restricted motion is on the time scale corresponding to this rotor period results into narrow spectral lines. In case, of incomplete sedimentation of these protein, certain slow motions that might exist would results into an incomplete CP transfer. The idea here was to determine if/how spinning at higher rates would assure averaging of the dipolar coupling and restrict the motions that might occur at short time scales i.e., microsecond range due to incomplete sedimentation

6.3.4 Correlating $T_{1\rho}$ relaxation to MAS dependent spectral resolution

Qualitative information on such protein molecular dynamics that occurs at the microsecond time scale is accessible by measuring the spin-lattice relaxation time in the rotating frame ($T_{1\rho}$). This solid-state near-rotary-resonance measurement of spin-lattice relaxation time i.e. with a small difference between the frequencies of magic-angle spinning (MAS) and spin-lock (SL), enables the detection of slow motions (Krushelnitsky et al. 2018). In the last decade a widespread application of ^{15}N detected rotating frame relaxation rate to study the molecular dynamics. MAS in combination with chemical perdeuteration protein samples, which dilutes the proton network provides a well resolved ^1H - ^{15}N protein correlation spectra. Additionally, it has also helped to measure site-specific relaxation rates, with a marginal dipolar spin contribution to the relaxation process (Zinkevich et al. 2013; Ma et al. 2015; Krushelnitsky et al. 2010).

In order to probe these slow motions, ^{15}N detected $T_{1\rho}$ relaxation measurements were performed. The $T_{1\rho}$ relaxation measured under MAS, that involves contribution from both the

heteronuclear dipolar and CSA relaxation mechanisms each of them is described by a combination of spectral-density function as follows:

$$\frac{1}{T_{1\rho}} = R_{1\rho} \propto (J(\omega_{SL} - 2\omega_{MAS}) + 2J(\omega_{SL} - \omega_{MAS}) + 2J(\omega_{SL} + \omega_{MAS}) + 2J(\omega_{SL} + 2\omega_{MAS})) \quad (33)$$

where, ω_{MAS} and ω_{SL} are the MAS and spin-lock frequencies. The term $\omega_{SL} - \omega_{MAS}$ provides the dominant contribution to the relaxation rate. Therefore, in order to compare the $T_{1\rho}$ at different spinning rate the difference $\omega_{SL} - \omega_{MAS}$ has to be kept constant. This dependence of frequency difference between the spin and MAS on the spectral density makes its feasible to measure very slow motions (Krushelnitsky et al. 2018) at their near-rotary-resonance conditions.

6.3.4.1 $T_{1\rho}$ relaxation measurements

Uniformly ^{15}N labeled proteins have been frequently used to investigate the local molecular motions of backbone amides using $^1\text{H}, ^{15}\text{N}$ T_1 , $T_{1\rho}$ and hetNOE experiments (Clore et al. 1990; Cho et al. 1996; Barbato et al. 1992). In this study, the slow motions that exist even after complete sedimentation of αB -crystallin were accessed using $T_{1\rho}$ at different spinning frequencies to test the hypothesis of the origin of the bad spectral resolution. Here, in order to have a direct comparison at all the spinning stages, a constant near-rotary-resonance condition was ensured, by choosing a difference of 4 kHz between spin-lock and MAS frequencies. As stated before, a properly calibrated Hartmann-Hahn match is necessary for cross polarization to occur between the abundant and dilute isotope, since it can easily be altered by factors such as power levels and even the chemical environment. Additionally, it is also important to calibrate the spin-lock pulse at the chosen spinning frequency. Here the experimental ^{15}N spin-lock nutation curve (Figure 51) was fitted using the following function,

$$y = A \cdot \cos(2\pi \cdot \nu_{SL} \cdot t + \varphi) \cdot \exp\left(-\frac{t}{T_2}\right) + P \quad (34)$$

where, A is the amplitude, ν_{SL} is the spinlock pulse frequency, φ is the phase of an apparent pulse, T_2 is the transverse relaxation time that mostly encodes rf inhomogeneity and P is a plateau value ($P = 0$).

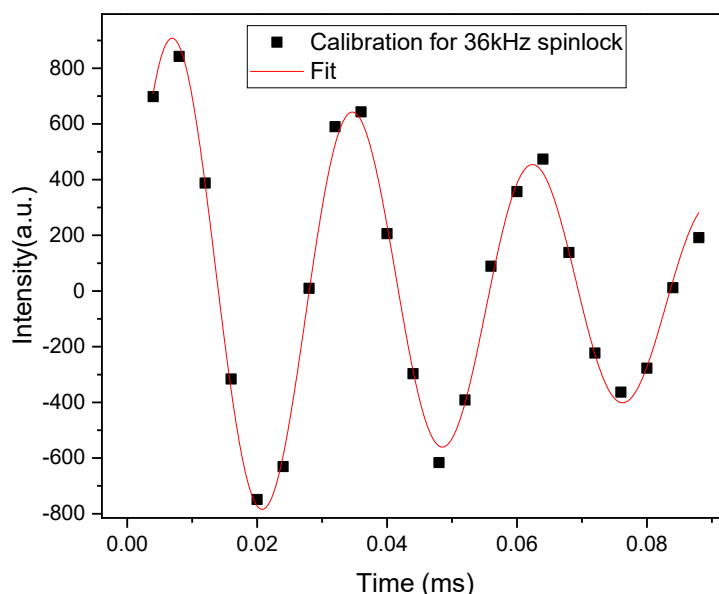


Figure 51: A representative nutation curve obtained for ^{15}N spinlock of 36 kHz for *h* αB -crystallin.

A fit of this nutation curve gave ν_{SL} of 36.07 kHz, and the corresponding power levels are calculated for a precise spin-lock pulse. ^{15}N -detected $T_{1\rho}$ experiments were then performed at all the different spinning speeds to assess the rocking motions or extend of motional restriction. The rocking motions are a type of molecular mobility, wherein the proteins are not fixed by intermolecular contacts and can undergo restricted motion as whole. The protein rocking motions only sets in once the overall tumbling of the protein is suspended. The $T_{1\rho}$ decays were measured using a routine CP pulse sequence, where the ^{15}N detected signal was obtained by magnetization transfer from amide protons to nitrogen with decoupling of protons during acquisition. At different durations of ^{15}N spinlock pulse one-dimensional amide spectra were measured and the $T_{1\rho}$ decay was obtained from integrated signal of the entire amide band as shown in Figure 52. One of the limitations here is that the site-specific characterization of protein dynamics is hardly possible, although insight into overall motion of protein can be acquired.

Figure 52 shows the normalized $T_{1\rho}$ decay curves obtained at different spinning speed with increasing spinlock duration. In all the cases, we observe a decreasing intensity with increasing spinlock duration. Due to poor signal-to-noise ratio a proper analysis of the decay curves was not feasible. But using a simple single-exponential function the $T_{1\rho}$ decay curves were fitted (see Figure 52). It has to mentioned here that the decays obtained are clearly multi-exponential, but because of the large experimental error fitting them using complicated fitting functions would be illogical, as the fits would be too uncertain. The $T_{1\rho}$ relaxation time obtained from

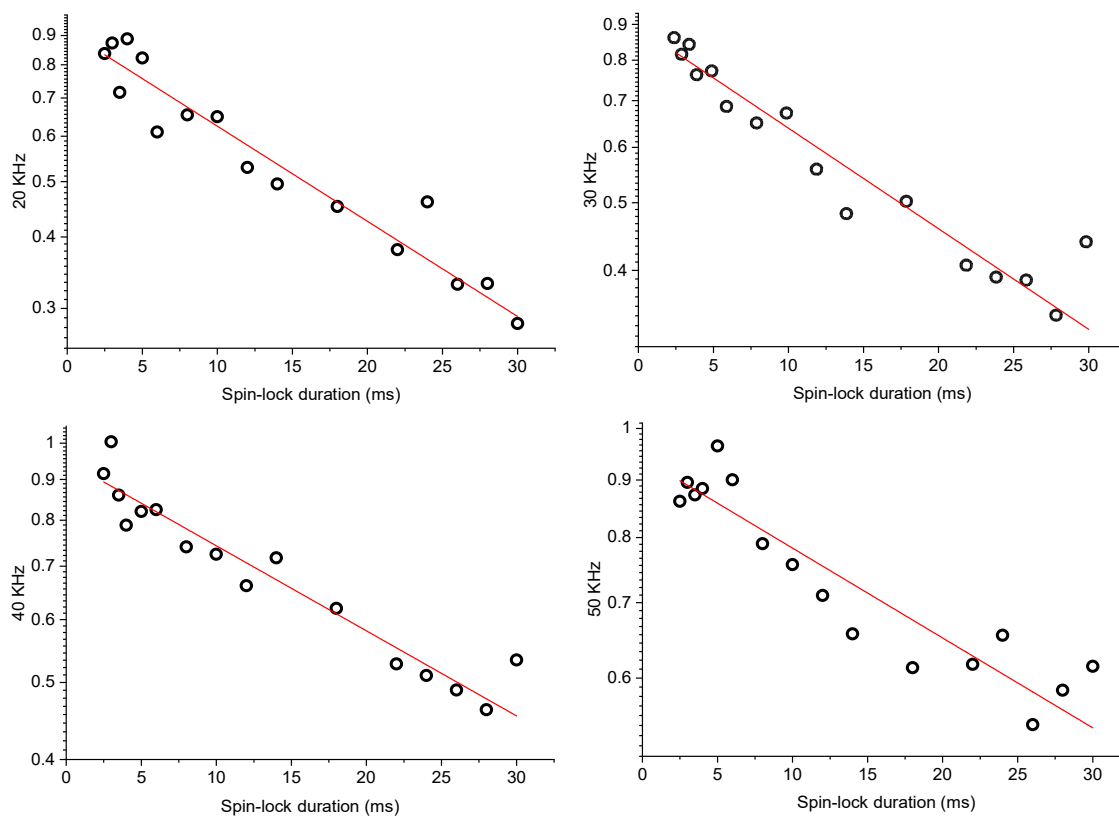


Figure 52: Normalized $T_{1\rho}$ decay curves obtained at different spinning speeds obtained for h α B-crystallin protein at ~ 200 mg/mL

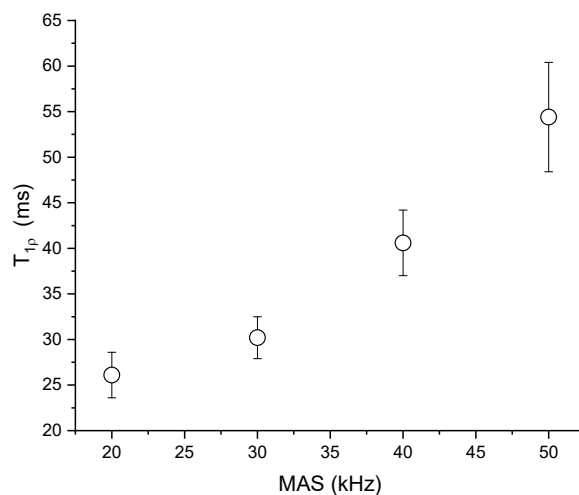


Figure 53: $T_{1\rho}$ values obtained from the single exponential fit of data in Figure 52 plotted against respective MAS spinning frequencies.

the fits were plotted against the respective MAS spinning frequencies in Figure 53. It can be clearly seen that with increasing spinning speed the $T_{1\rho}$ becomes slower implying slowing down of the rocking motion and a better ‘pseudo solidification’ of the protein. Here the main

purpose was not to determine absolute values rather demonstrate that the spinning and sedimentation had a certain tendency. And therefore, such an analysis was relevant.

6.3.4.2 Human α B-crystallin solid state spectra at different spin speeds

To obtain solid-state spectra of h α B-crystallin, the protein was immobilized in the rotor, since crystallization was not possible and investigated as a ‘pseudo solid’. These proteins were centrifugated and sedimented into a solid state thin walled 1.3 mm rotor at a starting concentration of 10 mg/ml. To probe the influence of spinning speed on the ^1H - ^{15}N correlation spectra resolution, the rotor was spun gradually with increasing spinning speed starting from 20 kHz to 50 kHz at 18 °C. At each spinning frequency the 2D spectrum was recorded within 3 days. In all the cases an indirect detection approach was involved, wherein the magnetization was initially transferred from ^1H to ^{15}N nuclei via cross polarization, the chemical shift then evolves on the ^{15}N nuclei, and eventually transferred back to ^1H and FID is acquired on ^1H nuclei. The spectra were processed using the same processing parameters, which can therefore be directly compared.

Figure 54 shows the ^1H - ^{15}N correlation spectra obtained for h α B crystallin at 20 kHz. Although the spectral resolution is mediocre, with mostly broad peaks, a few of the residues G147, T132, G141, G112, G102 and R116 could be identified. In some case the peak intensity was even comparable to the noise and hence could not be distinguished.

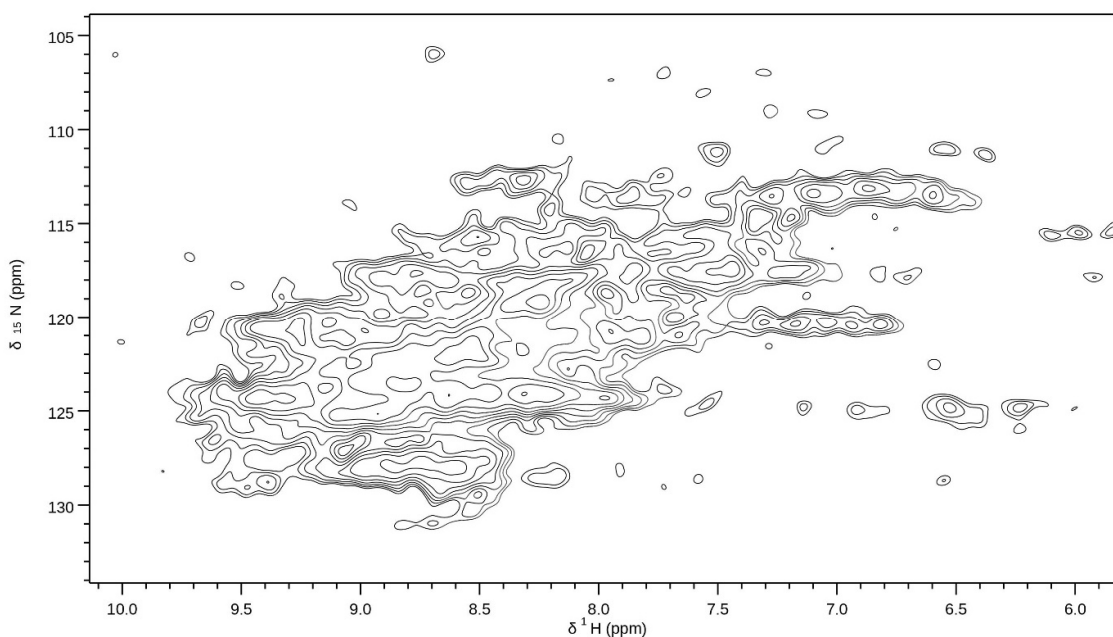


Figure 54: ^1H - ^{15}N correlation spectra of h α B crystallin (~200 mg/mL) at 20 kHz

With further increase of spinning frequency to 30kHz (Figure 55), yielded a similar correlation spectrum as for 20kHz. In comparison to the spectra at 20 kHz, at 30 kHz the resolution did

not improve, which made it impractical to identify the residues. The signature peak pattern, within the ^{15}N ppm range 105 -110 and ^1H ppm range 9.5 – 7.0 were also missing.

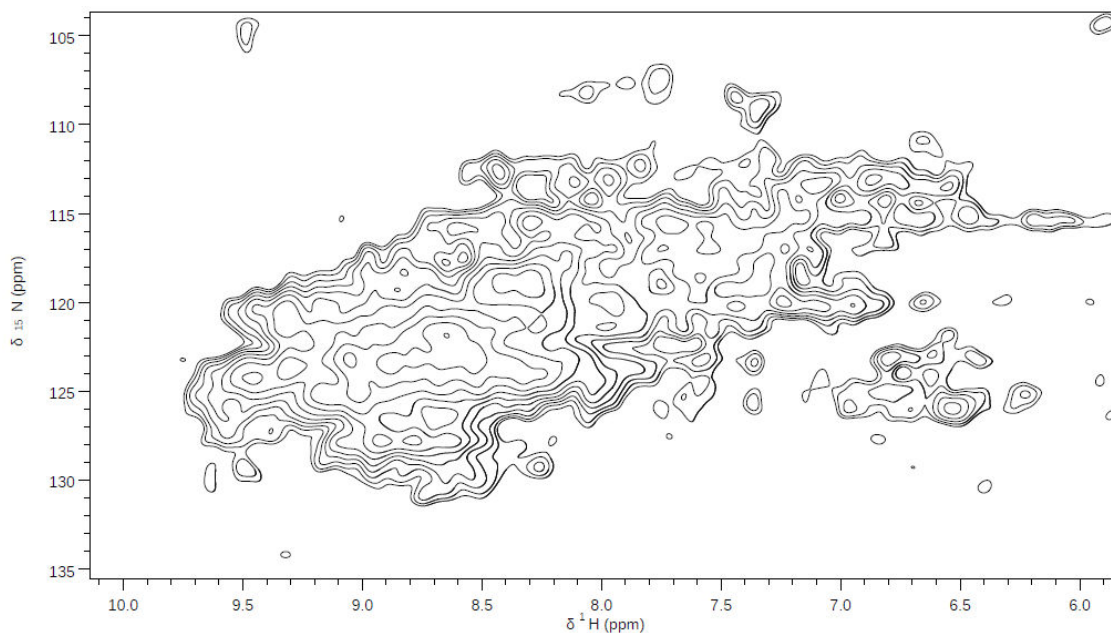


Figure 55: ^1H - ^{15}N correlation spectra of h αB crystallin (~ 200 mg/mL) at 30 kHz

Similarly, the 2D correlation spectra obtained at 40 kHz (Figure 56), exhibited broader peaks. This was fairly comparable to the spectra at 30 kHz, where nearly all the residues were indistinguishable and the signature peak pattern was missing as well.

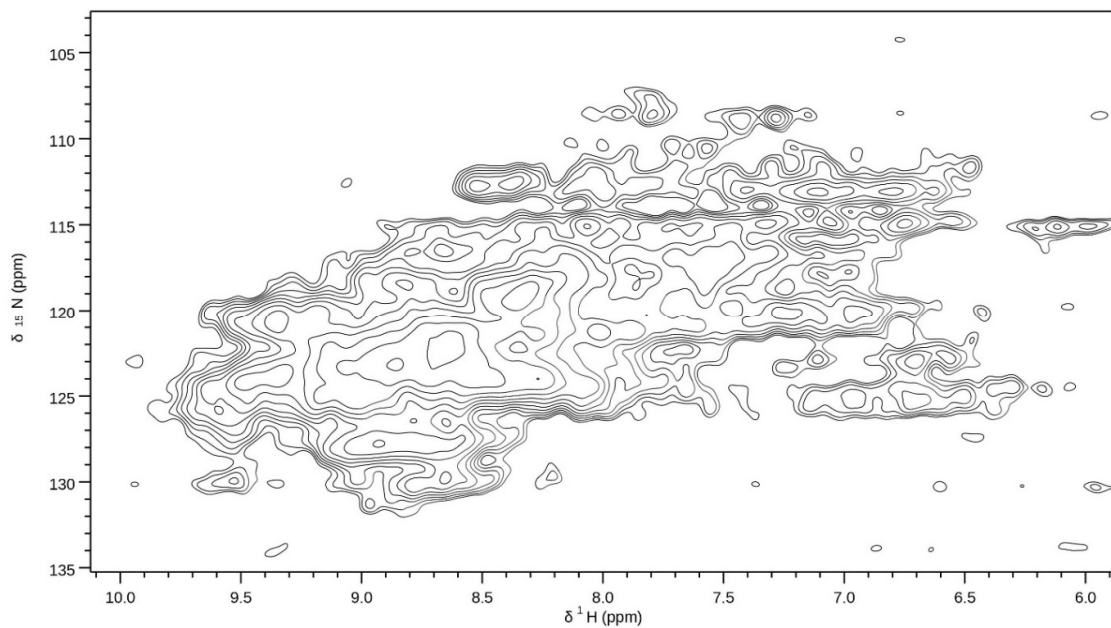


Figure 56: ^1H - ^{15}N correlation spectra of h αB crystallin (~ 200 mg/mL) at 40 kHz

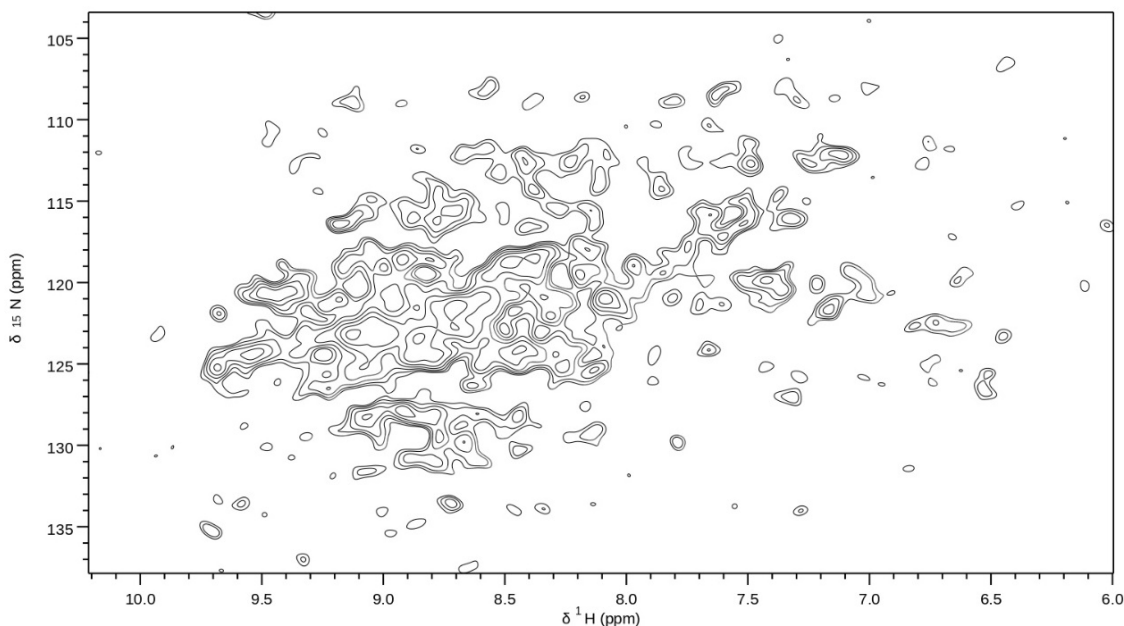


Figure 57: ^1H - ^{15}N correlation spectra of h αB crystallin (~ 200 mg/mL) at 50 kHz

At a first glance, the 2D spectra at 50kHz (Figure 57), shows a remarkable difference in comparison to those at lower spinning speed, with the peaks now being much narrower. Although as was observed for the earlier spectra, the comparable intensity of noise and signal renders the many relevant residues indistinguishable. A more careful analysis of the spectra could reveal a few of the amino acid residues, but they may be ambiguous.

In general, stepwise increment of spinning frequency did not remarkably improve the resolution of the ^1H - ^{15}N correlation spectra of h αB crystallin, except perhaps above 50 kHz. This, in combination with the $T_{1\rho}$ decays, that slows down with increasing spinning, implies a more solid-like protein and hence a marginally resolved spectra at 50 kHz.

This could further be complicated due to the uneven sedimentation of protein. There may possibly be a packing density gradient of the protein within the rotor from its center to the periphery. This perhaps is pressure dependent, where on the wall the protein is compressed and the overall protein tumbling is suppressed, while along the axis of the rotor it can freely rotate. This in turn could also affect the CP efficiency. Additionally, when these 2D spectra are compared to the solid-state correlation spectra that was published by Mainz et al. 2015, the spectral match was not exactly identical. One reason could be the different temperature at which the experiment was performed and other could be the packing of the protein. The amount of protein present is also crucial, in this case since the signal-to-noise was poor even after 3 days of spectrum acquisition, it could also be speculated that the amount of protein present was unfortunately inadequate.

6.3.5 Conclusion

In this study the influence of increasing magic angle spinning (MAS) frequency on the ^1H - ^{15}N spectral resolution of h αB crystallin was probed. Initially, to get a better insight into the structural details of h αB crystallin protein, a combination of solution state and solid state NMR was used, and the results were comparable to the previously published data for αB (Jehle et al. 2010; Mainz et al. 2015). The extend of sedimentation was further quantified using $T_{1\rho}$ relaxation measurements. A closer look at the $T_{1\rho}$ decay curves showed a slowing down of molecular motion, with increasing spinning speed from 20 kHz to 50 kHz. This could be an implication of better sedimentation and concomitant increase in spectral resolution was expected. It has to be emphasized here that, albeit $T_{1\rho}$ gives information regarding the dynamics, it may not necessarily give a complete dynamic information that relates to the spectral resolution, but only provide a rough qualitative estimation. The correlation spectra were further acquired at increasing spinning speed. At 20 kHz, the characteristic signal pattern (Figure 54) was observed, which was absent at 30 and 40 kHz. Primarily in all the cases a broad spectrum was obtained. The broad nature of peaks primarily could be attributed to the incomplete averaging of the interactions, which is on the time scale of the MAS frequency. In contrast, at 50 kHz, the 2D spectra was seemingly narrower, but due to the poor signal to noise the peaks were indistinguishable. This spectrum obtained at 50 kHz (Figure 57), qualitatively supports the idea of this work, although the quality of the acquired data is not adequate to make a definite conclusion. Therefore, correlating this increased resolution to the slowing down of $T_{1\rho}$ is not possible to given the sparsity of data. Additional experiments under different conditions could have aided in confirming the idea presented here but the limited sample availability hindered the further progress of the experimental work.

7 Summary

The work presented in this thesis aims at obtaining a more comprehensive understanding of the functionalities of the crystallin proteins, the major constituents of the eye lens milieu. The changes in the crystallins over time due to ageing or certain mutation, can affect the transparency of the lens and lead to cataract. In this study the two important aspects have been considered which is the effect of molecular crowding and the influence of heat-induced perturbations of these crystallins below its denaturation temperature. This allows for investigation of these proteins under the condition that mimicks the slow ageing of the lens.

In the first part of this work NMR relaxometry was used to characterize the aggregation kinetics of two specific proteins, (i) bovine γ B and (ii) bovine α -crystallin. Here, it was demonstrated that in comparison to other spectroscopic techniques, NMR transverse relaxation can be easily used to monitor the protein aggregation, its most important feature being that a quantitative estimate of the aggregate protein was possible. Although these crystallins belong to the same class of lens proteins, a qualitative difference in the heat-induced aggregation process was observed. The bovine γ B crystallin formed solid aggregates while the bovine α -crystallin formed a transparent gel on prolonged exposure at 60 °C. Since the bovine γ B crystallin formed solid aggregates, it was possible to estimate the percentage of aggregated protein in each time point. Interestingly, the concentration dependence of aggregation kinetics was distinct for both the proteins. The γ B crystallin exhibited a concentration-independent aggregation kinetics, while for α -crystallin a concentration dependent aggregation kinetics was observed. The transverse relaxation decay of the water component for the bovine α crystallin could be directly correlated to the relaxation decay of the protein aggregation itself, where the decay curves showed a similar trend. This indicated indeed that the α -crystallins formed a gel, wherein the motion of the water molecules become restricted. The formation of this transparent gel by the chaperone protein α -crystallin, at long exposure to 60°C below its denaturation temperature, was intriguing. Therefore, in the following chapter a detailed investigation of the gelation of α -crystallin protein was conducted.

In the second part, several different biophysical characterization techniques were used to characterize the heat induced gelation of α -crystallin protein. Throughout the study, a comparison of gel formation by bovine α -crystallin, a hetero oligomer containing both α A and α B subunits and h α B crystallin, a homooligomer with α B subunits, was investigated. The approach towards this study involved starting from a more globular/ general aspect of the gel, i.e., transparency to molecular-level gel network formation. Light transmission at 800 nm was used to demonstrate the transparency of gels formed by these crystallin proteins. In comparison to human α B, bovine α was more transparent, while the former formed larger aggregates making the system more opaque. In order to get a better insight into the change in size of these crystallins over heat-induced exposure time, dynamic light scattering was employed. Here, only lowly concentrated crystallin samples were used to avoid multiple scattering. It was found that h α B formed aggregates that settled to the bottom, while bovine α remained soluble,

although it showed a steady and gradual increase in particle size. Transmission electron microscopy was used to get a visualization of the particles when the proteins gel. For both the proteins TEM experiments indicated that the globular structure was intact even after the gel formation. This was additionally confirmed by ATR-FTIR, where the heat-induced secondary structural changes were negligible. Small-angle X-ray scattering was further used to get a more comprehensive understanding of the gel formation of these crystallin protein at a molecular level. When compared to BSA, the gel formation of the crystallins were slower, which was evident from the slow increase in intensity at smaller q -values. When heated at 60 °C for about 15 h, BSA formed larger aggregates and at 200 mg/ml the formed gels had a fractal dimension of 1.2, which indicates formation of a short extended but slightly branched network. H α B crystallin protein when annealed at 60 °C, increased in size from $60.95 \pm 0.49 \text{ \AA}$ to $75.9 \pm 1.18 \text{ \AA}$, and at low concentrations a fractal dimension of 1.4 was obtained, forming a short branched and less dense network. At high concentrations of 200 mg/ml a fractal dimension of 1 indicated that these formed an unbranched 1D network. Similarly, for bovine α -crystallin the R_g , increased from $70 \pm 1.5 \text{ \AA}$ to $75 \pm 1.14 \text{ \AA}$, although the increase was not very significant. At low concentrations for bovine α , a fractal dimension of 1.8 implied a dense network formation. The highly concentrated sample when annealed at 60 °C showed a dominant repulsive interaction. The bovine α -crystallin gel obtained after the ATR-FTIR analysis was also investigated using SAXS, which indicated a slight onset of gel formation. The determination of the fractal dimension was not possible in this case. In general, both the crystallin over time formed larger oligomers or superstructures, with h α B forming a gel composed of independent 'sticky' sphere with extended unbranched 1D aggregate, while bovine α crystallin forms a rather dynamic network, where mutual aggregation occurs due to weak hydrophobic surface-surface interactions. Additionally, both the crystallins again demonstrated to maintain the globular structure as was evident from Kratky plots.

To further the gelation studies, an attempt was made to investigate the α -crystallin, especially h α B using MAS solid state NMR spectroscopy. Initially, the solution state HSQC and solid-state NMR spectra were obtained which were comparable to the already published data. Furthermore, with increasing spinning speed from 20 kHz to 50 kHz, the improvement in spectral resolution was probed. In comparison to 20, 30 and 40 kHz, the spectra obtained at 50 kHz showed an improved resolution. In general, compare to the spectra from TUM the spectral resolution obtained at Halle, was quite inferior. Potential slow motions were accessed by $T_{1\rho}$ measurements, and with increasing spinning speed the $T_{1\rho}$ decay indeed became slower. This indicated that the protein solution was a 'pseudo-solid' and can be linked to the better resolved spectra at 50 kHz. Qualitatively this supports the idea of this work, but since the quality of the acquired data was still poor, a definite conclusion could not be made. Therefore, correlating this increased resolution to the slowing down of $T_{1\rho}$ was uncertain, additional experiments under different conditions could aid in confirming the idea presented here

It is relatively evident that the α -crystallin protein, which is a combination of two subunits α A and α B is more resistant to heat-induced changes. As opposed to the presence of

homooligomers, α B-crystallin in other tissues, the α -crystallin proteins are exclusively present only in the eye lens. One could speculate that the α A subunit might be providing this additional stability. Therefore, a similar heat stress study on α A crystallin might give a better insight into its structural and conformational stability. In this study the ageing of these lens crystallin was investigated, which showed that over time even under certain stress the α -crystallin may still help maintain the lens transparency, owing to its chaperoning function. It would be further ideal to investigate this chaperoning function of the α -crystallins in combination with other lens crystallins.

Lens crystallins are fascinating proteins, that help in maintaining the functionality of the eye lens. The studies based on these crystallins are still ongoing, in order to get a better understanding of lens cataract disease that is associated with crystallin protein aggregation. The conventional way of cataract treatment has been replacement of the lens with an artificial lens. An improved comprehension of the different interaction between the proteins in the eye lens that leads to or prevents such cataract formation could help in furthering the development of improved treatments for cataractogenesis.

8 Table of figures

Figure 1: a. Clear eye lens permits the light to focus sharply on the retina, b. Clouded lens scatters or blocks the light from falling on to the retina. (Pictures made using Biorender)	6
Figure 2: Organization within the eye lens a. cross-section of lens depicting the cell distribution of epithelium (Kalligeraki et al. 2020) reused with permission according to CC BY 4.0 DEED license (http://creativecommons.org/licenses/by/4.0/), b. Short ranged ordered packing of lens fiber cells (Song et al. 2009) reused with permission according to Copright Clearance Center, Inc, License ID – 1449356 - 1, c. Three major crystallin proteins (Goodsell 2010) reused with permission according to CC BY 4.0 license.	7
Figure 3: Oligomerization of α -crystallin via different interactions (Delbecq et al. 2015) adapted and reused according to ACS usage agreement.	8
Figure 4: Basic secondary structure construct of γ -Crystallin, a. Two Greek key motif per domain formed from antiparallel b sheets, b. Structure of Bovine γ B crystallin: pdb code: 1GCS (Najmudin et al. 1994), processed using pyMol	10
Figure 5: Depending on the type of the globular protein, its native state denatures (completely or partially) to form elementary units, that further aggregate to form self-similar units. These can further associate and form either fine network or coarse network gels which can be distinguished by their fractal dimensions.	16
Figure 6: Domain organization for α B-crystallin protein.....	20
Figure 7: When a $\pi/2$ pulse is applied on an ensemble of spins for a duration of tp , generates transverse magnetization that decays exponentially, where d_c is the dead time. The Fourier transformation of such an exponentially decaying function yields a Lorentzian peak, where the peak width at half height equal to $1/\pi T_2$ (Levitt 2015).....	24
Figure 8: Pake pattern obtained under static rigid limit and the time domain signal obtained after Fourier transformation.	29
Figure 9: Schematic representation of cross polarization (CP) pulse sequence for a polarization transfer from ^1H to ^{15}N	32
Figure 10: Schematic representation of small angle X-ray scattering experiment.	34
Figure 11: Combining FID and CPMG-based relaxometry (bovine α -crystallin, 60 mg/mL).	42
Figure 12: A simplified schematic representation of a sample within the Linkam stage. a. Glass capillary, b. Sample of interest, c. heating stage connected to a thermocouple and d. window with a diameter of 1 mm.	45
Figure 13: Scattering intensity curve of BSA, h α B crystallin and bovine α -crystallin at 20mg/ml at 20 °C.	46
Figure 14: R_g obtained for BSA 20mg/ml using Guinier approximation at 20 °C.	47
Figure 15: Scattering intensity of BSA at 20 mg/ml at 20 °C.	48
Figure 16: Comparison of X-ray scattering intensity of BSA at 20 mg/ml (grey) and 200 mg/ml (red) at room temperature.	49
Figure 17: The nature of network structure formed during aggregation and its corresponding fractal dimension (Lazzari et al. 2016)	50
Figure 18: Schematic of Kratky plot adapted from Kikhney and Svergun (2015).	51

Figure 19: Transverse relaxation decays of bovine α -crystallin at 60 mg/ml (AC60) and 200 mg/ml (AC200), recombinant bovine γ B-crystallin at 60 mg/ml (GC60) and at 135 mg/ml (GC135) at the first point of aggregation kinetics measurements. The dashed red lines here depict the long exponential relaxation component of the residual water proteins, which was subtracted from the integral signal.....	56
Figure 20: Protein transverse relaxation decays obtained after the subtraction of water component from Figure 19, of bovine α -crystallin at 60 mg/ml (AC60) and 200 mg/ml (AC200), recombinant bovine γ B-crystallin at 60 mg/ml (GC60) and at 135 mg/ml (GC135) at the first point of aggregation kinetics measurements (at 0 h). For a comparison, the relaxation decay of GC135 after 66 h at 60 °C is also shown, along with the fits to the initial parts (Equation (29)) are depicted by solid line.....	57
Figure 21: Protein transverse relaxation decay curves for recombinant γ B -crystallin during thermally induced aggregation at 60 °C at 60 mg/ml (GC60) and 135 mg/ml (GC135) (left panel: log-linear plots; right panel: log-log plots)	58
Figure 22: Protein transverse relaxation decay curves for bovine α -crystallin during thermally induced aggregation at 60°C at 60 mg/ml (AC60) and 200mg/ml (AC200) (Left panel: log-linear plots; right panel: log-log plots).....	59
Figure 23: Time dependence of mean transverse T_2 relaxation time for (a) bovine γ B-crystallin and (b) bovine α -crystallin.	60
Figure 24: Aggregated (i) γ B-crystallin at 135 mg/ml and (ii) α -crystallin at 200 mg/ml.....	61
Figure 25: The time dependence of the percentage of aggregated γ B-crystallin at 60 mg/ml (GC60) and 135 mg/ml (GC135) are shown, which have been fitted with an exponential growth function $I(t)=A \cdot (1-\exp(-t/\tau))$, where $I(t)$ is the intensity at time t , and A is the amplitude of the slowly aggregating species. The aggregation time constant can be derived from the main fit result i.e. τ	62
Figure 26: The time dependence of residual water proton T_2 relaxation time during the aggregation of bovine α -crystallin (AC60 and AC200) and γ B-crystallin (GC60 and GC135).	63
Figure 27: The change in % transmission of h α B crystallin haB20 (20 mg/ml), haB200 (200 mg/ml), bovine α -crystallin Bovine a20 (20 mg/ml), Bovine a200 (200mg/ml) and NaP-buffer when thermally stressed at 60 °C at 800 nm.....	66
Figure 28: The time dependent changes in the hydrodynamic radii of h α B and Bovine α crystallin at 20 mg/ml when thermally stressed at 60°C	67
Figure 29: Transmission electron microscopy image of negatively stained α crystallin from bovine eye lens at 10mg/ml at RT in 50mM NaP-buffer at pH 7.5.....	69
Figure 30: Transmission electron microscopy image of a. human α B-crystallin and b. bovine α -crystallin gels embedded in epoxy resin	69
Figure 31: The temperature dependent changes in FTIR spectra of a. h α B and b. bovine α -crystallin at 200 mg/ml	71

Figure 32: The time dependent changes in the amide I region of the FTIR spectra of a. h α B, b. h α B rescaled, c bovine α -crystallin and d. bovine α -crystallin rescaled at 200mg/ml when thermally stressed at 60 °C	72
Figure 33: Peak deconvolution of of h α B crystallin spectra at 0 h and 54 h and for bovine α crystallin spectra at 0 h and 52 h.....	73
Figure 34: Peak deconvolution of h α B and bovine α crystallin spectra at 20 °C and 85 °C.	74
Figure 35: Change in the peak amplitudes for a. h α B crystallin and b. bovine α -crystallin when heated at 60 °C and when heated at 85 °C.....	75
Figure 36: Scattering intensity curves of BSA at 20mg/ml, before heating, at 60°C and after heating at 20°C.....	77
Figure 37: a. Scattering intensity curve obtained over the course of thermal stress at 60°C of BSA at 200mg/ml. b. Structure factor obtained from the data in 'a'.....	78
Figure 38: Scattering curves of h α B. low concentration 20 mg/ml when thermally stressed over 72 h at 60 °C.	79
Figure 39: Kratky plot of human α B-crystallin at a concentration of 20 mg/ml, at different waiting times at 60 °C.....	80
Figure 40: a. Effect of increased concentration on the scattering intensity, b. Scattering curves and c. Structure factor curves of h α B 200 mg/ml when thermally stressed over 67 h at 60 °C.	81
Figure 41: Scattering curve of Bovine α crystallin low concentration 20 mg/ml when thermally stressed over 72 h.....	82
Figure 42: Kratky plots of bovine α -crystallin at a concentration of 20 mg/ml, at different waiting times at 60 °C.....	82
Figure 43: a. Effect of increased concentration on the scattering intensity, b. Scattering curves and c. Structure factor curves of Bovine α 200mg/ml when thermally stressed over 45 h at 60 °C	83
Figure 44: Fits of the structure factor of bovine α -crystallin 200 mg/mL after 10 mins and 45 h.....	84
Figure 45: Fits of the structure factor of human α B-crystallin 200 mg/mL after 2 h and 45 h	85
Figure 46: Force curve obtained for h α B-crystallin at 200 mg/mL.	86
Figure 47: H α B crystallin: pdb code:2YGD, processed using pyMol (Braun et al. 2011a) and 1D proton spectra of h α B crystallin at 30°C pH 7.5 in D ₂ O	89
Figure 48: ¹ H- ¹⁵ N HSQC spectra of h α B crystallin at 20 °C, pD 7.2. Major states indicated in black and minor states in blue.....	90
Figure 49: ¹ H- ¹⁵ N solid-state NMR spectra of human α B-crystallin protein (at 4°C, MAS – 30 kHz, in 1.9mm rotor, at magnetic field strength – 18.8T)	91
Figure 50: ¹ H- ¹⁵ N solid-state NMR spectra of human α B-crystallin protein (at 13 °C, MAS – 20 kHz, in 1.3 mm rotor, at magnetic field strength – 14.1 T)	92
Figure 51: A representative nutation curve obtained for ¹⁵ N spinlock of 36 kHz for h α B-crystallin.....	95

Figure 52: Normalized $T1\rho$ decay curves obtained at different spinning speeds obtained for h α B-crystallin protein at ~ 200 mg/mL.....	96
Figure 53: $T1\rho$ values obtained from the single exponential fit of data in Figure 52 plotted against respective MAS spinning frequencies.	96
Figure 54: ^1H - ^{15}N correlation spectra of h α B crystallin (~ 200 mg/mL) at 20 kHz.....	97
Figure 55: ^1H - ^{15}N correlation spectra of h α B crystallin (~ 200 mg/mL) at 30 kHz.....	98
Figure 56: ^1H - ^{15}N correlation spectra of h α B crystallin (~ 200 mg/mL) at 40 kHz.....	98
Figure 57: ^1H - ^{15}N correlation spectra of h α B crystallin (~ 200 mg/mL) at 50 kHz.....	99

9 References

- Alperstein, Ariel M.; Ostrander, Joshua S.; Zhang, Tianqi O.; Zanni, Martin T. (2019): Amyloid found in human cataracts with two-dimensional infrared spectroscopy. In *Proceedings of the National Academy of Sciences of the United States of America* 116 (14), pp. 6602–6607. DOI: 10.1073/pnas.1821534116.
- Anderson, P. W.; Weiss, P. R. (1953): Exchange Narrowing in Paramagnetic Resonance. In *Rev. Mod. Phys.* 25 (1), pp. 269–276. DOI: 10.1103/RevModPhys.25.269.
- Andreas, Loren B.; Reese, Marcel; Eddy, Matthew T.; Gelev, Vladimir; Ni, Qing Zhe; Miller, Eric A. et al. (2015): Structure and Mechanism of the Influenza A M218-60 Dimer of Dimers. In *Journal of the American Chemical Society* 137 (47), pp. 14877–14886. DOI: 10.1021/jacs.5b04802.
- Anitas, Eugen Mircea (2019): Small-Angle Scattering from Weakly Correlated Nanoscale Mass Fractal Aggregates. In *Nanomaterials (Basel, Switzerland)* 9 (4). DOI: 10.3390/nano9040648.
- Aquilina, J. Andrew; Benesch, Justin L. P.; Bateman, Orval A.; Slingsby, Christine; Robinson, Carol V. (2003): Polydispersity of a mammalian chaperone: mass spectrometry reveals the population of oligomers in alphaB-crystallin. In *Proceedings of the National Academy of Sciences of the United States of America* 100 (19), pp. 10611–10616. DOI: 10.1073/pnas.1932958100.
- Augusteyn, R. C.; Stevens, A. (1998): Macromolecular structure of the eye lens. In *Progress in Polymer Science* 23 (3), pp. 375–413. DOI: 10.1016/S0079-6700(98)80008-7.
- Barbato, G.; Ikura, M.; Kay, L. E.; Pastor, R. W.; Bax, A. (1992): Backbone dynamics of calmodulin studied by ¹⁵N relaxation using inverse detected two-dimensional NMR spectroscopy: the central helix is flexible. In *Biochemistry* 31 (23), pp. 5269–5278. DOI: 10.1021/bi00138a005.
- Barth, Andreas (2007): Infrared spectroscopy of proteins. In *Biochimica et biophysica acta* 1767 (9), pp. 1073–1101. DOI: 10.1016/j.bbabi.2007.06.004.
- Barth, Andreas; Zscherp, Christian (2002): What vibrations tell us about proteins. In *Quarterly reviews of biophysics* 35 (4), pp. 369–430. DOI: 10.1017/S0033583502003815.
- Benedek, G. B. (1971): Theory of transparency of the eye. In *Applied optics* 10 (3), pp. 459–473. DOI: 10.1364/AO.10.000459.
- Benedek, G. B. (1997): Cataract as a protein condensation disease: the Proctor Lecture. In *Invest. Ophthalmol. Vis. Sci.* 38 (10), pp. 1911–1921.
- Benedek, George B.; Pande, Jayanti; Thurston, George M.; Clark, John I. (1999): Theoretical and experimental basis for the inhibition of cataract. In *Progress in Retinal and Eye Research* 18 (3), pp. 391–402. DOI: 10.1016/S1350-9462(98)00023-8.

- Berg, John C. (2010): An introduction to interfaces & colloids: the bridge to nanoscience: World Scientific.
- Bettelheim, Frederick A.; Chen, Alex (1998): Thermodynamic stability of bovine α -crystallin in its interactions with other bovine crystallins. In *International Journal of Biological Macromolecules* 22 (3-4), pp. 247–252. DOI: 10.1016/S0141-8130(98)00022-1.
- Bloemendal, Hans; Jong, Wilfried de; Jaenicke, Rainer; Lubsen, Nicolette H.; Slingsby, Christine; Tardieu, Annette (2004): Ageing and vision: structure, stability and function of lens crystallins. In *Progress in biophysics and molecular biology* 86 (3), pp. 407–485. DOI: 10.1016/j.pbiomolbio.2003.11.012.
- Blundell, T.; Lindley, P.; Miller, L.; Moss, D.; Slingsby, C.; Tickle, I. et al. (1981): The molecular structure and stability of the eye lens: x-ray analysis of gamma-crystallin II. In *Nature* 289 (5800), pp. 771–777. DOI: 10.1038/289771a0.
- Bodenhausen, Geoffrey; Ruben, David J. (1980): Natural abundance nitrogen-15 NMR by enhanced heteronuclear spectroscopy. In *Chemical Physics Letters* 69 (1), pp. 185–189. DOI: 10.1016/0009-2614(80)80041-8.
- Borzova, Vera A.; Markossian, Kira A.; Chebotareva, Natalia A.; Kleymenov, Sergey Yu; Poliansky, Nikolay B.; Muranov, Konstantin O. et al. (2016): Kinetics of Thermal Denaturation and Aggregation of Bovine Serum Albumin. In *PloS one* 11 (4), e0153495. DOI: 10.1371/journal.pone.0153495.
- Boye, Joyce I.; Alli, Inteaz; Ismail, Ashraf A. (1996): Interactions Involved in the Gelation of Bovine Serum Albumin. In *J. Agric. Food Chem.* 44 (4), pp. 996–1004. DOI: 10.1021/jf950529t.
- Boyle, D.; Takemoto, L. (1994): Characterization of the alpha-gamma and alpha-beta complex: evidence for an in vivo functional role of alpha-crystallin as a molecular chaperone. In *Experimental eye research* 58 (1), pp. 9–15. DOI: 10.1006/exer.1994.1190.
- Braun, N.; Zacharias, M.; Peschek, J.; Kastenmueller, A.; Zou, J.; Hanzlik, M. et al. (2011a): Molecular architectures of the 24meric eye lens chaperone alphaB- crystallin elucidated by a triple hybrid approach.
- Braun, Nathalie; Zacharias, Martin; Peschek, Jirka; Kastenmüller, Andreas; Zou, Juan; Hanzlik, Marianne et al. (2011b): Multiple molecular architectures of the eye lens chaperone α B-crystallin elucidated by a triple hybrid approach. In *Proceedings of the National Academy of Sciences of the United States of America* 108 (51), pp. 20491–20496. DOI: 10.1073/pnas.1111014108.
- Brodkorb, André; Croguennec, Thomas; Bouhallab, Said; Kehoe, Joseph J. (2016): Heat-Induced Denaturation, Aggregation and Gelation of Whey Proteins. In Paul L. H. McSweeney, James A. O'Mahony (Eds.): *Advanced Dairy Chemistry*. New York, NY: Springer New York, pp. 155–178.

- Burgio, M. R.; Bennett, P. M.; Koretz, J. F. (2001): Heat-induced quaternary transitions in hetero- and homo-polymers of α -crystallin. In *Molecular Vision* 7, pp. 228–233.
- Burgio, M. R.; Kim, C. J.; Dow, C. C.; Koretz, J. F. (2000): Correlation between the chaperone-like activity and aggregate size of α -crystallin with increasing temperature. In *Biochemical and biophysical research communications* 268 (2), pp. 426–432. DOI: 10.1006/bbrc.1999.2036.
- Camilles, Maria; Link, Susanne; Balbach, Jochen; Saalwächter, Kay; Krushelnitsky, Alexey (2018): Quantitative NMR study of heat-induced aggregation of eye-lens crystallin proteins under crowding conditions. In *Biochimica et biophysica acta. Proteins and proteomics*. DOI: 10.1016/j.bbapap.2018.07.007.
- Carver, J. (1999): Probing the structure and interactions of crystallin proteins by NMR spectroscopy. In *Progress in Retinal and Eye Research* 18 (4), pp. 431–462. DOI: 10.1016/S1350-9462(98)00027-5.
- Carver, J. A.; Aquilina, J. A.; Truscott, R. J. (1994): A possible chaperone-like quaternary structure for α -crystallin. In *Experimental eye research* 59 (2), pp. 231–234. DOI: 10.1006/exer.1994.1101.
- Carver, John A.; Aquilina, J. Andrew; Truscott, Roger J.W. (1993): An investigation into the stability of α -crystallin by NMR spectroscopy; evidence for a two-domain structure. In *Biochimica et Biophysica Acta (BBA) - Protein Structure and Molecular Enzymology* 1164 (1), pp. 22–28. DOI: 10.1016/0167-4838(93)90107-3.
- Carver, John A.; Grosas, Aidan B.; Ecroyd, Heath; Quinlan, Roy A. (2017): The functional roles of the unstructured N- and C-terminal regions in α B-crystallin and other mammalian small heat-shock proteins. In *Cell stress & chaperones* 22 (4), pp. 627–638. DOI: 10.1007/s12192-017-0789-6.
- Cavanagh, John (2010): Protein NMR Spectroscopy. Principles and Practice. 2nd ed. Burlington: Elsevier Science. Available online at <https://ebookcentral.proquest.com/lib/kxp/detail.action?docID=287969>.
- Cetinel, Sibel; Semenchenko, Valentyna; Cho, Jae-Young; Sharaf, Mehdi Ghaffari; Damji, Karim F.; Unsworth, Larry D.; Montemagno, Carlo (2017): UV-B induced fibrillization of crystallin protein mixtures. In *PloS one* 12 (5), e0177991. DOI: 10.1371/journal.pone.0177991.
- Cheung, Margaret S.; Klimov, Dmitri; Thirumalai, D. (2005): Molecular crowding enhances native state stability and refolding rates of globular proteins. In *Proceedings of the National Academy of Sciences of the United States of America* 102 (13), pp. 4753–4758. DOI: 10.1073/pnas.0409630102.
- Cho, H. S.; Liu, C. W.; Damberger, F. F.; Pelton, J. G.; Nelson, H. C.; Wemmer, D. E. (1996): Yeast heat shock transcription factor N-terminal activation domains are unstructured as probed by heteronuclear NMR spectroscopy. In *Protein science : a publication of the Protein Society* 5 (2), pp. 262–269. DOI: 10.1002/pro.5560050210.

- Ciryam, Prajwal; Kundra, Rishika; Morimoto, Richard I.; Dobson, Christopher M.; Vendruscolo, Michele (2015): Supersaturation is a major driving force for protein aggregation in neurodegenerative diseases. In *Trends in pharmacological sciences* 36 (2), pp. 72–77. DOI: 10.1016/j.tips.2014.12.004.
- Clark, A. H.; Judge, F. J.; Richards, J. B.; Stubbs, J. M.; Suggett, A. (1981a): Electron microscopy of network structures in thermally-induced globular protein gels. In *International journal of peptide and protein research* 17 (3), pp. 380–392. DOI: 10.1111/j.1399-3011.1981.tb02005.x.
- Clark, A. H.; Kavanagh, G. M.; Ross-Murphy, S. B. (2001): Globular protein gelation—theory and experiment. In *Food Hydrocolloids* 15 (4-6), pp. 383–400. DOI: 10.1016/S0268-005X(01)00042-X.
- Clark, A. H.; Saunderson, D. H.; Suggett, A. (1981b): Infrared and laser-Raman spectroscopic studies of thermally-induced globular protein gels. In *International journal of peptide and protein research* 17 (3), pp. 353–364. DOI: 10.1111/j.1399-3011.1981.tb02002.x.
- Clore, G. M.; Driscoll, P. C.; Wingfield, P. T.; Gronenborn, A. M. (1990): Analysis of the backbone dynamics of interleukin-1 beta using two-dimensional inverse detected heteronuclear ^{15}N - ^1H NMR spectroscopy. In *Biochemistry* 29 (32), pp. 7387–7401. DOI: 10.1021/bi00484a006.
- Cooper, P. G.; Aquilina, J. A.; Truscott, R. J.; Carver, J. A. (1994): Supramolecular order within the lens: ^1H NMR spectroscopic evidence for specific crystallin-crystallin interactions. In *Experimental eye research* 59 (5), pp. 607–616. DOI: 10.1006/exer.1994.1146.
- Dalvit, Claudio; Santi, Sara; Neier, Reinhard (2017): A Ligand-Based NMR Screening Approach for the Identification and Characterization of Inhibitors and Promoters of Amyloid Peptide Aggregation. In *ChemMedChem* 12 (17), pp. 1458–1463. DOI: 10.1002/cmde.201700319.
- Das, B. K.; Liang, J. J.; Chakrabarti, B. (1997): Heat-induced conformational change and increased chaperone activity of lens alpha-crystallin. In *Current eye research* 16 (4), pp. 303–309. DOI: 10.1076/ceyr.16.4.303.10691.
- Delaye, M.; Tardieu, A. (1983): Short-range order of crystallin proteins accounts for eye lens transparency. In *Nature* 302 (5907), pp. 415–417. DOI: 10.1038/302415a0.
- Delbecq, Scott P.; Klevit, Rachel E. (2013): One size does not fit all: the oligomeric states of αB crystallin. In *FEBS letters* 587 (8), pp. 1073–1080. DOI: 10.1016/j.febslet.2013.01.021.
- Delbecq, Scott P.; Rosenbaum, Joel C.; Klevit, Rachel E. (2015): A Mechanism of Subunit Recruitment in Human Small Heat Shock Protein Oligomers. In *Biochemistry* 54 (28), pp. 4276–4284. DOI: 10.1021/acs.biochem.5b00490.
- Djabourov, Madeleine; Nishinari, Katsuyoshi; Ross-Murphy, Simon B. (Eds.) (2013): Physical Gels from Biological and Synthetic Polymers. Cambridge: Cambridge University Press.

- Doi, Etsushiro (1993): Gels and gelling of globular proteins. In *Trends in Food Science & Technology* 4 (1), pp. 1–5. DOI: 10.1016/S0924-2244(05)80003-2.
- Duer, Melinda J. (2001): *Solid-State NMR Spectroscopy Principles and Applications*. Oxford, UK: Blackwell Science Ltd.
- Elena, Bénédicte; Lesage, Anne; Steuernagel, Stefan; Böckmann, Anja; Emsley, Lyndon (2005): Proton to carbon-13 INEPT in solid-state NMR spectroscopy. In *Journal of the American Chemical Society* 127 (49), pp. 17296–17302. DOI: 10.1021/ja054411x.
- Ellis, R. John; Minton, Allen P. (2003): Cell biology: join the crowd. In *Nature* 425 (6953), pp. 27–28. DOI: 10.1038/425027a.
- Ellis, R. John (2001): Macromolecular crowding: obvious but underappreciated. In *Trends in biochemical sciences* 26 (10), pp. 597–604. DOI: 10.1016/S0968-0004(01)01938-7.
- Fagerholm, Per P.; Philipson, Bo T.; Lindström, Bo (1981): Normal human lens—the distribution of protein. In *Experimental eye research* 33 (6), pp. 615–620. DOI: 10.1016/S0014-4835(81)80101-7.
- Farnsworth, Patricia N.; Groth–Vasselli, B.; Greenfield, Norma J.; Singh, Kamalendra (1997): Effects of temperature and concentration on bovine lens α -crystallin secondary structure: a circular dichroism spectroscopic study. In *International Journal of Biological Macromolecules* 20 (4), pp. 283–291. DOI: 10.1016/S0141-8130(97)00028-7.
- Feigin, L. A.; Svergun, D. I. (1987): *Structure Analysis by Small-Angle X-Ray and Neutron Scattering*. Boston, MA: Springer US.
- Ferry, John D. (1948): Protein Gels. In, vol. 4: Elsevier (*Advances in Protein Chemistry*), pp. 1–78.
- Foffi, Giuseppe; Savin, Gabriela; Bucciarelli, Saskia; Dorsaz, Nicolas; Thurston, George M.; Stradner, Anna; Schurtenberger, Peter (2014): Hard sphere-like glass transition in eye lens α -crystallin solutions. In *Proceedings of the National Academy of Sciences of the United States of America* 111 (47), pp. 16748–16753. DOI: 10.1073/pnas.1406990111.
- Garrido, C.; Paul, C.; Seigneuric, R.; Kampinga, H. H. (2012): The small heat shock proteins family: the long forgotten chaperones. In *The international journal of biochemistry & cell biology* 44 (10), pp. 1588–1592. DOI: 10.1016/j.biocel.2012.02.022.
- Ghosh, Ranendu; Calero-Rubio, Cesar; Saluja, Atul; Roberts, Christopher J. (2016): Relating Protein-Protein Interactions and Aggregation Rates From Low to High Concentrations. In *Journal of pharmaceutical sciences* 105 (3), pp. 1086–1096. DOI: 10.1016/j.xphs.2016.01.004.
- Gimel, Jean Christophe; Durand, Dominique; Nicolai, Taco (1994): Structure and distribution of aggregates formed after heat-induced denaturation of globular proteins. In *Macromolecules* 27 (2), pp. 583–589. DOI: 10.1021/ma00080a037.

- Glassford, Stefanie E.; Byrne, Bernadette; Kazarian, Sergei G. (2013): Recent applications of ATR FTIR spectroscopy and imaging to proteins. In *Biochimica et biophysica acta* 1834 (12), pp. 2849–2858. DOI: 10.1016/j.bbapap.2013.07.015.
- Goodhew, Peter (2011): General Introduction to Transmission Electron Microscopy (TEM). In Rik Brydson (Ed.): *Aberration-Corrected Analytical Transmission Electron Microscopy*: Wiley, pp. 1–19.
- Goodsell, D. S. (2010): Crystallins. In *RCSB PDB*. DOI: 10.2210/rcsb_pdb/mom_2010_7.
- Graw, Jochen (2009): Genetics of crystallins: cataract and beyond. In *Experimental eye research* 88 (2), pp. 173–189. DOI: 10.1016/j.exer.2008.10.011.
- Guinier A., Fournet G. (1955): *Small-Angle Scattering of X-rays*. N.Y.: Wiley & Sons.
- Haley, D. A.; Horwitz, J.; Stewart, P. L. (1998): The small heat-shock protein, alphaB-crystallin, has a variable quaternary structure. In *Journal of Molecular Biology* 277 (1), pp. 27–35. DOI: 10.1006/jmbi.1997.1611.
- Harada, Ryuhei; Tochio, Naoya; Kigawa, Takanori; Sugita, Yuji; Feig, Michael (2013): Reduced native state stability in crowded cellular environment due to protein-protein interactions. In *Journal of the American Chemical Society* 135 (9), pp. 3696–3701. DOI: 10.1021/ja3126992.
- Haris, Parvez I.; Severcan, Feride (1999): FTIR spectroscopic characterization of protein structure in aqueous and non-aqueous media. In *Journal of Molecular Catalysis B: Enzymatic* 7 (1-4), pp. 207–221. DOI: 10.1016/S1381-1177(99)00030-2.
- Harn, N.; Allan, C.; Oliver, C.; Middaugh, C. R. (2007): Highly concentrated monoclonal antibody solutions: direct analysis of physical structure and thermal stability. In *Journal of pharmaceutical sciences* 96 (3), pp. 532–546. DOI: 10.1002/jps.20753.
- Hasan, Azeem; Yu, Jiong; Smith, David L.; Smith, Jean B. (2004): Thermal stability of human alpha-crystallins sensed by amide hydrogen exchange. In *Protein science : a publication of the Protein Society* 13 (2), pp. 332–341. DOI: 10.1110/ps.03180004.
- Haslbeck, Martin; Franzmann, Titus; Weinfurter, Daniel; Buchner, Johannes (2005): Some like it hot: the structure and function of small heat-shock proteins. In *Nature structural & molecular biology* 12 (10), pp. 842–846. DOI: 10.1038/nsmb993.
- Herzfeld, Judith (1996): Entropically Driven Order in Crowded Solutions: From Liquid Crystals to Cell Biology. In *Accounts of chemical research* 29 (1), pp. 31–37. DOI: 10.1021/ar9500224.
- Hofmann, Melanie; Winzer, Matthias; Weber, Christian; Gieseler, Henning (2016): Prediction of Protein Aggregation in High Concentration Protein Solutions Utilizing Protein-Protein Interactions Determined by Low Volume Static Light Scattering. In *Journal of pharmaceutical sciences* 105 (6), pp. 1819–1828. DOI: 10.1016/j.xphs.2016.03.022.

- Hoo, Christopher M.; Starostin, Natasha; West, Paul; Mecartney, Martha L. (2008): A comparison of atomic force microscopy (AFM) and dynamic light scattering (DLS) methods to characterize nanoparticle size distributions. In *J Nanopart Res* 10 (S1), pp. 89–96. DOI: 10.1007/s11051-008-9435-7.
- Horwitz, J. (1992): Alpha-crystallin can function as a molecular chaperone. In *Proceedings of the National Academy of Sciences of the United States of America* 89 (21), pp. 10449–10453. DOI: 10.1073/pnas.89.21.10449.
- Horwitz, J.; Bova, M. P.; Ding, L. L.; Haley, D. A.; Stewart, P. L. (1999): Lens alpha-crystallin: function and structure. In *Eye (London, England)* 13 (Pt 3b), pp. 403–408. DOI: 10.1038/eye.1999.114.
- Horwitz, Joseph (2003): Alpha-crystallin. In *Experimental eye research* 76 (2), pp. 145–153. DOI: 10.1016/S0014-4835(02)00278-6.
- Hunter, Robert J. (2001, 2009): Foundations of colloid science. 2nd ed. Oxford, New York: Oxford University Press.
- Ikeda, Shinya; Foegeding, E. Allen; Hagiwara, Tomoaki (1999): Rheological Study on the Fractal Nature of the Protein Gel Structure. In *Langmuir* 15 (25), pp. 8584–8589. DOI: 10.1021/la9817415.
- Indrawati, Linda; Stroshine, Richard L.; Narsimhan, Ganesan (2007): Low-field NMR: A tool for studying protein aggregation. In *J. Sci. Food Agric.* 87 (12), pp. 2207–2216. DOI: 10.1002/jsfa.2914.
- Israelachvili, Jacob N. (2011): Intermolecular and surface forces. San Diego, CA, USA: Elsevier Science & Technology Books.
- Jaeger, Christian; Hemmann, Felix (2014): EASY: a simple tool for simultaneously removing background, deadtime and acoustic ringing in quantitative NMR spectroscopy--part I: basic principle and applications. In *Solid state nuclear magnetic resonance* 57-58, pp. 22–28. DOI: 10.1016/j.ssnmr.2013.11.002.
- Jehle, Stefan; Rajagopal, Ponni; Bardiaux, Benjamin; Markovic, Stefan; Kühne, Ronald; Stout, Joseph R. et al. (2010): Solid-state NMR and SAXS studies provide a structural basis for the activation of alphaB-crystallin oligomers. In *Nature structural & molecular biology* 17 (9), pp. 1037–1042. DOI: 10.1038/nsmb.1891.
- Jehle, Stefan; Vollmar, Breanna S.; Bardiaux, Benjamin; Dove, Katja K.; Rajagopal, Ponni; Gonen, Tamir et al. (2011): N-terminal domain of alphaB-crystallin provides a conformational switch for multimerization and structural heterogeneity. In *Proceedings of the National Academy of Sciences of the United States of America* 108 (16), pp. 6409–6414. DOI: 10.1073/pnas.1014656108.
- Jong, W. W. de; Leunissen, J. A.; Voorter, C. E. (1993): Evolution of the alpha-crystallin/small heat-shock protein family. In *Molecular biology and evolution* 10 (1), pp. 103–126. DOI: 10.1093/oxfordjournals.molbev.a039992.

- Joshi, Varsha; Shivach, Tarun; Yadav, Nitin; Rathore, Anurag S. (2014): Circular dichroism spectroscopy as a tool for monitoring aggregation in monoclonal antibody therapeutics. In *Analytical chemistry* 86 (23), pp. 11606–11613. DOI: 10.1021/ac503140j.
- Kalligeraki, Alexia A.; Isted, Archie; Jarrin, Miguel; Uwineza, Alice; Pal, Robert; Saunter, Christopher D. et al. (2020): Three-dimensional data capture and analysis of intact eye lenses evidences emmetropia-associated changes in epithelial cell organization. In *Scientific reports* 10 (1), p. 16898. DOI: 10.1038/s41598-020-73625-9.
- Kamei, A.; Hamaguchi, T.; Matsuura, N.; Iwase, H.; Masuda, K. (2000): Post-translational modification of alphaB-crystallin of normal human lens. In *Biological & pharmaceutical bulletin* 23 (2), pp. 226–230. DOI: 10.1248/bpb.23.226.
- Kholová, I.; Niessen, H. W. M. (2005): Amyloid in the cardiovascular system: a review. In *Journal of clinical pathology* 58 (2), pp. 125–133. DOI: 10.1136/jcp.2004.017293.
- Kikhney, Alexey G.; Svergun, Dmitri I. (2015): A practical guide to small angle X-ray scattering (SAXS) of flexible and intrinsically disordered proteins. In *FEBS letters* 589 (19 Pt A), pp. 2570–2577. DOI: 10.1016/j.febslet.2015.08.027.
- Kim, K. K.; Kim, R.; Kim, S. H. (1998): Crystal structure of a small heat-shock protein. In *Nature* 394 (6693), pp. 595–599. DOI: 10.1038/29106.
- Kleinschmidt, Jörg H. (2019): Lipid-Protein Interactions. New York, NY: Springer New York (2003).
- Kono, M.; Sen, A. C.; Chakrabarti, B. (1990): Thermodynamics of thermal and athermal denaturation of gamma-crystallins: changes in conformational stability upon glutathione reaction. In *Biochemistry* 29 (2), pp. 464–470. DOI: 10.1021/bi00454a022.
- Kotlarchyk, Michael; Stephens, Richard B.; Huang, John S. (1988): Study of Schultz distribution to model polydispersity of microemulsion droplets. In *J. Phys. Chem.* 92 (6), pp. 1533–1538. DOI: 10.1021/j100317a032.
- Krushelnitsky, Alexey (2006): Intermolecular electrostatic interactions and Brownian tumbling in protein solutions. In *Physical chemistry chemical physics : PCCP* 8 (18), pp. 2117–2128. DOI: 10.1039/b517448a.
- Krushelnitsky, Alexey; Gauto, Diego; Rodriguez Camargo, Diana C.; Schanda, Paul; Saalwächter, Kay (2018): Microsecond motions probed by near-rotary-resonance R1ρ15N MAS NMR experiments: the model case of protein overall-rocking in crystals. In *Journal of biomolecular NMR* 71 (1), pp. 53–67. DOI: 10.1007/s10858-018-0191-4.
- Krushelnitsky, Alexey; Zinkevich, Tatiana; Reichert, Detlef; Chevelkov, Veniamin; Reif, Bernd (2010): Microsecond time scale mobility in a solid protein as studied by the 15N R(1rho) site-specific NMR relaxation rates. In *Journal of the American Chemical Society* 132 (34), pp. 11850–11853. DOI: 10.1021/ja103582n.

- Krushelnitsky, Alexey; Zinkevich, Tatiana; Reif, Bernd; Saalwächter, Kay (2014): Slow motions in microcrystalline proteins as observed by MAS-dependent ^{15}N rotating-frame NMR relaxation. In *Journal of magnetic resonance (San Diego, Calif. : 1997)* 248, pp. 8–12. DOI: 10.1016/j.jmr.2014.09.007.
- Kumar, Vineet; Dixit, Nitin; Zhou, Liqiang Lisa; Fraunhofer, Wolfgang (2011): Impact of short range hydrophobic interactions and long range electrostatic forces on the aggregation kinetics of a monoclonal antibody and a dual-variable domain immunoglobulin at low and high concentrations. In *International journal of pharmaceutics* 421 (1), pp. 82–93. DOI: 10.1016/j.ijpharm.2011.09.017.
- Kumosinski, Thomas F.; Farrell, Harold M. (1993): Determination of the global secondary structure of proteins by Fourier transform infrared (FTIR) spectroscopy. In *Trends in Food Science & Technology* 4 (6), pp. 169–175. DOI: 10.1016/0924-2244(93)90119-U.
- Lamba, Om P.; Borchman, Douglas; Sinha, S. K.; Shah, J.; Renugopalakrishnan, V.; Yappert, M. C. (1993): Estimation of the secondary structure and conformation of bovine lens crystallins by infrared spectroscopy: quantitative analysis and resolution by Fourier self-deconvolution and curve fit. In *Biochimica et Biophysica Acta (BBA) - Protein Structure and Molecular Enzymology* 1163 (2), pp. 113–123. DOI: 10.1016/0167-4838(93)90172-N.
- Lazzari, S.; Nicoud, L.; Jaquet, B.; Lattuada, M.; Morbidelli, M. (2016): Fractal-like structures in colloid science. In *Advances in colloid and interface science* 235, pp. 1–13. DOI: 10.1016/j.cis.2016.05.002.
- Le Bon, Christel; Nicolai, Taco; Durand, Dominique (1999): Kinetics of Aggregation and Gelation of Globular Proteins after Heat-Induced Denaturation. In *Macromolecules* 32 (19), pp. 6120–6127. DOI: 10.1021/ma9905775.
- Levitt, Malcolm H. (2015): Spin dynamics. Basics of nuclear magnetic resonance. 2. ed. Chichester: Wiley.
- Liang, J. J.; Chakrabarti, B. (1998): Intermolecular interaction of lens crystallins: from rotationally mobile to immobile states at high protein concentrations. In *Biochemical and biophysical research communications* 246 (2), pp. 441–445. DOI: 10.1006/bbrc.1998.8640.
- Liang, Lixin; Ji, Yi; Chen, Kuizhi; Gao, Pan; Zhao, Zhenchao; Hou, Guangjin (2022): Solid-State NMR Dipolar and Chemical Shift Anisotropy Recoupling Techniques for Structural and Dynamical Studies in Biological Systems. In *Chemical reviews*. DOI: 10.1021/acs.chemrev.1c00779.
- Liao, Jimmy Y. H.; Selomulya, Cordelia; Bushell, Graeme; Bickert, Götz; Amal, Rose (2005): On Different Approaches to Estimate the Mass Fractal Dimension of Coal Aggregates. In *Part. Part. Syst. Charact.* 22 (5), pp. 299–309. DOI: 10.1002/ppsc.200500978.
- Luz, Z.; Meiboom, S. (1963): Nuclear Magnetic Resonance Study of the Protolysis of Trimethylammonium Ion in Aqueous Solution—Order of the Reaction with Respect to Solvent. In *The Journal of chemical physics* 39 (2), pp. 366–370. DOI: 10.1063/1.1734254.

- Ma, Peixiang; Xue, Yi; Coquelle, Nicolas; Haller, Jens D.; Yuwen, Tairan; Ayala, Isabel et al. (2015): Observing the overall rocking motion of a protein in a crystal. In *Nature communications* 6, p. 8361. DOI: 10.1038/ncomms9361.
- MacRae, T. H. (2000): Structure and function of small heat shock/alpha-crystallin proteins: established concepts and emerging ideas. In *Cellular and molecular life sciences : CMLS* 57 (6), pp. 899–913. DOI: 10.1007/pl00000733.
- Mainz, Andi; Peschek, Jirka; Stavropoulou, Maria; Back, Katrin C.; Bardiaux, Benjamin; Asami, Sam et al. (2015): The chaperone α B-crystallin uses different interfaces to capture an amorphous and an amyloid client. In *Nature structural & molecular biology* 22 (11), pp. 898–905. DOI: 10.1038/nsmb.3108.
- Mainz, Andi; Reif, Bernd (2015): 1H, 15N and 13C chemical shift assignment of the alpha-crystallin domain and the C-terminal domain in human alpha-B crystallin oligomers.
- Maiti, Motilal; Kono, Masahiro; Chakrabarti, Bireswar (1988): Heat-induced changes in the conformation of α - and β -crystalline: Unique thermal stability of α -crystallin. In *FEBS letters* 236 (1), pp. 109–114. DOI: 10.1016/0014-5793(88)80295-3.
- Mandal, K.; Chakrabarti, B.; Thomson, J.; Siezen, R. J. (1987): Structure and stability of gamma-crystallins. Denaturation and proteolysis behavior. In *Journal of Biological Chemistry* 262 (17), pp. 8096–8102. DOI: 10.1016/S0021-9258(18)47533-3.
- Martin, Rachel W. (2007): NMR Studies of Eye Lens Crystallins. In Robin K. Harris, Roderick L. Wasylishen (Eds.): eMagRes. Chichester, UK: John Wiley & Sons, Ltd, pp. 139–152.
- Matheus, Susanne; Friess, Wolfgang; Mahler, Hanns-Christian (2006): FTIR and nDSC as analytical tools for high-concentration protein formulations. In *Pharmaceutical research* 23 (6), pp. 1350–1363. DOI: 10.1007/s11095-006-0142-8.
- McDermott, Martin J.; Gawinowicz-Kolks, Mary Ann; Chiesa, Rau'1; Spector, Abraham (1988): The disulfide content of calf γ -crystallin. In *Archives of Biochemistry and Biophysics* 262 (2), pp. 609–619. DOI: 10.1016/0003-9861(88)90413-4.
- Metz, G.; Wu, X. L.; Smith, S. O. (1994): Ramped-Amplitude Cross Polarization in Magic-Angle-Spinning NMR. In *Journal of Magnetic Resonance, Series A* 110 (2), pp. 219–227. DOI: 10.1006/jmra.1994.1208.
- Mezzena, Raffaele; Fischer, Peter (2013): The self-assembly, aggregation and phase transitions of food protein systems in one, two and three dimensions. In *Reports on Progress in Physics* 76 (4), p. 46601. DOI: 10.1088/0034-4885/76/4/046601.
- Miklos, Andrew C.; Li, Conggang; Sharaf, Naima G.; Pielak, Gary J. (2010): Volume exclusion and soft interaction effects on protein stability under crowded conditions. In *Biochemistry* 49 (33), pp. 6984–6991. DOI: 10.1021/bi100727y.

- Miklos, Andrew C.; Sarkar, Mohona; Wang, Yaqiang; Pielak, Gary J. (2011): Protein crowding tunes protein stability. In *Journal of the American Chemical Society* 133 (18), pp. 7116–7120. DOI: 10.1021/ja200067p.
- Minton, A. P. (2001): The influence of macromolecular crowding and macromolecular confinement on biochemical reactions in physiological media. In *Journal of Biological Chemistry* 276 (14), pp. 10577–10580. DOI: 10.1074/jbc.R100005200.
- Minton, Allen P. (2000): Implications of macromolecular crowding for protein assembly. In *Current Opinion in Structural Biology* 10 (1), pp. 34–39. DOI: 10.1016/S0959-440X(99)00045-7.
- Minton, Allen P. (2005): Models for excluded volume interaction between an unfolded protein and rigid macromolecular cosolutes: macromolecular crowding and protein stability revisited. In *Biophysical Journal* 88 (2), pp. 971–985. DOI: 10.1529/biophysj.104.050351.
- Mishra, Rajesh; Geyer, Matthias; Winter, Roland (2009): NMR spectroscopic investigation of early events in IAPP amyloid fibril formation. In *Chembiochem : a European journal of chemical biology* 10 (11), pp. 1769–1772. DOI: 10.1002/cbic.200900237.
- Mittal, Shruti; Chowhan, Rimpay Kaur; Singh, Laishram Rajendrakumar (2015): Macromolecular crowding: Macromolecules friend or foe. In *Biochimica et biophysica acta* 1850 (9), pp. 1822–1831. DOI: 10.1016/j.bbagen.2015.05.002.
- Moran, Sean D.; Zhang, Tianqi O.; Zanni, Martin T. (2014): An alternative structural isoform in amyloid-like aggregates formed from thermally denatured human γ D-crystallin. In *Protein science : a publication of the Protein Society* 23 (3), pp. 321–331. DOI: 10.1002/pro.2422.
- Moreau, Kate L.; King, Jonathan A. (2012): Protein misfolding and aggregation in cataract disease and prospects for prevention. In *Trends in molecular medicine* 18 (5), pp. 273–282. DOI: 10.1016/j.molmed.2012.03.005.
- Morgan, C. F.; Schleich, T.; Caines, G. H.; Farnsworth, P. N. (1989): Elucidation of intermediate (mobile) and slow (solidlike) protein motions in bovine lens homogenates by carbon-13 NMR spectroscopy. In *Biochemistry* 28 (12), pp. 5065–5074. DOI: 10.1021/bi00438a025.
- Mylonas, Efstratios; Svergun, Dmitri I. (2007): Accuracy of molecular mass determination of proteins in solution by small-angle X-ray scattering. In *J Appl Crystallogr* 40 (s1), s245-s249. DOI: 10.1107/S002188980700252X.
- Najmudin, S.; Lindley, P.; Slingsby, C.; Bateman, O.; Myles, D.; Kumaraswamy, S.; Glover, I. (1994): Structure of the Bovine Gamma-B Crystallin at 150K.
- Nakai, Shuryo (1983): Structure-function relationships of food proteins: with an emphasis on the importance of protein hydrophobicity. In *J. Agric. Food Chem.* 31 (4), pp. 676–683. DOI: 10.1021/jf00118a001.

- Nakamura, Ryo; Sugiyama, Hisako; Sato, Yasushi (1978): Factors Contributing to the Heat-induced Aggregation of Ovalbumin. In *Agricultural and Biological Chemistry* 42 (4), pp. 819–824. DOI: 10.1080/00021369.1978.10863067.
- Narberhaus, Franz (2002): Alpha-crystallin-type heat shock proteins: socializing minichaperones in the context of a multichaperone network. In *Microbiology and molecular biology reviews : MMBR* 66 (1), 64-93; table of contents. DOI: 10.1128/MMBR.66.1.64-93.2002.
- Nicolai, Taco (2007): Structure of self-assembled globular proteins. In *Food colloids. Interactions, microstructure and processing*, pp. 35–56.
- Nicolai, Taco (2019): Gelation of food protein-protein mixtures. In *Advances in colloid and interface science* 270, pp. 147–164. DOI: 10.1016/j.cis.2019.06.006.
- Oakes, John (1976a): Protein hydration. Nuclear magnetic resonance relaxation studies of the state of water in native bovine serum albumin solutions. In *J. Chem. Soc., Faraday Trans. 1* 72 (0), p. 216. DOI: 10.1039/F19767200216.
- Oakes, John (1976b): Thermally denatured proteins. Nuclear magnetic resonance, binding isotherm and chemical modification studies of thermally denatured bovine serum albumin. In *J. Chem. Soc., Faraday Trans. 1* 72 (0), p. 228. DOI: 10.1039/F19767200228.
- Paravastu, Anant K.; Leapman, Richard D.; Yau, Wai-Ming; Tycko, Robert (2008): Molecular structural basis for polymorphism in Alzheimer's beta-amyloid fibrils. In *Proceedings of the National Academy of Sciences of the United States of America* 105 (47), pp. 18349–18354. DOI: 10.1073/pnas.0806270105.
- Parker, Roger; Noel, Timothy R.; Brownsey, Geoffrey J.; Laos, Katrin; Ring, Stephen G. (2005): The nonequilibrium phase and glass transition behavior of beta-lactoglobulin. In *Biophysical Journal* 89 (2), pp. 1227–1236. DOI: 10.1529/biophysj.105.064246.
- Pascolini, Donatella; Mariotti, Silvio Paolo (2012): Global estimates of visual impairment: 2010. In *The British journal of ophthalmology* 96 (5), pp. 614–618. DOI: 10.1136/bjophthalmol-2011-300539.
- Peschek, Jirka; Braun, Nathalie; Franzmann, Titus M.; Georgalis, Yannis; Haslbeck, Martin; Weinkauf, Sevil; Buchner, Johannes (2009): The eye lens chaperone alpha-crystallin forms defined globular assemblies. In *Proceedings of the National Academy of Sciences of the United States of America* 106 (32), pp. 13272–13277. DOI: 10.1073/pnas.0902651106.
- Peschek, Jirka; Braun, Nathalie; Rohrberg, Julia; Back, Katrin Christiane; Kriehuber, Thomas; Kastenmüller, Andreas et al. (2013): Regulated structural transitions unleash the chaperone activity of α B-crystallin. In *Proceedings of the National Academy of Sciences of the United States of America* 110 (40), E3780-9. DOI: 10.1073/pnas.1308898110.
- Pouzot, M.; NICOLAI, T.; Visschers, R. W.; Weijers, M. (2005): X-ray and light scattering study of the structure of large protein aggregates at neutral pH. In *Food Hydrocolloids* 19 (2), pp. 231–238. DOI: 10.1016/j.foodhyd.2004.06.003.

- Putilina, Tatiana; Skouri-Panet, Fériel; Prat, Karine; Lubsen, Nicolette H.; Tardieu, Annette (2003): Subunit exchange demonstrates a differential chaperone activity of calf alpha-crystallin toward beta LOW- and individual gamma-crystallins. In *The Journal of biological chemistry* 278 (16), pp. 13747–13756. DOI: 10.1074/jbc.M208157200.
- Ralston, G. B. (1990): Effects of "crowding" in protein solutions. In *J. Chem. Educ.* 67 (10), p. 857. DOI: 10.1021/ed067p857.
- Rasmussen, Tue; van de Weert, Marco; Jiskoot, Wim; Kasimova, Marina R. (2011): Thermal and acid denaturation of bovine lens α -crystallin. In *Proteins* 79 (6), pp. 1747–1758. DOI: 10.1002/prot.22998.
- Ravera, Enrico; Parigi, Giacomo; Mainz, Andi; Religa, Tomasz L.; Reif, Bernd; Luchinat, Claudio (2013): Experimental determination of microsecond reorientation correlation times in protein solutions. In *The journal of physical chemistry. B* 117 (13), pp. 3548–3553. DOI: 10.1021/jp312561f.
- Reddy, G. Bhanuprakash; Kumar, P. Anil; Kumar, M. Satish (2006): Chaperone-like activity and hydrophobicity of alpha-crystallin. In *IUBMB life* 58 (11), pp. 632–641. DOI: 10.1080/15216540601010096.
- Regini, J. W.; Grossmann, J. G.; Burgio, M. R.; Malik, N. S.; Koretz, J. F.; Hodson, S. A.; Elliott, G. F. (2004): Structural Changes in α -Crystallin and Whole Eye Lens During Heating, Observed by Low-angle X-ray Diffraction. In *Journal of Molecular Biology* 336 (5), pp. 1185–1194. DOI: 10.1016/S0022-2836(03)00814-3.
- Riedl, Mareike; Strauch, Annika; Catoci, Dragana A. M.; Haslbeck, Martin (2020): Proteinaceous Transformers: Structural and Functional Variability of Human sHsps. In *International journal of molecular sciences* 21 (15). DOI: 10.3390/ijms21155448.
- Roberts, Gordon C. K. (Ed.) (2013): *Encyclopedia of Biophysics*. Berlin, Heidelberg: Springer Berlin Heidelberg.
- Robinson, M. L. (2010): Lens Fiber Cell Differentiation. In : *Encyclopedia of the Eye*: Elsevier, pp. 543–550.
- Roos, Matthias; Hofmann, Marius; Link, Susanne; Ott, Maria; Balbach, Jochen; Rössler, Ernst et al. (2015a): The "long tail" of the protein tumbling correlation function: observation by (1)H NMR relaxometry in a wide frequency and concentration range. In *Journal of biomolecular NMR* 63 (4), pp. 403–415. DOI: 10.1007/s10858-015-0001-1.
- Roos, Matthias; Link, Susanne; Balbach, Jochen; Krushelnitsky, Alexey; Saalwächter, Kay (2015b): NMR-detected brownian dynamics of α B-crystallin over a wide range of concentrations. In *Biophysical Journal* 108 (1), pp. 98–106. DOI: 10.1016/j.bpj.2014.11.1858.
- Roos, Matthias; Ott, Maria; Hofmann, Marius; Link, Susanne; Rössler, Ernst; Balbach, Jochen et al. (2016): Coupling and Decoupling of Rotational and Translational Diffusion of Proteins under Crowding Conditions. In *Journal of the American Chemical Society* 138 (32), pp. 10365–10372. DOI: 10.1021/jacs.6b06615.

- Roskamp, Kyle W.; Montelongo, David M.; Anorma, Chelsea D.; Bandak, Diana N.; Chua, Janine A.; Malecha, Kurtis T.; Martin, Rachel W. (2017): Multiple Aggregation Pathways in Human γ S-Crystallin and Its Aggregation-Prone G18V Variant. In *Invest. Ophthalmol. Vis. Sci.* 58 (4), pp. 2397–2405. DOI: 10.1167/iovs.16-20621.
- Roskamp, Kyle W.; Paulson, Carolyn N.; Brubaker, William D.; Martin, Rachel W. (2020): Function and Aggregation in Structural Eye Lens Crystallins. In *Accounts of chemical research* 53 (4), pp. 863–874. DOI: 10.1021/acs.accounts.0c00014.
- Ross, Christopher A.; Poirier, Michelle A. (2004): Protein aggregation and neurodegenerative disease. In *Nature medicine* 10 Suppl, S10-7. DOI: 10.1038/nm1066.
- Ross-Murphy, Simon B. (1998): Reversible and irreversible biopolymer gels - Structure and mechanical properties. In *Berichte der Bunsengesellschaft für physikalische Chemie* 102 (11), pp. 1534–1539. DOI: 10.1002/bbpc.19981021104.
- Ryazantsev, Sergey N.; Poliansky, Nikolai B.; Chebotareva, Natalia A.; Muranov, Konstantin O. (2018): 3D structure of the native α -crystallin from bovine eye lens. In *International Journal of Biological Macromolecules* 117, pp. 1289–1298. DOI: 10.1016/j.ijbiomac.2018.06.004.
- Sarkar, Mohona; Li, Conggang; Pielak, Gary J. (2013): Soft interactions and crowding. In *Biophysical reviews* 5 (2), pp. 187–194. DOI: 10.1007/s12551-013-0104-4.
- Sauter, Andrea; Zhang, Fajun; Szekely, Noemi K.; Pipich, Vitaliy; Sztucki, Michael; Schreiber, Frank (2016): Structural Evolution of Metastable Protein Aggregates in the Presence of Trivalent Salt Studied by (V)SANS and SAXS. In *The journal of physical chemistry. B* 120 (24), pp. 5564–5571. DOI: 10.1021/acs.jpcc.6b03559.
- Schägger, H.; Jagow, G. von (1987): Tricine-sodium dodecyl sulfate-polyacrylamide gel electrophoresis for the separation of proteins in the range from 1 to 100 kDa. In *Analytical biochemistry* 166 (2), pp. 368–379. DOI: 10.1016/0003-2697(87)90587-2.
- Schütz, Anne K.; Vagt, Toni; Huber, Matthias; Ovchinnikova, Oxana Y.; Cadalbert, Riccardo; Wall, Joseph et al. (2015): Atomic-resolution three-dimensional structure of amyloid β fibrils bearing the Osaka mutation. In *Angewandte Chemie (International ed. in English)* 54 (1), pp. 331–335. DOI: 10.1002/anie.201408598.
- Selivanova, Olga M.; Galzitskaya, Oxana V. (2020): Structural and Functional Peculiarities of α -Crystallin. In *Biology* 9 (4). DOI: 10.3390/biology9040085.
- Sen, A. C.; Walsh, M. T.; Chakrabarti, B. (1992): An insight into domain structures and thermal stability of gamma-crystallins. In *Journal of Biological Chemistry* 267 (17), pp. 11898–11907. DOI: 10.1016/S0021-9258(19)49782-2.
- Shahid, Shakeel Ahmad; Bardiaux, Benjamin; Franks, W. Trent; Krabben, Ludwig; Habeck, Michael; van Rossum, Barth-Jan; Linke, Dirk (2012): Membrane-protein structure determination by solid-state NMR spectroscopy of microcrystals. In *Nature methods* 9 (12), pp. 1212–1217. DOI: 10.1038/nmeth.2248.

- Shih; Kim; Liu; Aksay (1990): Scaling behavior of the elastic properties of colloidal gels. In *Physical review. A, Atomic, molecular, and optical physics* 42 (8), pp. 4772–4779. DOI: 10.1103/PhysRevA.42.4772.
- Siezen, R. J.; Bindels, J. G.; Hoenders, H. J. (1978): The quaternary structure of bovine alpha-crystallin. Size and charge microheterogeneity: more than 1000 different hybrids? In *European journal of biochemistry* 91 (2), pp. 387–396. DOI: 10.1111/j.1432-1033.1978.tb12691.x.
- Song, Shuhua; Landsbury, Andrew; Dahm, Ralf; Liu, Yizhi; Zhang, Qingjiong; Quinlan, Roy A. (2009): Functions of the intermediate filament cytoskeleton in the eye lens. In *The Journal of clinical investigation* 119 (7), pp. 1837–1848. DOI: 10.1172/JCI38277.
- Spurr, Arthur R. (1969): A low-viscosity epoxy resin embedding medium for electron microscopy. In *Journal of Ultrastructure Research* 26 (1-2), pp. 31–43. DOI: 10.1016/s0022-5320(69)90033-1.
- Steadman, B. L.; Trautman, P. A.; Lawson, E. Q.; Raymond, M. J.; Mood, D. A.; Thomson, J. A.; Middaugh, C. R. (1989): A differential scanning calorimetric study of the bovine lens crystallins. In *Biochemistry* 28 (25), pp. 9653–9658. DOI: 10.1021/bi00451a017.
- Stetefeld, Jörg; McKenna, Sean A.; Patel, Trushar R. (2016): Dynamic light scattering: a practical guide and applications in biomedical sciences. In *Biophysical reviews* 8 (4), pp. 409–427. DOI: 10.1007/s12551-016-0218-6.
- Sun, T. X.; Liang, J. J. (1998): Intermolecular exchange and stabilization of recombinant human alphaA- and alphaB-crystallin. In *The Journal of biological chemistry* 273 (1), pp. 286–290. DOI: 10.1074/jbc.273.1.286.
- Surewicz, W. K.; Olesen, P. R. (1995): On the thermal stability of alpha-crystallin: a new insight from infrared spectroscopy. In *Biochemistry* 34 (30), pp. 9655–9660. DOI: 10.1021/bi00030a001.
- Suzuki, Yuta; Brender, Jeffrey R.; Hartman, Kevin; Ramamoorthy, Ayyalusamy; Marsh, E. Neil G. (2012): Alternative pathways of human islet amyloid polypeptide aggregation distinguished by (19)f nuclear magnetic resonance-detected kinetics of monomer consumption. In *Biochemistry* 51 (41), pp. 8154–8162. DOI: 10.1021/bi3012548.
- Takemoto, L.; Emmons, T.; Horwitz, J. (1993): The C-terminal region of alpha-crystallin: involvement in protection against heat-induced denaturation. In *The Biochemical journal* 294 (Pt 2), pp. 435–438. DOI: 10.1042/bj2940435.
- Taraban, Marc B.; DePaz, Roberto A.; Lobo, Brian; Yu, Y. Bruce (2017): Water Proton NMR: A Tool for Protein Aggregation Characterization. In *Analytical chemistry* 89 (10), pp. 5494–5502. DOI: 10.1021/acs.analchem.7b00464.
- Tardieu, A.; V  r  tout, F.; Krop, B.; Slingsby, C. (1992): Protein interactions in the calf eye lens: interactions between beta-crystallins are repulsive whereas in gamma-crystallins they are attractive. In *European biophysics journal : EBJ* 21 (1), pp. 1–12. DOI: 10.1007/BF00195438.

- Tardieu, Annette; Laporte, Dominique; Licinio, Pedro; Krop, Brigitte; Delaye, Mireille (1986): Calf lens α -crystallin quaternary structure. In *Journal of Molecular Biology* 192 (4), pp. 711–724. DOI: 10.1016/0022-2836(86)90023-9.
- Tatulian, Suren A. (2019): FTIR Analysis of Proteins and Protein-Membrane Interactions. In *Methods in molecular biology (Clifton, N.J.)* 2003, pp. 281–325. DOI: 10.1007/978-1-4939-9512-7_13.
- Tobitani, Atsumi; Ross-Murphy, Simon B. (1997): Heat-Induced Gelation of Globular Proteins. 1. Model for the Effects of Time and Temperature on the Gelation Time of BSA Gels. In *Macromolecules* 30 (17), pp. 4845–4854. DOI: 10.1021/ma970112j.
- Totosaus, Alfonso; Montejano, Jose G.; Salazar, Juan A.; Guerrero, Isabel (2002): A review of physical and chemical protein-gel induction. In *Int J Food Sci Tech* 37 (6), pp. 589–601. DOI: 10.1046/j.1365-2621.2002.00623.x.
- Treweek, Teresa M.; Ecroyd, Heath; Williams, Danielle M.; Meehan, Sarah; Carver, John A.; Walker, Mark J. (2007): Site-directed mutations in the C-terminal extension of human α B-crystallin affect chaperone function and block amyloid fibril formation. In *PloS one* 2 (10), e1046. DOI: 10.1371/journal.pone.0001046.
- Treweek, Teresa M.; Rekas, Agata; Walker, Mark J.; Carver, John A. (2010): A quantitative NMR spectroscopic examination of the flexibility of the C-terminal extensions of the molecular chaperones, α A- and α B-crystallin. In *Experimental eye research* 91 (5), pp. 691–699. DOI: 10.1016/j.exer.2010.08.015.
- Trokel, Stephen (1962): The Physical Basis for Transparency of the Crystalline Lens. In *Invest. Ophthalmol. Vis. Sci.* 1 (4), pp. 493–501.
- Uversky, Vladimir N.; Dunker, A. Keith (2010): Understanding protein non-folding. In *Biochimica et biophysica acta* 1804 (6), pp. 1231–1264. DOI: 10.1016/j.bbapap.2010.01.017.
- van Boekel, Martinus A.M; Lange, Frank de; Grip, Willem J. de; Jong, Wilfried W. de (1999): Eye lens α A- and α B-crystallin: complex stability versus chaperone-like activity. In *Biochimica et Biophysica Acta (BBA) - Protein Structure and Molecular Enzymology* 1434 (1), pp. 114–123. DOI: 10.1016/S0167-4838(99)00178-8.
- van Kleef, F. S. (1986): Thermally induced protein gelation: gelation and rheological characterization of highly concentrated ovalbumin and soybean protein gels. In *Biopolymers* 25 (1), pp. 31–59. DOI: 10.1002/bip.360250105.
- van Montfort, R. L.; Basha, E.; Friedrich, K. L.; Slingsby, C.; Vierling, E. (2001a): Crystal structure and assembly of a eukaryotic small heat shock protein. In *Nature structural biology* 8 (12), pp. 1025–1030. DOI: 10.1038/nsb722.
- van Montfort, Rob; Slingsby, Christine; Vierling, Elizabeth (2001b): Structure and function of the small heat shock protein/ α -crystallin family of molecular chaperones. In : Protein Folding in the Cell, vol. 59: Elsevier (Advances in Protein Chemistry), pp. 105–156.

- Vanhoudt, J.; Abgar, S.; Aerts, T.; Clauwaert, J. (2000): Native quaternary structure of bovine alpha-crystallin. In *Biochemistry* 39 (15), pp. 4483–4492. DOI: 10.1021/bi990386u.
- Verheul, M.; Roefs, S.P.F.M. (1998): Structure of whey protein gels, studied by permeability, scanning electron microscopy and rheology. In *Food Hydrocolloids* 12 (1), pp. 17–24. DOI: 10.1016/S0268-005X(98)00041-1.
- Verheul, Marleen; Roefs, Sebastianus P. F. M.; Mellema, Jorrit; Kruif, Kees G. de (1998): Power Law Behavior of Structural Properties of Protein Gels. In *Langmuir* 14 (9), pp. 2263–2268. DOI: 10.1021/la9708187.
- Vermeer, Arnoldus W.P.; Norde, Willem (2000): The Thermal Stability of Immunoglobulin: Unfolding and Aggregation of a Multi-Domain Protein. In *Biophysical Journal* 78 (1), pp. 394–404. DOI: 10.1016/S0006-3495(00)76602-1.
- Walsh, M. T.; Sen, A. C.; Chakrabarti, B. (1991): Micellar subunit assembly in a three-layer model of oligomeric alpha-crystallin. In *Journal of Biological Chemistry* 266 (30), pp. 20079–20084. DOI: 10.1016/S0021-9258(18)54893-6.
- Wang, Cheng Hsin; Damodaran, Srinivasan (1991): Thermal gelation of globular proteins: influence of protein conformation on gel strength. In *J. Agric. Food Chem.* 39 (3), pp. 433–438. DOI: 10.1021/jf00003a001.
- Wang, Yaqiang; Sarkar, Mohona; Smith, Austin E.; Krois, Alexander S.; Pielak, Gary J. (2012): Macromolecular crowding and protein stability. In *Journal of the American Chemical Society* 134 (40), pp. 16614–16618. DOI: 10.1021/ja305300m.
- Weijers, Mireille; Visschers, Ronald W.; Nicolai, Taco (2002): Light Scattering Study of Heat-Induced Aggregation and Gelation of Ovalbumin. In *Macromolecules* 35 (12), pp. 4753–4762. DOI: 10.1021/ma0120198.
- Wistow, G. (1993): Possible tetramer-based quaternary structure for alpha-crystallins and small heat shock proteins. In *Experimental eye research* 56 (6), pp. 729–732. DOI: 10.1006/exer.1993.1090.
- Xia, J. Z.; Aerts, T.; Donceel, K.; Clauwaert, J. (1994): Light scattering by bovine alpha-crystallin proteins in solution: hydrodynamic structure and interparticle interaction. In *Biophysical Journal* 66 (3), pp. 861–872. DOI: 10.1016/S0006-3495(94)80862-8.
- Xu, Zhi-Xue; Ma, Gong-Li; Zhang, Qiang; Chen, Cong-Heng; He, Yan-Ming; Xu, Li-Hui et al. (2017): Inhibitory Mechanism of Epigallocatechin Gallate on Fibrillation and Aggregation of Amidated Human Islet Amyloid Polypeptide. In *Chemphyschem : a European journal of chemical physics and physical chemistry* 18 (12), pp. 1611–1619. DOI: 10.1002/cphc.201700057.
- Zaccarelli, Emanuela (2007): Colloidal gels: equilibrium and non-equilibrium routes. In *Journal of Physics: Condensed Matter* 19 (32), p. 323101. DOI: 10.1088/0953-8984/19/32/323101.

- Zhang, Q. (2013): Selection of an artificial binding protein against the ectodomain of PTH1R. Naturwissenschaftliche Fakultät I. Martin-Luther-Universität Halle-Wittenberg: Halle (Saale).
- Zimmerman, S. B.; Minton, A. P. (1993): Macromolecular crowding: biochemical, biophysical, and physiological consequences. In *Annual review of biophysics and biomolecular structure* 22, pp. 27–65. DOI: 10.1146/annurev.bb.22.060193.000331.
- Zinkevich, Tatiana; Chevelkov, Veniamin; Reif, Bernd; Saalwächter, Kay; Krushelnitsky, Alexey (2013): Internal protein dynamics on ps to μ s timescales as studied by multi-frequency (^{15}N) solid-state NMR relaxation. In *Journal of biomolecular NMR* 57 (3), pp. 219–235. DOI: 10.1007/s10858-013-9782-2.

10 Acknowledgement

My PhD journey was an exciting challenge, although with some hardships on the way it ended with a rewarding outcome. This would not have been possible by the help and support of a lot of people I interacted with. I would therefore like to thank and acknowledge all who supported me in this journey.

Firstly, I would like to express my heartfelt gratitude to Prof. Dr. Kay Saalwächter who trusted me with this wonderful chance to be a part of his research team and to work on this project. His scientific expertise as well as the support and guidance steered me to fruitfully complete this thesis.

Dr. Alexey Krushelnitsky introduced me to NMR and to the experimental part of this project. I would always be grateful to him for helping me with all the NMR measurements and for the discussions that I benefited from immensely.

I would like to thank the collaborators of this project, Prof. Dr. Jochen Balbach for the discussions that furthered this project, Dr. Susanne Weininger (Link) for initially providing the crystallin proteins and eventually introducing me to protein expression and purification and lastly Malte Neudorf for supporting me with this project and suggesting new ideas.

I am further grateful to several people who dedicated their time for me by conducting experiments and introducing me to the working principles of different characterization techniques. Dr. Maria Ott (Institute of Biochemistry and Biotechnology, MLU Halle) was kind enough to perform SAXS measurements as well as its data interpretation. Dr. Gerd Hause (Biocenter, MLU Halle), provided the TEM images of the proteins. Dr. Andreas Kerth (Formerly Institute for Chemistry, MLU Halle) introduced me to ATR FTIR and Dr. Christian Schwieger (Institute of Chemistry, MLU Halle) helped me with FTIR data analysis. Kevin Hagmann (TU Darmstadt) performed AFM measurements. Dr. Riddiman Sarkar (TU Munich) provided the solid-state spectra of α B crystallin protein.

I would also like to thank Prof. Dr. Bernd Reif (TU Munich) for giving me the opportunity to work in his group and to the AG Reif members who were kind enough to teach me the techniques involved in the sample preparation and measurements to acquire the solid-state NMR spectra of crystallin proteins.

My sincere thanks to Prof. Dr. Dariush Hinderberger (Institute of Chemistry, MLU Halle) for allowing me to work with the ATR - FTIR and DLS instruments and his team members for easily allocating me within their measurement schedules, which proved to be an integral part of this thesis.

I am grateful to the Biophysics group Shubhra Sachan, Kathrin Waldheim, Celia González Moya, Bruno Voigt, Dr. Matthias Dreydoppel, Dr. Tobias Gruber, Dr. Ulrich Weininger and

Stefan Gröger for a very pleasant working atmosphere in the Bio-lab and for being always available to help.

I had the privilege to work with a wonderful NMR research group. I will always fondly remember the time we spent during the get-togethers and the non-scientific discussions we had over lunch. I thank Akshay Karekar, Dr. Anna Naumova, Dr. Mareen Schaller (Schäfer), Mozhdeh Abbasi, Anika Wurl, Lucas Löser, David Haselberger, Afiq Anuar, Assam Raja, Dr. Tiago Mendes Ferriera, Dr. Yury Golitsyn, Pierre Seiboth, Dr. Günter Hempel and Prof. Dr. Detlef Reichert. I would like to thank Rositta Mothes for all the administrative support.

I couldn't ask for any better officemates than Dr. Anton Mordvinkin and Dr. Farhad Shahsavan. Thank you so much for the funny conversations and for lighting the mood on a dull day. The most exciting times were when we created games for the graduation parties.

I am extremely grateful for the funding by the Deutsche Forschungsgemeinschaft (DFG) towards the integrated research training group of the SFB/TRR 102 project A08. Additionally, I would like to thank Dr. Ann-Kristin Fliieger and Dr. Thomas Michael for the organization and administrative support of the SFB related workshops, soft-skill courses, advanced training modules and doctoral students' seminar. I am thankful to Prof. Dr. Wolfgang Binder for being my mentor in the graduate school of the iRTG.

Though there were a lot of ups and downs in my life here in Germany, it was all made bearable due to the company of a group of people that I call 'family'. I am extremely grateful to Chinku, Nilu, Nishanth, Joji, Anish, Mithun, Arya, Jai, Kuriakose, Ajeesh, Nalin, Khyati, Jubin chettan, Susha chechi, Renee and Abby.

Last but not the least my family in India. Being away from them was not always easy but they always supported me and pushed me to reach my goals. They knew what I am capable of and never let me lose hope in my troubled times. Thank you so much Achachan, Amma and Savio for raising me to be a strong independent woman.

Finally, I want to thank my husband Milan. Although he came in to my life after my PhD, he played a huge role in helping me reach the end of my thesis writing. I will forever be grateful for all his love and encouragement.

11 List of Publications

Publication from this thesis

M. Camilles; S. Link, J. Balbach, K Saalwächter, A Krushelnitsky, (2018): Quantitative NMR study of heat-induced aggregation of eye-lens crystallin proteins under crowding conditions. In *Biochimica et biophysica acta. Proteins and proteomics*. DOI: 10.1016/j.bbapap.2018.07.007

M. Camilles; S. Link, J. Balbach, K Saalwächter, A Krushelnitsky, (2019): Corrigendum to quantitative NMR study of heat-induced aggregation of eye-lens crystallin proteins under crowding conditions. *BBAPAP Volume 1866/10 2018 1055-1061*. In *Biochimica et biophysica acta. Proteins and proteomics* 1867 (4), pp. 453–454. DOI: 10.1016/j.bbapap.2019.02.001

Other publications

D. Chadar, M Camilles, R Patil, A Khan, T Weyhermüller, S Salunke-Gawali, (2015): Synthesis and characterization of n-alkylamino derivatives of vitamin K3: Molecular structure of 2-propylamino-3-methyl-1,4-naphthoquinone and antibacterial activities. In *Journal of Molecular Structure* 1086, pp. 179–189. DOI: 10.1016/j.molstruc.2015.01.029:

12 Curriculum Vitae

Personal details

First name: Maria
Family name: Camilles
Nationality: Indian

Education

07.2016 – 03.2022 Doctoral Studies
Martin-Luther-Universität, Halle – Wittenberg
Halle (Saale), Germany
08.2012 – 04.2014 Master of Science (Inorganic chemistry)
Savitribai Phule Pune University (SPPU)
Pune, India
07.2009 – 05.2012 Bachelor of Science (Chemistry)
H. P. T Arts and R.Y.K Science College (Affiliated to SPPU, India)
Nashik, India

Work experience

11.2022 – present Junior Scientist
R – Pharm Germany GmbH
Illertissen, Germany
08.2014 – 05.2016 Research Assistant
National Chemical Laboratory
Pune, India

Halle (Saale), den 30.10.2024

Maria Camilles

13 Erklärung

Hiermit versichere ich, die vorliegende Arbeit selbstständig und ohne fremde Hilfe verfasst und die von mir angegeben Quellen und Hilfsmittel verwendet zu haben. Die den benutzten Werken wörtlich oder inhaltlich entnommenen Stellen habe ich als solche kenntlich gemacht.

Ich erkläre, keine anderweitigen Promotionsversuche unternommen und die vorliegende Dissertatin weder in der jetzigen noch in einer anderen Fassung einer anderen wissenschaftlichen Einrichtung vorgelegt zu haben.

Halle (Saale), den 30.10. 2024

Maria Camilles